MATECO

- "New Coating Deposited by PACVD for Corrosion Protection" -

FP6 Project: NMP3-CT-2003-505928

Instrument: STREP
Priority: 3- NMP

PUBLISHABLE FINAL ACTIVITY REPORT

Project Co-ordinator: HEF (F)

Partners: **CSIC (E)**
UNIBA (I)
INSA (F)
CNRS (F)
POLITO (I)
CRF (I)
EADS (D)
TEFAL (F)
ALMA (F)

PROJECT START DATE: 01st February 2004 **DURATION**: 36 months

PERIOD COVERED: from 1st February 2004 to 31st January 2007

Due Date: 15th March 2007

Actual Submission Date: 15th March 2007

Document Information

Document Name: Final PublishableActivity Report **Draft**
ID: MATECO-Final-Publishable-Report-V01.doc
Revision: Version 01
Revision Date: 24/07/2007
Author: Stéphane GAMEZ - ALMA Consulting Group
Dissemination level: Confidential

Diffusion list

Consortium and EC by PRODIGE

Approvals

	Name	Company	Date	Visa
Author	Stéphane GAMEZ	ALMA	12/02/07	
WP Leader	-	-	-	-
Coordinator	Christophe HEAU	HEF R&D		
Quality Manager	Stéphane GAMEZ	ALMA		

Documents history

Revision	Date	Modification	Author
Version 01	12/02/07	First draft	S. GAMEZ

Content

Section 1 – Project Execution

1.1. Overview of general project objectives

This project has been designed so as to develop smart multifunctional coatings based on [Si-O-N] materials. They have to combine corrosion resistance and tribology, decorative and anti-sticking properties. Developing such a kind of material is only possible if fundamental knowledge on materials and associated coating process is gained. Therefore, the global objectives of this project are:

- To develop, understand and characterise new materials related to the [SiOx - SiNx - SiOxNy] ternary system;
- To manufacture coatings with these new materials using vapour deposition process;
- To develop, understand and characterise new coatings made with these materials.

Objective 1: Development and modelling of new materials

Regarding the materials for coatings, the objectives will focus on the increase of fundamental knowledge on:

- The [Si - O - N] materials and their behaviours concerning properties expected. Models and deep nano-characterisation will be performed (**Milestone M 3.1**);
- The preparation methods of these materials. A careful attention will be paid on the effect of the gas feed composition on the chemical composition of the coating and its basic mechanical and electrical properties. Indeed, gas feed composition is a crucial parameter for obtaining a coating with the desired chemical composition.

As the coatings quality is directly linked to the surface state of the substrate, MATECO project will also focus on the understanding and improvement of substrate surface. The objectives are:

- Basic knowledge:
  - To identify the corrosion sources (kind and nature of defect) according to the nature of the substrates (**Milestone M 1.1**).
- Study on the surface preparation methods:
  - To design suitable surface preparation methods to obtain defect-free coatings (**Milestone M 4.2**).

Objective 2: Study and understanding of Vapour deposition process

The process to be studied will be the PACVD. MATECO project proposes to study and develop a new technology, which separates the control of plasma generation (precursor dissociation) from ion bombardment of the growing coating. For this, it is proposed to generate ECR microwave plasma by small sources distributed on the wall of the chamber.

Theoretical understanding:

- To model the production and diffusion of plasma;
- To model the PACVD deposition process;
- To model the cleaning process.

Study, optimisation and development of process:

- To design a microwave plasma reactor, which produces a plasma density of 1 012 cm^{-3} at 0.133 Pa (**Milestone M 2.2**);
- To design a low temperature process < 100 °C for corrosion protection alone;
- To design a low temperature process < 200 °C for corrosion protection and tribology properties;
- To combine two different layer types for wear and corrosion resistance in one production unit, which normally have to be prepared by different processes. This will be disruptive for the cost reduction in deposition and for the increase in quality of the coating;
- To improve the deposition rate of PACVD process up to 7 µm / h (**Milestone M 2.1**);
- To develop a suitable cleaning process for the reactor and related tools.

Objective 3: Coatings properties (Milestone M 4.1)

The coatings developed will have to fulfil the following general objectives:

- To obtain homogeneous coating and properties (less than 10 % variation in the whole batch);
- To define the correlation between coating materials and corrosion protection. To achieve this objective, a deep study based upon electrochemical, morphological, and chemical characterisation will be carried out.

Regarding the objectives in terms of properties, coatings developed must have (**Milestone M 6.1**):

- Coated part achieving the objectives in terms of corrosion and wear protection;
- For Corrosion protection alone:
  - Optical transparency > 80 %;
  - Colourless (constant optical transparency from 400 to 900 nm);
  - Corrosion protection > 144 h salt spray test;
  - Scribe creepage (1 - 2 mm in cyclic testing.
- For adhesion:
  - Cross hatch test GT 0 (wet and dry);
  - Scratch resistant: no delamination.
- For corrosion and tribology properties:
  - Surface hardness > 25 GPa;
  - Dry friction coefficient < 0.2;
  - Corrosion protection > 96 h salt spray test.

Objective 4: Validation

Validation on the following applications:

- The coated parts have to fulfil the requirements of **CRF** in terms of mirroring, corrosion and wear resistance for automotive application;
- The coated parts have to fulfil the requirements of **EADS** regarding wear (fretting and galling), corrosion and anti-sticking properties;
- The coated parts have to fulfil the requirement of **HEF** in terms of decorative properties and protection of corrosion & wear resistance and protection of electromagnetic shielding metal coatings;
- The coated parts have to fulfil the requirement of **TEFAL** in terms of anti-sticking an wear protection;

- To maintain the same corrosion resistance of actual used hazardous "chromium-based or nickel-based..." coating treatments for light alloys components applications with a reduction of industrial coating process cost of about 10 %.

To prepare sustainable coatings, a life cycle analysis and a socio / economical / health study will be done (**Milestone M 5.1**). The objectives related to this are:

- To define methods for the recycling of the coating at the end of life;
- To define the economical and environmental impact of such recycling;
- To provide a database on technical, economical and environment analysis of coatings;
- To provide a life cycle analysis of the coatings prepared expecting a lower impact of this coatings.

1.2. General Coordinator's assessment and Conclusions

Objective 1 : Development and modelling of new materials

Various coating materials have been elaborated in the SiON diagram to obtain corrosion protective coatings. The real diagram is wider as the coatings were elaborated from organo-silicon precursors. They also contain carbon and hydrogen then SiOCNH coatings were explored. Two main composition have given interesting behaviour in term of corrosion protection efficiency, they are SiO_x coatings and SiC_xN_y. This corresponds to **milestone 3.1.** At the early stage of the project, several materials were selected and characterised in term of corrosion behaviour. This aspect was related to **milestone 1.1**. Corrosion mechanism of Al alloys, Ti alloys, stainless steel and low carbon steel have been identified.
The protection mechanism of these coatings have been investigated. It was found that SiO_x is the material performing the highest corrosion protection efficiency. The protection is brought by the combination of a dense amorphous structure and insulating properties of SiO_x. The addition of nitrogen to SiO_x result in general to the degradation of the corrosion protection efficiency. The SiC_xN_y materials are semiconductors. It was demonstrated in the project that the amount of nitrogen introduced in the coating changes the doping level and the nature of charge carrier. At the same time, the chemical bonding changes from Si-C to Si-N. When the nitrogen content is properly adjusted, the semiconductor is intrinsic and shows the lowest electrical conductivity. For all the coatings tested, it was also shown that the corrosion efficiency was linked to the electrical conductivity. For all the coating materials, it is important to use deposition conditions which allow the formation of inorganic compounds which are effective for corrosion protection. Organic compound contain bonds like –OH, CH_x. hey have a lower density that allow the diffusion of the corrosive agents. In some case, the organic compound could show some instability and they could be corroded.
The influence of organo-silicon precursors has also been investigated. It was shown that it was possible to obtain good SiO_x coatings using a large variety of precursors. Of course, it is necessary to adapt the deposition conditions to reach similar coating properties. It was also shown that the nitrogen incorporation was not so easy particularly when the aim was to deposit oxinitride as silicon has a much higher affinity to oxygen than to nitrogen. It was then necessary to use a nitrogen containing precursor. It was demonstrated that using different ways to produce plasma, that nitrogen incorporation was weak when using N_2 even when highly dissociating plasmas were used. This is probably explained by the high binding energy in the N_2 molecule.

Due to weak mechanical properties, SiO_x can be used in applications where only corrosion protection is required. The addition of DLC on top of SiO_x was not possible as adhesive failure occurred systematically at the interface between the layers. It has been possible to deposit DLC on the top of SiCN coatings, and to have high mechanical performances. Such coatings allow to combined corrosion protection and friction reduction, corrosion protection and wear reduction and also corrosion protection and anti-fretting behaviour.
At the beginning of the project, the study of the influence of the initial preparation of parts has been investigated. To ways have been explored. The first one has consisted to evaluate the influence of plasma pre-treatment before coating deposition. It was seen that an oxygen or hydrogen pre-treatment is able to enhance the corrosion protective efficiency of the coating. NH_3 pre-treatment has not given satisfactory results. The second one has consisted to investigate the effect of the initial surface morphology on the corrosion resistance. It was observed that corrosion pits were aligned along machining grooves, or polishing scratches. The optimum surface morphology does not coincide with the lowest roughness but with the smoothest one. The surface defects before coating deposition are clearly one source of corrosion. A polishing process has been developed to obtain the desired surface morphology that allow to obtain a nearly defect free coated surface.
By combining the appropriate surface preparation and coating materials, it has been possible to obtain coatings with a porosity level below 0.2% and in some case as low as 0.0002%. This porosity level fits to the objective of **milestone 4.2**.

Objective 2 : Study and understanding of Vapour deposition process

Various PACVD processes have been investigated during the project. Some classical PACVD processes like pulsed DC and radio-frequency with different configurations like CCP, ICP… were studied, as well as some newer PACVD processes like pulsed radio-frequency, ECR microwave coupled to pulsed DC biasing, high pressure microwave.
In the cases of microwave processes, a large work of modelling has been carried out, especially to predict electron trajectories, their collisions and their diffusion in the plasma. This work has allowed a better comprehension on the physics involved around the ECR sources and to propose some ways of modification to improve their performances. Electrostatic and optical characterisations of the plasma were carried out for confrontation with the model and to check the plasma homogeneity in multi-sources reactors. The simulations have also been focused on the coupling between microwave and electrons of the plasma to understand the energy transfers between electromagnetic wave and electrons. One single source could achieve a plasma density of 5.10^{11} cm^{-3} at 150 W. The distribution of sources around the periphery of a reactor has allowed to further increase the plasma density up to 10^{12} cm^{-3} which was the **milestone 2.2**. In this conditions, 20 sources were used at 150 W microwave power per source. When coupling the ECR plasma and pulsed DC bias, it was seen that when increasing the power above a critical value, there was not significant influence on the deposition rate. This indicates that low pressure PACVD process is limited by the partial pressure of gas precursors. It was confirmed by the evolution of deposition rate being proportional to gas flow. In this deposition configuration, deposition rate up to 2.5µm/h were obtained when using a fully loaded rotating substrate holder. Deposition on parts standing in front of ECR sources have allowed deposition rate over 10µm/h, the **milestone 2.1** being at 7µm/h. Indeed, the ECR power was directly linked to the ion flow to the substrate holder but was not influencing the deposition rate. The consequence of this was an increase of stress in the coating and consequently an increase of brittleness. Moreover, the increase of the microwave power induces an increase of the temperature at the substrate location. Then for some application, the power was limited to keep

the temperature low enough to prevent degradation of the substrates, this was the case for the 100Cr6 steel substrates.
A new high pressure microwave process was also developed. This new process has shown very high plasma density. The gas temperature is more important and seems to rapidly increase with the pressure. This can be a limitation for the use of this new process. However, very high deposition rate could be achieved, up to 60 µm/h far beyond **milestone 2.1**. Such process would probably suitable for the treatment of planar objects.
Reactive plasmas were also investigated using light emission. More particularly, H, O, CH, CO and CO_2^+ species were evidenced in the plasma phase. Correlation could be established between the presence of species in the plasma and the constitution of the coating material. For example, the inorganic character of SiO_x coatings was correlated to the absence of CH_x emission in the plasma which was also correlated to high RF power working conditions. Spectroscopy of the plasma has also allowed a better understanding of the difficulty to incorporate N in the coatings when oxygen was added. The Si-N bond in the precursors seem to be highly fragmented in the plasma.
The process study has also involved research on the effect of pulsing the RF signal. It was seen some benefit to pulse the RF signal in term of corrosion protection of SiO_x coatings. However, when the off time becomes too large, some organic groups appear in the coating which gradually looses its efficiency for corrosion protection.
It has been shown to that precursors and the nature of the plasma generation could have in some cases some influence of on the nature of the coating.
Pulsed DC process produce low heating to the parts and can be used on parts which must be coated at a maximum temperature of 150°C. In this process, it is not possible to decrease further the power to reduce the temperature of parts has the plasma does not ignite anymore. Then the new microwave process, coupled with pulsed DC has allowed to work at lower deposition temperature. Has the plasma is not generated on the parts but on ECR sources, there is a lower impact of power on the temperature of parts. However, for low temperature deposition, it was necessary to reduce the power to minimize ion flow to the parts. The bias voltage cannot be used to reduce the incoming power on the parts as it also influences the coating properties. It was observed that the inorganic character was obtained at high bias voltage. Inorganic character means hard coatings able to bring corrosion protection.
Some bi-layers were deposited. They have combined SiCN+DLC or $SiO+CF_x$. This has been tested using the pulsed DC process, the pulsed DC combined with ECR and by RF PACVD process. Beyond the economic benefit of carrying out the 2 coatings in the same equipment, this allows to prevent some contamination between the layers and the adhesion problems associated to such contamination. By combining the appropriate layers, it has been possible to have corrosion protection and wear or friction reduction. For example, this was the case by combining SiCN and DLC. SiO layers, having better corrosion protection revealed to be unsuitable for their low mechanical resistance. Some multilayers were also deposited, but the mechanical behaviour was not improved and corrosion protection was a bit reduced.
Finally, reactor cleaning by using etching plasma was investigated. The principle is based on the formation of gaseous species formed by reaction enhanced by the plasma. Basically, carbon is etched by using oxygen plasma while Si is etched by fluorine atoms. The other elements in the coating like O, N and H form directly gaseous species. The principle of plasma etching was also successfully applied to the removal of the coating form the parts without modification of the roughness of the parts. The reactor cleaning process necessitate a soft ion bombardment to enhance reaction and desorption. A specific biasing of the substrate holder has been used to allow soft ion bombardment on the chamber walls.

Objective 3: Coatings properties

The microwave processes have been investigated in term of process homogeneity. For the high pressure process, the homogeneity is obtain by the disposition of sources in a matrix way. The thickness profile is flat in front of the sources and shows a drop at the extremities of the matrix. For the low pressure ECR microwave process, the homogeneity has been achieved by a combination of sources distribution and substrate holder motion.
The coatings characterisations have allowed to understand corrosion protection mechanism. For all the coatings, it was observed that the corrosion protection efficiency is correlated to the electrical resistance through the coating thickness. In that sense, SiO_x coatings show the highest corrosion protection efficiency. For SiCN coatings, their composition influence their electrical properties and then their corrosion protection. All the coatings deposited are amorphous. In most of the cases they have a glassy morphology favourable for the coverage of the surface. Nevertheless, some composition have a less glassy structure like SiON compared to SiO_x making them less efficient for corrosion protection. The deposition parameters have also an influence as it was observed for the ECR process combined with pulsed DC. When decreasing bias voltage, coatings develop a nodular growth, less favourable for corrosion protection.
Combination of coatings and architectures were defined to fit the specification of the different applications and their multifunctional requirements. This part of the work corresponds to the **milestone 4.1**. 2 coatings were defined for corrosion protection, SiO_x being the most efficient in pure corrosion conditions. SiCN coatings have a good efficiency for corrosion protection and their hardness level allow them to be used as tribology coating. Friction and wear resistance are further improved by depositing a DLC layer on the top of SiCN coatings. Low surface energy coatings were also studied. It consists to incorporate fluorine in the layers. Such coatings were deposited on SiO_x or SiCN coatings.
There were several objectives related to the coatings properties related to **milestone 6.1**.
For corrosion protection alone, the objectives were essentially link to applications for which mechanical characteristics are not important. It was initially concerning some optical application and more particularly the protection of metal coated plastic parts. For this kind of application, the coating must have high optical transparency. This was achieved with the coatings of the SiO_x family. The most transparent coating has shown transparency between 90 and 100% in the visible range. This is greater than the initial objective of 80%. For these coatings, there was also a requirement related to the aspect. The coatings must also be colourless. SiO_x coatings are intrinsically colourless but some coloration can appear due to the formation of interference fringes of visible light. One of the solution is to deposit a coating thinner than 0.08 µm. In that case, no interference of visible light occur. The difficulty with low thickness is that the coatings can be very easily scratch on soft substrates like metal coated parts. The alternative is to grow thick coatings. A thickness of 1 µm should be sufficient. In the practice, the thickness should be at least 7 to 8 µm to prevent interferences with artificial light. In that case the problem becomes economical. The deposition on plastic parts requires low deposition temperature which also means low deposition rate. This means that the deposition time would be excessive to achieve a sufficiently high thickness to prevent interference of light. As mentioned previously, SiO_x coatings have very high protection efficiency. The first corrosion pits in salt spray test appeared after 168 h for a 1.5 µm thick coating. Since no industrial partner in the specification phase selected scribe creepage as a criteria for its application this property was not tested.
For adhesion, the coatings have shown a good adhesion. In fact the adhesion is more related to initial surface preparation than to the coating material. More precisely, the removal of the residual contamination by bias etching has allowed to obtain high adhesion of SiO_x and SiCN

to substrates. good adhesion of the coatings with grid test values of 0 was reached on metallic substrates when an appropriate pre-treatment of the substrate was selected. For one of the end user parts, delamination has progressively occurred during the test of the real parts while this phenomenon was not observed on test samples during the project. One can suspect in this particular case that argon bias etching was not sufficient. On these parts a soft bias etching was carried out to keep the parts below 180°C. As no delamination was observed on steel samples etched at higher power, one can expect that it is only a matter of optimisation. Adhesion should be improved by increasing the etching duration or by etching at a higher power, keeping the parts below 180°C.
Particularly interesting results were obtained for the combination of corrosion protection and tribology. High surface hardness has been achieved by the deposition of a DLC top layers. Hardness between 30 and 35 GPa were obtained which is higher than the objective of 25 GPa. Of course the DLC top Layers have allowed to reduce dry friction coefficient. In the case of a metal/DLC contact, stabilised friction coefficient are comprised between 0.10 and 0.15 which is below the objective of 0.2. Finally, salt spray test were also carried out on bilayer structures combines a SiCN base layer and a top DLC. The first corrosion pits generally appeared between 144 and 162 h. In some cases, on small samples, the first corrosion pits were observed after more than 480h. The potential for corrosion protection of the coating materials is high but it seems to be strongly influenced by the surface morphology of the parts. The corrosion results are then over the initial goal which was 96 h.
Hence looking back to the properties aimed in **milestone 6.1**, the objective related to adhesion, corrosion protection and tribology properties are reached. The only point which is not achieved concerns the case of the protection for decorative applications.

Objective 4 : Validation

During the project, CRF has chosen an industrial application. It concerns the deposition of a hard coating on a shim to reduce the friction in the contact with the cam. Some shims were coated with one solution developed in MATECO. These shims were tested on an engine head and compared to a standard industrial solution. The normal validation test on an engine head last 250 h. It was observed a lower friction torque when using the MATECO solution compared to the standard one. During the 200 remaining hours, the friction torque has been increasing slowly with the MATECO solution and slowly decreasing with the standard one. At the end of the 250 h test, the friction torque for both solutions is similar. SEM examination have shown a degradation of the coating having adhesive failure expending with the duration of test. At the end of the test the MATECO solution has nearly completely flaked off explaining that the torque is similar to the standard solution. The adhesive failure is probably due to under-etching of the shims due to the fact that the parts required a low temperature deposition process. Adhesion can probably be increased on these parts keeping low the temperature during deposition process. It is then expected that the friction torque provided by the MATECO solution, would remain low all along the test.
EADS has focussed its interest on an application for which parts are degraded by fretting. EADS has received steel bolts coated with a coating solution combining anti corrosion and tribology top layer. These bots were tested using a fretting test developed by EADS. It was compared to uncoated bolts which are damaged by a fretting mechanism after only 100000 cycles. For these first tests, uncoated bolts were tested against steel and titanium bushings. Testing the MATECO solution in the same configuration, nearly no damage was observed after 2 million cycles. A second test campaign was also carried out. In this second campaign, the bolts coated with the MATECO solution were compared to surface treatment available on the

market. Once again, the MATECO solution was undamaged after 600000 cycles while the market solutions were damaged.
HEF has identified and tested 2 potential markets. The first one concerns a low carbon steel rod which is part of a mechanical component. Parts were coated with a MATECO solution combining corrosion protection and improved tribology properties. The parts were mainly characterised by corrosion test using salt spray test. Two test series were carried out. In the first one, corrosion pits were observed after 72 h. The corrosion pits are aligned along machining grooves, revealing an insufficient mechanical preparation before the coating deposition. In the second series of tests, the parts were carefully prepared before coating. However, the first corrosion pits appeared again at 72 h on one side of the rods, revealing an homogeneity defect of the coating. This defect should be resolved by using a 3 rotation substrate holder, allowing an homogeneous coverage of the steel rods. The second application concerns the protection of metal coated plastic parts. The metal is deposited on plastic parts to bring electromagnetic shielding properties. The parts were coated with a very thin coating adapted to corrosion protection alone. The corrosion tests have shown that the parts are still protected after 70 minutes corrosion test while the unprotected metal coated parts were corroded.
TEFAL has tested coated sole plate of iron. In this case, the parts were coated with a bilayer coating including corrosion protective layer and a low surface energy layer. The coated parts were compared to enamel coated standard parts and stainless steel ones. Sliding tests of the various MATECO solution have given higher sliding effort than enamelled parts. The scratch resistance of MATECO coatings was also compared to market solutions. The MATECO coatings were qualified as good.
Some work was also carried on the life cycle analysis and a study related to socio/economical/health aspects was done. This work corresponds to **milestone 5.1**. A plasma process for coating removal was developed in the project. The initial objective was the removal of the coating at the end of life of the parts. In fact, the plasma removal of the coating can be applied to the parts at any moment. This process can remove the coating without damaging of the surface of the parts which can then be coated again. This allows to recover parts after a deposition batch failure. For metal parts, the coating is so thin (1 to 3 µm) that they could probably be recycled without coating removal. The environmental aspect of recycling was investigated. As for plasma deposition process, the environmental aspect of plasma de-coating concerns electricity consumption. It was seen in the project that the environment impact is strongly linked to the means used for electricity production. The cost related to energy consumption were also investigated. Rather important differences of costs were found depending on the country considered, this is also probably linked to the means used for electricity production. Similar work was also carried out on the impact of coating production. The impact of coatings investigated in the project was compared to classical electrodeposited coatings. The work carried out has necessitated several iterations to obtain consistent results. It has been necessary to precise the surface of coated parts. The energy consumption of vacuum deposited coatings depends partly of the quantity of parts. This means that the environment impact can be unfavourable to vacuum technology when the batch is not fully loaded which particularly the case in research work. Additionally, coatings where initially compared with a thickness of 1 µm which is favourable to electro deposition as these coatings usually are at least 10 times thicker while it corresponds to the order of magnitude of the thickness of the PACVD coatings. Finally, it has also been necessary to correct the results, taking into account functional properties of the coatings. In this particular case, the corrosion protection brought by the coatings was considered. This could have been extended to other properties like wear resistance or friction resistance which are favourable to the vacuum deposited coatings investigated in the

project. The final results have allowed to conclude to the lower environment impact of the developed coatings compared to a state of the art electrodeposited coating.

1.3. WP 1: Understanding and Optimisation of the Surface Properties of Substrate Materials – Surface Engineering (WP Leader: ICMSE)

WP Leader	ICMSE
Participants	HEF – UNIBA – CRF – EADS - POLITO

1.3.1 Objectives

The general objectives of this workpackage (WP) comprised the identification of the corrosion sources according to the chosen substrates and the definition of the surface preparation before PACVD process in order to improve the corrosion protection. This WP1 concluded at month 18 however some extended surface treatment tests and optimization of mechanical preparation procedure with more substrates were extended along 2nd year.
In the first six months of the MATECO project, the specific objectives concerned the preparation and delivery of the substrates for their analysis and characterization (task 1.2) and a theoretical study of the corrosion mechanisms on chosen substrates (task 1.1). Later, we focused on the study of surface preparation methods of the substrates by mechanical (subtask 1.3.1) and plasma pre-treatment (subtask 1.3.2) in order to define a an optimized procedure for the surface finishing of the chosen substrate.

1.3.2 Progress towards objectives

1.3.2.1 Task 1.1: Theoretical understanding of corrosion and anti-sticking phenomena on the substrates. (**EADS**, **POLITO**)

EADS has performed a theoretical study on corrosion behaviour and other substrate properties like wear and fretting for the materials of relevance for EADS application with respect to protection schemes to be developed. The considered materials are precipitation hardenable stainless steel and titanium alloy TiAl6V4. Results have shown that both materials are very corrosion resistant. But, stainless steel as well as titanium can be heavily damaged by wear and especially fretting processes.
As far as these materials are concerned, the new coating systems have to improve the fretting and wear behaviour in the first approach. But, with the coating process, the substrate properties can be strongly affected and the corrosion behaviour of the coating may not be worse than the original substrate. Therefore, besides fretting properties, specific attention has to be given to the corrosion properties of the coatings as well.
POLITO strictly cooperated with EADS in the description of the corrosion mechanism of chosen substrates (low carbon and stainless steels, aluminum, etc.), according to their industrial applications.
The selected materials for coating by all end-users have been listed in detail in the report on "Material requirements for achieving suitable properties, requirements and specifications of end-users" (D 3.1). Different types of substrates were chosen according to the special requirements of each partner (automotive, aeronautic, decorative, electrical appliances, etc). In the following list we summarize the chosen materials and the main trouble they show in practical performance.

End-user	Substrate material	Application	Main trouble
EADS	Low C Steel 1.4548.4	Bolts (aeronautics)	Fretting
	Ti-alloy (TiAl6V4)	Bolts (aeronautics)	Wear, Fretting
TEFAL	Steel (austenitic) AISI304 Steel (ferritic) AISI436	Cookware	Corrosion, fretting
	Al5005 (1% Mg)	Cookware	Corrosion, Anti-sticking
HEF	Steel 42CrMo4	Gas spring axis	Corrosion
	Metal (Al, Ag) coated plastics (polysulfones)	Decorative Electrical	Corrosion
CRF	Steel 100Cr6 16MnCr5	Shim	Corrosion, fretting

The basic information on degradation mechanisms collected by all partners have been written down in deliverable D1.1: "Report on the theoretical study on corrosion and other properties of substrates". In the enclosed table we highlight the main characteristics of each material extracted from this deliverable:

Material	Corrosion mechanism
Al	Pitting corrosion (most commonly produced by halide ions) Corrosion potential between matrix and particles (intercrystalline) Presence of 1% Mg in solid solution →corrosion resistance better to alkaline solutions
Ti	High strength and corrosion resistance (formation of TiO_x film) Oxide film breakdown in acid conditions Embrittlement by long exposures to air at T>340ºC or H_2 Low wear and fretting resistance
Stainless Steel	Good corrosion and oxidation resistance (up to 12% Cr) AISI304: sensitive to halogen (Cl^-), salty elements AISI436: Difficult for fine polishing Fretting mechanisms: adhesion and tribochemical reaction
Low carbon steel; 42CrMo4	Pitting corrosion Creviced corrosion (severe pitting at restricted areas) Intergranular corrosion (Cr-depleted zones) Stress corrosion cracking

1.3.2.2 Task 1.2: Assessment of the model (**HEF**, **POLITO**, **ICMSE**, **UNIBA**, **EADS**, **CRF**)

Sub-task 1.2.1: Preparation of substrates for properties and phenomena understanding (**HEF R&D**, **EADS**, **CRF**)

A delivery table with the selected substrates from previous subtask was prepared in order to exchange them in an appropriate manner and schedule among different partners.
In this task, HEF has contributed to the preparation of sample materials for the various studies in the project. It has consisted to provide low carbon steel related to an industrial potential application selected by HEF and requiring both corrosion protective coating and wear resistance (42 CrMo4). HEF has also used tool steel (X85WCrMoV06-05-04-02) which is a standard steel used for research purpose for hard coatings. These substrate materials were mechanically polished and sent to partners. HEF has also contributed to the polishing of the substrate materials provided by partners, it consists of 2 stainless steels and an aluminium alloy from Tefal, a steel from CRF and one steel and one titanium alloy from EADS.
The end-users EADS, TEFAL and CRF have provided samples to the partners for basic testing and characterisation of the surface state.
- EADS: steel (1.4548) and titanium alloy (TiAl6V4);
- TEFAL: Steel (austenitic) AISI304, Steel (ferritic) AISI436, Al5005;
- CRF: Steel 100Cr6; 16MnCr5.

Sub-task 1.2.2: Characterisation of the substrates and testing (**POLITO**, **ICMSE**, **UNIBA**, **CRF**)

The next sketch presents schematically the distribution of the substrates among the partners involved in this task and the type of characterization performed:

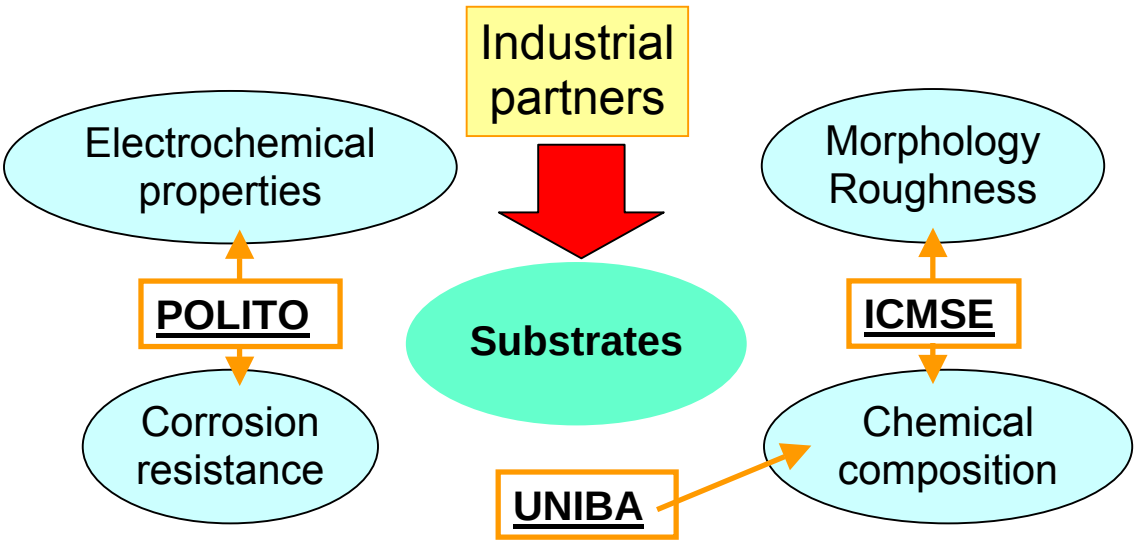

ICMSE has carried out chemical and morphological characterization of the substrates by Scanning Electron Microscopy (SEM)/ Energy Dispersive X-ray spectroscopy (EDX) technique. SEM technique allows showing the surface texture of the different substrates. EDX establishes the chemical composition by allowing the identification of the main elements and their atomic concentration present in the samples. The surface state has been studied by means of profilometry and XPS. These aspects are quite important since the corrosion phenomenon is highly dependent on the surface properties of the substrate (roughness and cleaning). The

roughness R_a and R_z have been measured for all the samples. R_z the mean surface roughness is an important parameter as it represents the regularity of the surface. Different surface polishing has been found between the steel substrates provided by **HEF** and **TEFAL**. Nevertheless, both cases could be considered satisfactory with mirror polished surface compared to the surface finishing of aluminium substrates. In task 1.3, new methods of surface treatment are explored and this characterization was therefore necessary to be used for comparison purposes.

Steel 304_TEFAL	Al5005_TEFAL	Steel 42CrMo4_HEF
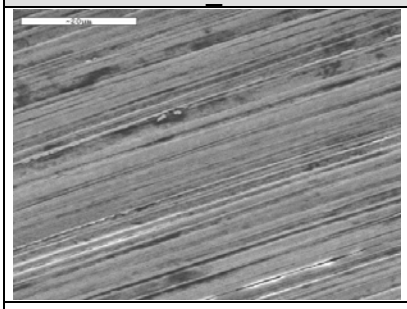	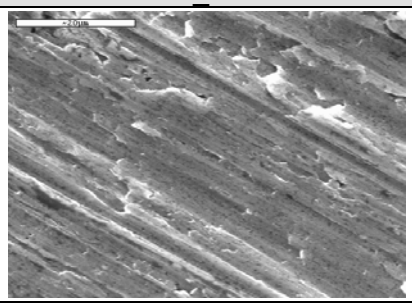	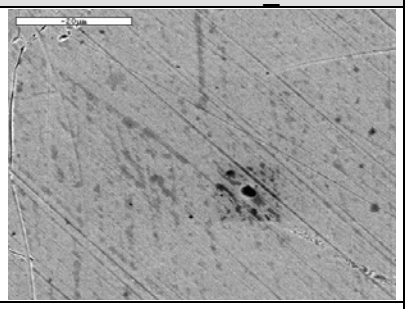
Ra: 0.037 µm Rz: 0.308 µm R_{max}: 0.373 µm	Ra: 0.268 µm Rz: 2.062 µm R_{max}: 3.060 µm	Ra: 0.006 µm Rz: 0.076 µm R_{max}: 0.156 µm

SEM micrographs and roughness estimation of different substrates employed in the project

The second family of coatings studied is metal coatings deposited on plastic parts. It includes aluminium coating which is used for decorative application on plastic parts. Samples of PS with better surface quality have been found for the deposition of Al for optical (decorative) applications. Aluminium coatings are interesting because of its low cost and exhibit rather high optical reflectivity as shown on the picture above. The Al coatings seem to be very smooth as they present a very good optical reflectivity as a mirror. **ICMSE** has measured the roughness of the coated plastics parts. The R_a and R_z roughness are very low and about 0.01 and 0.16 µm respectively. The aluminium coating does not affect the surface morphology of the substrate.

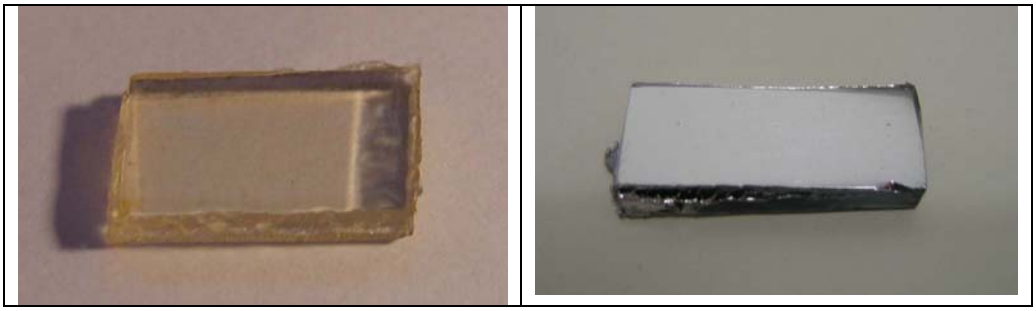

Images of a polysulfone substrate uncoated and coated with an aluminium film

UNIBA has carried out ESCA analysis of the metal of interest in MATECO. The table below reports the atomic concentration of the surface considered:

	C1s	O1s	Al2p	Fe2p	Cr2p	Ni2p	Ti2p	V2p	Mo3d
Al 5005	8.0	57.3	34.7	-	-	-	-	-	-
Inox 304	0.00	19.1	-	60.5	10.7	9.7	-	-	-
Inox 444	0.4	37.0	-	44.5	18.1	-	-	-	-
42CrMo4 steel	8.2	41.3	-	50.5	0.0	-	-	-	0.0
100Cr6 steel	6.2	38.7	-	54.1	1.0	-	-	-	-
TiAl6V4	14.2	35.6	6.4	-	-	-	40.5	3.3	-

ESCA surface atomic concentration of various MATECO substrates

The work made by POLITO concerned the morphological and electrochemical characterization of the selected substrates: low carbon steel, austenitic stainless steel 304, ferritic stainless steel 436, steel 42CrMo4 and aluminum series 5005. The corrosion behavior of the selected specimens has been assessed by means of electrochemical impedance spectroscopy (EIS). Impedance measurements have been performed at room temperature in aerated 0.1M sodium chloride solution, using a EIS300 Frequency Response Analyzer (Gamry Instruments). The experimental data have been analyzed by fitting them to an equivalent circuit model in order to obtain the value of the charge transfer resistance, R_{ct}, which can be correlated to the corrosion process occurring at the metal/solution interface: the higher R_{ct} value, the higher corrosion resistance.

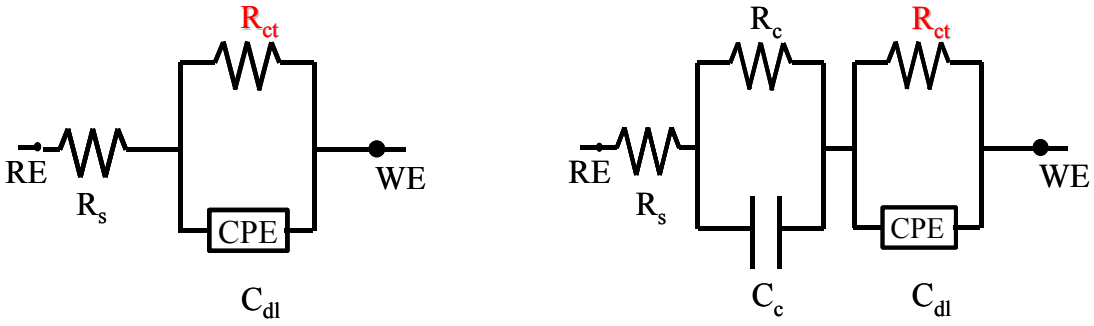

(a) (b)

Equivalent circuit models used for fitting the impedance diagrams: (a) spectra recorded on 100Cr6 and 42CrMo4 steel, (b) spectra recorded on stainless steel samples

Low R_{ct} values (about 150–350 $\Omega \cdot cm^2$) have been obtained for low carbon and 42CrMo4 steels, while good corrosion performance have been observed, as expected, for Al and stainless steel substrates (R_{ct} values ranged from 9.5 $k\Omega \cdot cm^2$ to 1.96 $M\Omega \cdot cm^2$).

SEM and AFM observations of the samples morphology have been carried out in order to evaluate the surface roughness and to define the requirements for the coatings.
The corrosion resistance evaluation has been performed also by means of anodic polarisation curves, employing a new instrument, PARSTAT 2263 Electrochemical System, acquired on purpose for the project.
The above plot shows the anodic polarization curve recorded on austenitic stainless steel 304 after 1h exposure to 0.1 M NaCl solution. The sample exhibit a pseudo-passive behaviour characterized by a very high critical passivating current density, about 20 mA / cm^2, and a pseudo-passive current density about 15 mA / cm^2, thereby indicating a poor corrosion resistance in the aggressive environment. The steep increase of anodic current density observed at E > + 1 000 mV / SCE may be ascribed to transpassive phenomena.

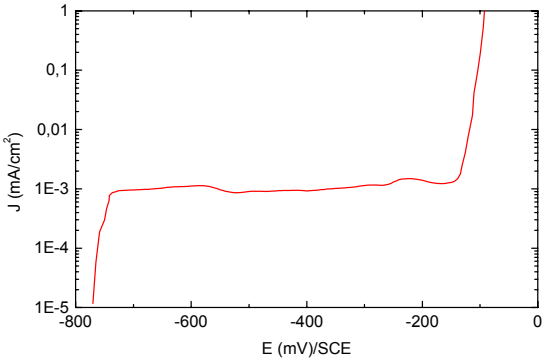

Anodic polarisation curve recorded on 5005 aluminium alloy after 1 h of immersion in 0.1 M NaCl solution

The above plot shows the anodic polarization curve recorded on 5 005 aluminium alloy after 1 h exposure to 0.1 M NaCl solution. The sample exhibit a passive potential range characterized by low current density values (not exceeding 1 µA / cm^2). The passive range is followed by a steep increase of current density which may be ascribed to the onset of localized corrosion phenomena (pitting). From the analysis of anodic polarization curve the breakdown potential, Eb, and the extent of passive range, ΔE, can be assessed.

Ecorr (mV)	Eb (mV)	ΔE = | Ecorr - Eb | (mV)
-780	-150	630

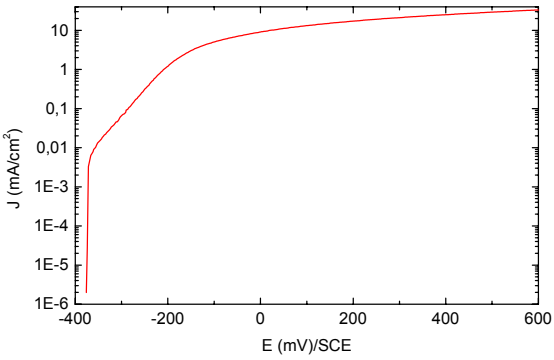

Anodic polarisation curve recorded on 100Cr6 steel after 1h of immersion in 0.1 M NaCl solution

The above plot shows the anodic polarization curve recorded on 100Cr6 steel after 1 h exposure to 0.1 M NaCl solution. The sample exhibit an active dissolution regime characterized by a progressive increase of current density with increasing the potential, then reaching the value of 30 mA / cm^2 at E = + 600 mV / SCE.

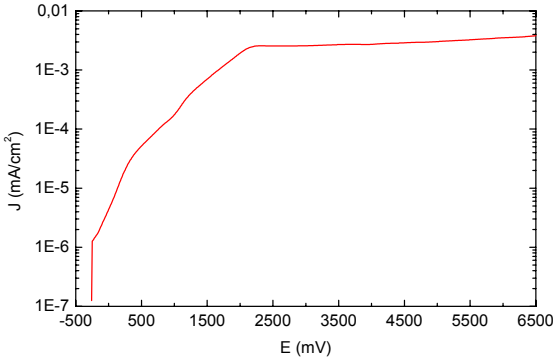

Anodic polarisation curve recorded on Ti6Al4V alloy after 1h of immersion in 0.1 M NaCl solution

The above plot shows the anodic polarization curve recorded on Ti6Al4V alloy after 1 h exposure to 0.1 M NaCl solution. Due to a highly protective TiO_2 surface layer the sample exhibits an excellent corrosion resistance as evidenced by the wide passive potential range, extending from the corrosion potential to + 6 500 mV / SCE, where the current density never exceeds 5 µA / cm^2. This activity is concluded during the first year of the project as scheduled in the work plan.

1.3.2.3 Task 1.3: Study on the substrates surface preparation method on final properties (**HEF**, **UNIBA** and **ICMSE**)

Sub-task 1.3.1: Mechanical preparation of the substrates (**HEF R&D**)

The purpose of this task was to study preparation means to improve surface morphology. It has rapidly appeared that one of the corrosion sources was the surface morphology before coating deposition.
The table below schematises the surface morphologies and their ability to receive a corrosion protective coating.

Schematic surface morphology	Ability to receive corrosion protective coatings
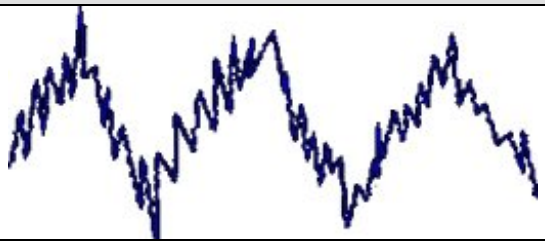	Inappropriate surface Grinded surfaces have a roughness showing sharp edges. Such morphology can induce shadowing during coating growth leaving defects from the substrate to the surface.

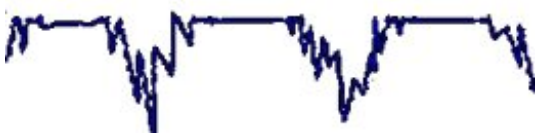	<u>Inappropriate surface</u> Mechanical polishing removes the large peaks of the roughness but grooves can remain. The shadowing occurs in the grooves and growth defects are still their. It is also only applicable to simple geometries.
	<u>Appropriate surface</u> Such surfaces are smooth. They are not characterised by a low roughness value. The smoothness of the surface allows an excellent coverage by coatings.

In the pictures below, one can see the effect of the initial surface morphology on coated steel samples after accelerated corrosion test.

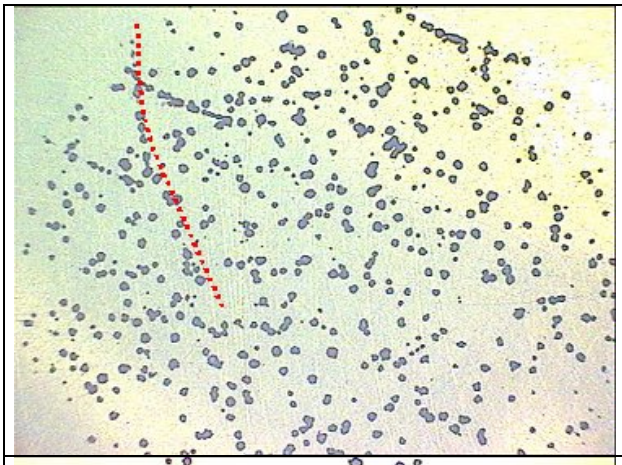	On the rough surface, the coating presents a large density of growth defects at which corrosion takes place. The steel sample was grinded and polished with a 240 grit paper. Some of the corrosion pits are aligned along remaining scratches.
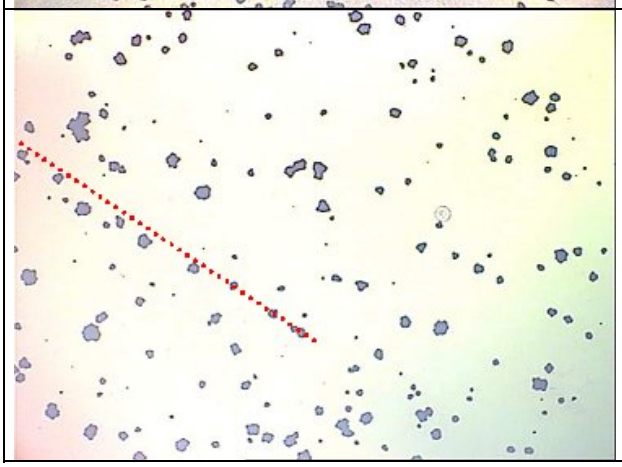	A diamond paste polishing was also carried out to obtain mirror polished surface with very low Ra. It becomes evident that pit density has decreased. However, it is still too high and steel is corroded. The diamond polishing also makes some scratches. Despite their very small dimensions, they can be the source of corrosion sites as indicated by the alignment of some corrosion pits.

When using an appropriate polishing mean, it becomes possible to obtain smooth surfaces on which the coating can have a very high covering efficiency, allowing corrosion protection.
In the pictures below, one can see roughness profiles of as received grinded steel samples and the roughness profile on the optimised appropriate polishing mean.

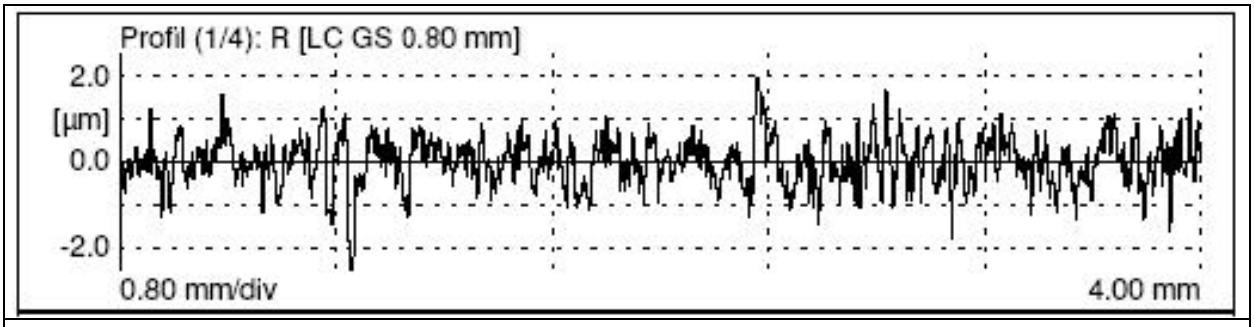

As received grinded 42 CrMo4 steel samples : Ra : 0.44 µm, RHSC[0-50] : 200

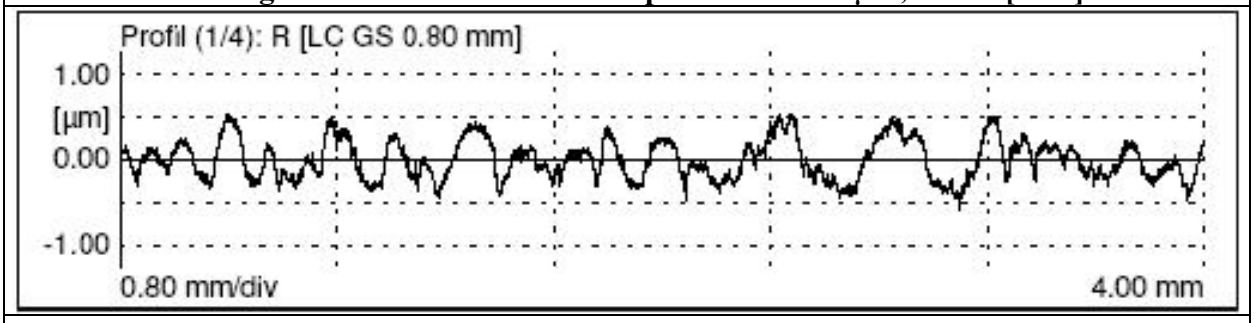

Adapted polishing of 42 CrMo4 steel samples : Ra : 0.18 µm, RHSC[0-50] : 12

As illustrated here, the optimised polishing to deposit corrosion protective coatings does not lead to low Ra value but to a smoother surface. Generally, diamond paste mirror polishing results in Ra as low as 0.02 µm which are not suitable for an efficient corrosion protection.
The description of the polishing mean allowing the appropriate surface morphology is considered as confidential.

Sub-task 1.3.2: Study of the influence of different plasma pre-treatment on final properties **(ICMSE, UNIBA)**

Even if it was not scheduled in the previous work plan, **POLITO** strictly cooperated with **UNIBA** in order to assess the effect of different plasma pre-treatment on the corrosion behaviour of SiO_x coatings. Impedance measurements play a fundamental role in the optimisation of the PECVD process in order to obtain well-adherent and high corrosion protective coatings.
Different plasma pre-treatments have been tested. The metals investigated for can be grouped in four categories from the surface chemistry point of view:
- Stainless steel (304 austenitic and 436 ferritic stainless steel);
- Low carbon steel (C40, 42CrMo4, 100Cr6, 1.4548.4);
- Ti alloys (TiAl6V4);
- Al Alloys (Al 5005).

The main part of the experiments have been carried out in parallel plate RF reactor, though some trials have been tested onto an inductive coupled reactor (ICP) and have been planned with the aim of:
- Cleaning the surface by removal of the organic contamination;
- Formating a passivating layer;
- Grafting functional groups which can enhance the coating adhesion.

H_2, O_2 and Ar plasma pre-treatment have been optimized and Rct values from EIS measurements have been determined for coating deposited on treated or untreated metal surfaces.
It has been found that plasma pre-treatment increases the coating performance in terms of Rct values. For example when low carbon steel (Rct is 250 $\Omega \cdot cm^2$) is considered as substrate, resistance at charge transfer is enhanced by the plasma deposited coating, but a several order magnitude increase (Rct value of 2.9×10^5 $\Omega \cdot cm^2$) is observed if deposition is preceded by a H_2 plasma treatment. In the table below it can be observed that the Rct value for SiO_x Coated Ti alloy increases mainly when O_2 is considered. XPS analysis in depth profile mode have evidenced an increase in the thickness of the oxidized layer passivated layer when Ti is exposed to O_2 plasma.

Plasma pre-treatment	Rct ($\Omega \cdot cm^2$)		
	1 day	10 day	50 day
Ar	$2.00 \cdot 10^8$	$1.18 \cdot 10^8$	$6.25 \cdot 10^7$
O_2	$3.06 \cdot 10^9$	$1.69 \cdot 10^9$	$1.50 \cdot 10^9$
H_2	$3.46 \cdot 10^8$	$5.14 \cdot 10^8$	$4.96 \cdot 10^8$
Non pretreated	$1.65 \cdot 10^8$	$7.92 \cdot 10^7$	$1.54 \cdot 10^8$

Values for plasma processed Ti alloy

In the case of Stainless Steel, figure below, both H_2 and O_2 plasma pre-treatment can drastically enhance the coating protection. In this case XPS analysis reveals only organic contamination removal with both kinds of plasma pre-treatment.

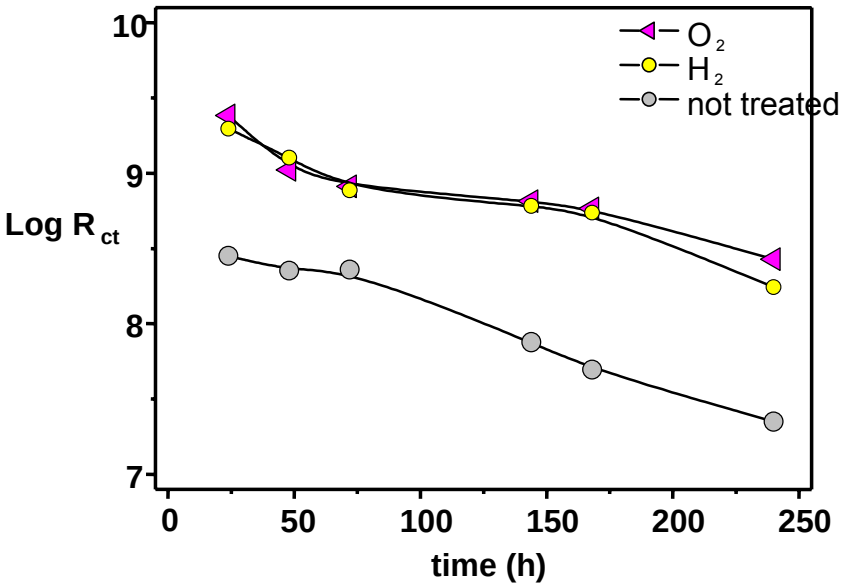

In summary, the main conclusions obtained for this study are the following:
- Plasma pre-treatment substantially increases the performance of the protective layer, with entity which depend on the gas feed and on the substrate;

- H_2 and Ar plasma role on the various categories of metal considered is that of removing carbon contamination by means of H atoms etching and ion sputtering respectively. This in turn enhances coating adhesion and protective performance;
- O_2 plasma, instead, have a different chemical effect on the surface depending on the metal group considered. When highly passivated metals are considered, Stainless steel and aluminium alloys surfaces in this case, O_2 plasma simply exhibits a organic contamination scavenger; no changes in the oxidation state of metal, or oxide thickness is revealed. On the other hand, when O_2 plasma is carried out onto low carbon steel or Ti alloys, besides removal of carbon contamination, an increment in the thickness of the oxide layer can be observed. Both factors can lead to increase of the adhesion of the coating, or increase of passivation layer, and in turn to a better corrosion resistance.

Sub-task 1.3.3: Determination of the surface morphological and chemical properties (**ICMSE**)

The SEM analyses presented on the following figures exhibit that the SiO_x films formed during the plasma pre-treatment performed by **UNIBA** do not modify significantly the surface morphology and the films seem to be homogenous. Preliminary GD-OES (Glow Discharge Optical Emission Spectroscopy) experiments in DC mode have shown the films were insulating and consequently not porous.

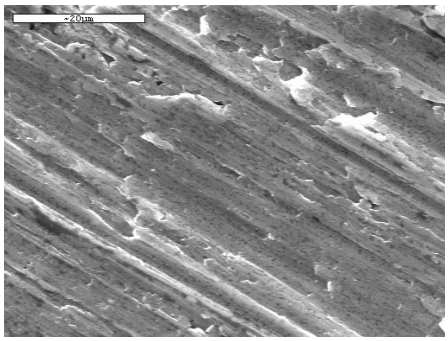

Polished Al 5 005 (TEFAL)

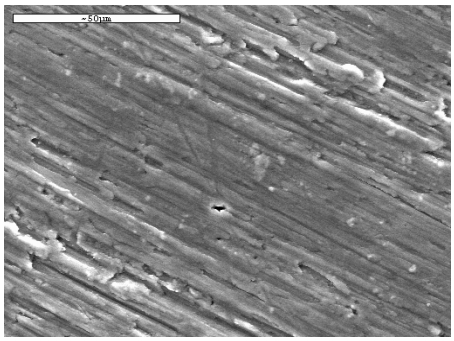

Pre-treated Al 5 005 (UNIBA)

SEM micrographs of Al 5 005 substrate before and after pre-treatment

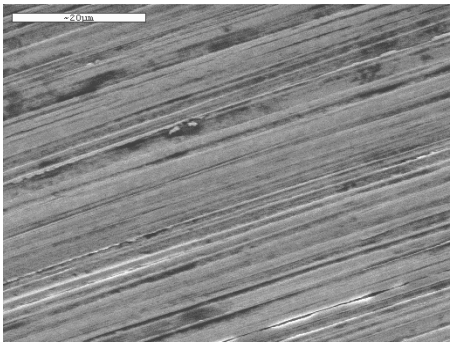

Steel 304 TEFAL

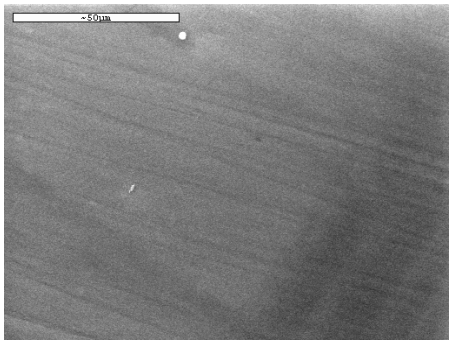

Steel 304 TEFAL after pre-treatment

SEM micrographs of Steel 304 substrate before and after pre-treatment

The surface state has been studied by means of profilometry as planned in the last activity report. The R_a and R_z roughness of the pre-treated samples are reported in the table below.

Sample	Ra (µm)	Rz (µm)
Polished Al 5005	0.268	2.062
Pre-treated Al 5005	0.283	1.850
Steel 304	0.005	0.071
Steel 304 after pre-treatment	0.029	0.317

Roughness of steel 304 and Al 5005 substrates before and after plasma pre-treatment

As **ICMSE** had already concluded based on preliminary SEM observations, the roughness measurements confirm the plasma pre-treatment do not affect significantly the surface morphology of the substrate.
ICMSE has realised TEM (Transmission Electron Microscopy), EELS (Electron Energy Loss Spectroscopy) and XPS (X-ray photoelectron) measurements on SiO_x thin films deposited on silicon substrate in the conditions resumed in the following table. Three types of pre-treatments have been investigated: H_2, O_2 and Ar plasma pre-treatment. A sample without pre-treatment has also been investigated (see table below) for comparison purposes. Afterwards, a SiO_x layer is grown on top by using TEOS precursor in an Ar/O_2 discharge.

	Chemical compound	Flow (sccm)	Power (W)	Pressure (mtorr)	Time (min)
Pre-treatment	A) H_2	20	16	1 000	30
	B) O_2	15	50	500	10
	C) No	0	0	0	0
	D) Ar	20	30	500	30
Treatment	Ar	22	250	100	90
	O_2	45			
	TEOS	2			

PECVD conditions of UNIBA treatments

The characterization of the interface between the substrate and the plasma modified layer was of special interest to assess the effectiveness of the plasma pre-treatment and to distinguish the result among different types. For this purpose, ICMSE prepared cross-sectional views of the four types of pre-treated films deposited by **UNIBA**. The next figure shows the micrographs a), b), c), and d) taken from the TEM cross-section observations. We clearly observe the interface between the silicon substrate and the SiO_x film in all the cases. This interface is very sharp and well-defined without evidences of crystalline features, defects or pores. The SiO_x films appear to be amorphous and very dense. The modifications induced by pre-treatments are probably in the range of 1 nm. However, it is not possible to conclude significant differences between the types of pre-treatment from HRTEM observations. Finally, the modified depth of plasma pre-treatment can not be distinguished and appears to be in the order of 1 nm or 2-3 atomic monolayers.

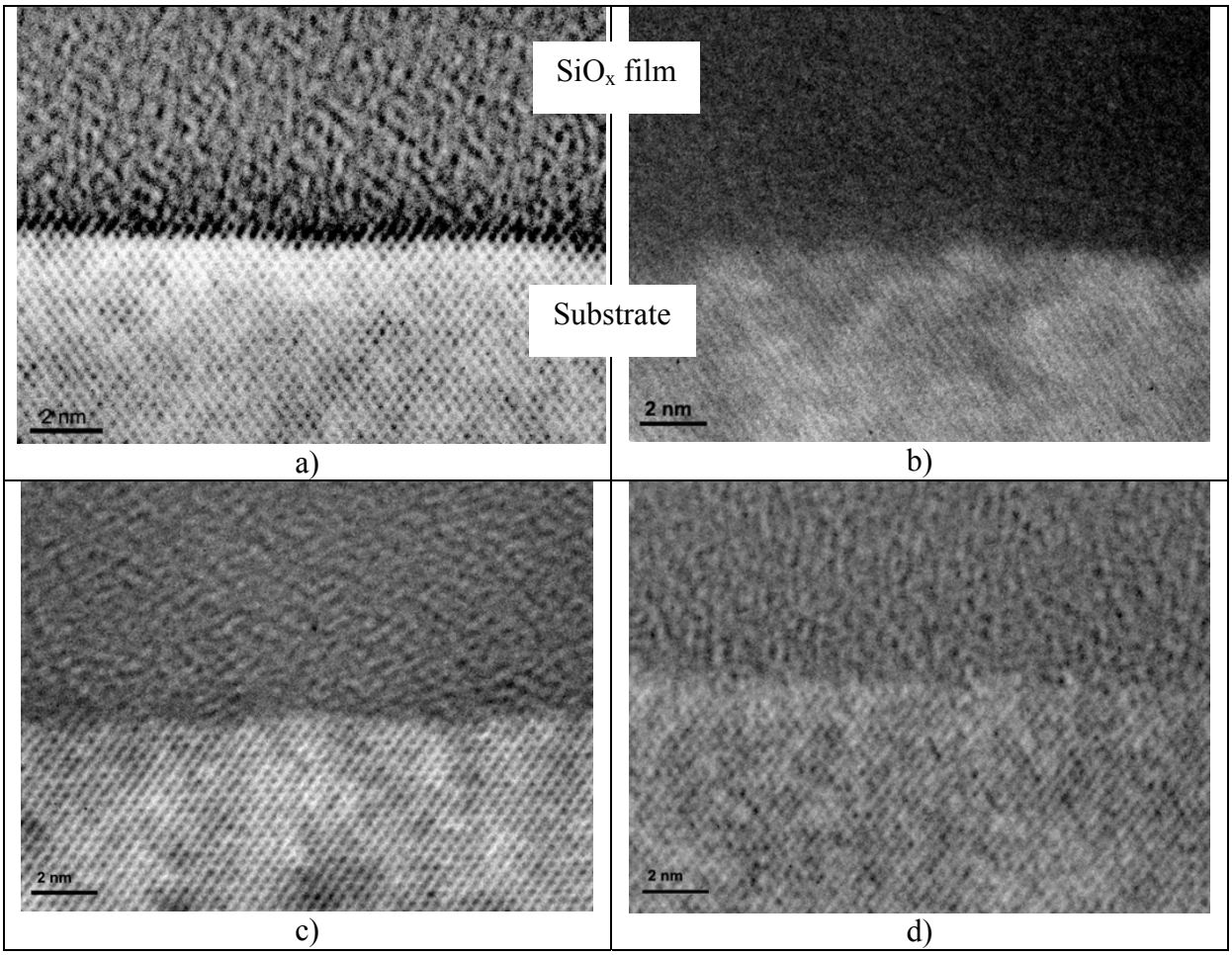

HRTEM micrographs of SiO_x film deposited with an a) H_2, b) O_2, c) Ar and d) without plasma pre-treatment at the interface substrate-coating

These results are the subject of an article in collaboration with **INSA**: "Analysis of the corrosion protective ability of PACVD silica-based coatings deposited on steel", D. Pech *et al.*, *Surf. Coat. Technol.* **201**, 347-352 (2006).

XPS analyses performed on SiO_x films in order to determine their nature and chemical composition. A depth profiling of the samples was carried out by Ar^+ ions sputtering (2.10^{-5} mtorr, 6 mA, 3.5 kV) during 0, 120 and 240 seconds before analysis. The composition of SiO_x thin films is independent of the type of substrates and is rather homogeneous in depth. The atomic ratio is about 75 % for oxygen and 25 % for silica whatever the sputtering conditions. Complementary analysis carried out on a SiO_2 standard sent by **UNIBA** in order to check the atomic ratios measured for the SiO_2-like films put in evidence that a correction factor must be applied to the elemental atomic concentrations. Finally silica-based films deposited by UNIBA present a Si/O ratio of 2.07 after correction. This value is slightly higher than 2 as usually observed for SiO_x-like films deposited by PECVD.

The binding energy of the Si_{2p} and O_{1s} photoelectrons peaks was found to be ≈ 103.5 and ≈ 533.0 eV respectively. These values are in the range of those reported for SiO_2-like layers varied between 1 711.3 and 1 712.3 eV. These values are in agreement with the values found in the literature for SiO_2 films.

EELS spectroscopy was used in order to obtain further chemical information on these structures. The figure below presents the low-loss electron energy spectra of the different

coatings compared to the ones of a SiO_2 reference and Si substrate and the oxygen K-edge spectra. In each case, the legends follow the order of the curves.

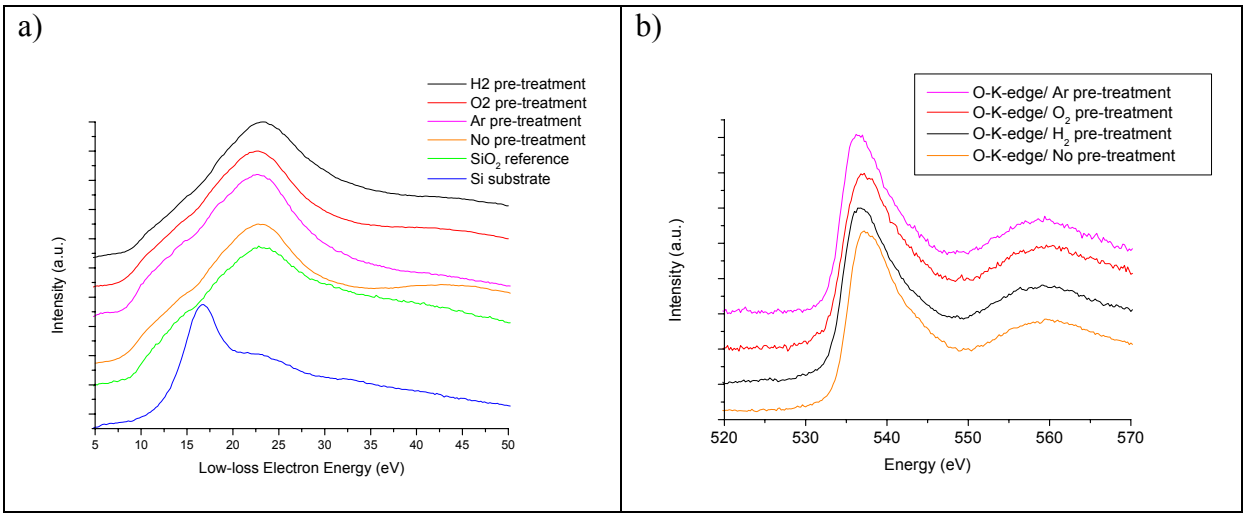

a) Low-loss spectra of SiO_x film deposited with an H_2, O_2, Ar or without plasma pre-treatment; Reference of SiO_2 film and Si substrate are included for comparison purposes, b) Near edge structure of the O K-edge from SiO_x film deposited with an H_2, O_2, Ar or without plasma pre-treatment on Si substrate

In this energy domain (i.e. 0 - 150 eV), the valence electrons are excited in a collective manner and the corresponding signature of EELS spectra is an intense distribution centred at the energy called the plasmon energy. The maximum of the plasmon peak for the SiO_x coatings is about 23 eV whereas the maximum one for Si substrate is around 16 eV. Concerning the SiO_2 reference, the position of the maximum plasmon peak is also at 23 eV. In the literature, it is explained that the reduction of the densities of Si atomic orbitals in the crystal valence states implies a modification of intensity of the SiO_2 plasmon peak. Moreover the broadening of the plasmon peak could be explained by the fact that the plasmon width depends on the structure of the compounds. It will be larger for amorphous compounds than for crystalline ones according to the fact that occupied and unoccupied bands are more delocalized in the case of non-crystalline compounds. As a consequence, the band-band transitions will exist over a larger domain. For each sample, we observed a broad plasmon peak compared to the one of Si substrate. This observation indicates that all the samples are completely amorphous.
ICMSE has also studied the oxygen K-edge of both films. The following figure presents the different spectra which exhibits the same structure. According to the literature these spectra represent the typical features of amorphous SiO_2 films. EELS analysis indicated that all the pre-treatments led to very similar structure and chemical compositions based on SiO_x.

1.3.3 WP Leader Assessment and Conclusions

WP 1 concerns the understanding and the optimisation of the surface properties of substrate materials. According to the DOW document, the 3 main objectives related to this part are:

- To identify the corrosion sources (kind and nature of defects) of the substrates selected by the different partners (**HEF R&D, EADS**, **CRF** and **TEFAL**);
- To improve the surface preparation (by mechanical and plasma means) before PACVD for corrosion protection purpose;
- To correlate the experimental results with the theoretical analysis of the substrates.

In this sense, WP 1 has covered successfully the following aspects described in the DOW:

- Selection of appropriated materials depending on the industrial applications foreseen for each partner. Delivery of chosen substrates among the different partners for their study and characterization;
- Identification of the corrosion sources: The presence of defects as scratches, holes, pores, surface roughness, impurities has been highlighted that favour the initiation and propagation of corrosion phenomena. These features must be avoided in order to have an uniform covering of the sample and warrant the protection ability of the coating. The correlation between experimental results in terms of properties (adhesion and corrosion ability) and structure and morphology of the coatings allows to propose the next solutions to address this phenomena:
- Surface finishing of the substrate material: A method identified and developed at HEF conveys a very smooth surface without scratches but leaving some waviness very useful in mechanical applications to keep lubricant in a contact;
- Plasma-pre-treatment of the substrate: O_2 and H_2 (benefit), NH_3 (not favourable). A significant improvement of the corrosion is obtained for the two first with similar results between them. Their mechanisms of action are removal of carbon surface contamination and increment of film adhesion to the substrate;
- The EIS measurements carried out with substrates submitted to the surface finishing procedure (polishing+plasma pre-treatment) have demonstrated an improvement of the corrosion resistance manifested in terms of R_{ct} values 10 to 10^4 higher than initial values depending on the kind of substrate.

1.4. WP 2: Understanding and Optimisation of PACVD Process (WP Leader: EPM)

WP Leader	EPM
Participants	HEF – UNIBA – ICMSE – EADS - POLITO

1.4.1 Objectives

The general objective of WP 2, the understanding and optimisation of PACVD process, includes more specific objectives such as the development, the comprehension and the improvement of deposition processes. Therefore, this workpackage includes experimental and theoretical studies on plasma modelling for a better knowledge of plasma production, on plasma diagnostics for a better control of process parameters, and on the effect of process parameters on the properties of the coatings. The tasks and subtasks in WP2 bring specific contributions to the general objective of WP2.

In Task 2.1, Sub-task 2.1.1 concerns the results obtained by **UNIBA** on the deposition process parameters, with a contribution of **POLITO** (not planned initially in the MATECO program). Development, comprehension and optimization of the RF PECVD have been carried out for producing effective protective coatings. Specifically the sub-task 2.1.1 is devoted to the correlation of experimental parameters to gas phase data (UV-OES, FTIR and GC-MS) for the detection and, when possible, the quantification, of the species populating the discharge and likely interacting with the surface. In sub-task 2.1.2 by **EPM**, experimental and theoretical results on plasma modelling of an elementary dipolar plasma source have been obtained on magnetic field configurations and trajectories of fast electrons accelerated at ECR.

Task 2.2 is devoted to reactor design and testing. In fact, this work has been divided, as indicated during the kick-off meeting, into two parts. The first one corresponds to the

development of a low pressure (0.1 Pa range), cylindrical microwave plasma reactor (thesis of Mr. TRAN Tan Vinh). The second consists in developing a medium pressure (100 Pa range), planar microwave plasma reactor (thesis of Mr. Louis LATRASSE, recruited for the MATECO project). Task 2.2 includes a milestone (M2.2) whose specification have been met. Louis Latrasse has successfully defended his thesis (Conception, caractérisation et applications des plasmas micro-onde en configuration matricielle) on November 29, 2006 in Grenoble, and Tan Vinh Tran (Caractérisation et modélisation des plasmas micro-onde multi-dipolaires) on December 20, 2006. Their thesis manuscripts will be soon available on line on the website http://tel.archives-ouvertes.fr.
Task 2.3 corresponds to the development of the coating processes. This task includes contributions of **HEF R&D** and **EADS**. The milestone M 2.1, corresponding to the deposition rate, has been met by **HEF and EPM**. The functional properties of deposited layers have been tested as a function of plasma deposition parameters. The objective of sub-tasks 2.3.2 and 2.3.3 concerns the correlation of experimental parameters (power, pressure, substrate bias and temperature, pulsing) with the chemical and physical properties of the coatings. Both sub-tasks converge in giving a process understanding and optimization in deposition of protective Si-O-N coatings, object of the research of MATECO. Characterization of the coatings by **UNIBA, EADS** and **EPM** has been carried out in collaboration with **POLITO** and **ICMSE**.
Finally, in WP2, a reflection was opened in Task 2.4 on the different ways of cleaning microwave plasma reactors by using reactive gas plasmas in order to obtain the chemical etching of films unintentionally deposited on reactor walls. The cleaning process proposed in MATECO project is based on conventional etching processes with reactive gases currently used in microelectronics. Due to the innovative character of the solution proposed, a patent (FR 06 02 787) has been deposited in France by CNRS-EPM on June 13, 2006.

1.4.2 Progress towards objectives

1.4.2.1 Task 2.1: Theoretical study on the parameters influencing the coating process (**UNIBA**, **POLITO** and **EPM**)

Sub-task 2.1.1. Parameters linked to the deposition processes (**UNIBA** and **POLITO**)

Since the aim of this tasks is the definition of the process parameters suitable to deposit inorganic, non-conductive and dense silicon based coatings, this task has been bound to task 2.3.3.

SiO_x deposition process has been studied in a RF capacitive reactor. The effect of various experimental parameters onto the plasma phase and the coating chemistry has been studied:
- Monomer nature (HMDSO, HMDSN, TEOS);
- RF Power;
- Feed composition (O_2 / monomer flow rate ratio).

Except for HMDSO at low O_2 / monomer ratio and low power, the absorption features are consistent with an inorganic SiO_x matrix since under all the input power conditions investigated no evidence of the typical bands of organic moieties have been detected. Few features can be observed in the spectra: the Si-O-Si stretching and bending absorption bands, at 1 068 cm^{-1} and 820 cm^{-1}, respectively and the features of silanols (Si - OH) at 935 cm^{-1} (bending) and 3 450 cm^{-1} (stretching). The absorptions of silanol groups decrease by increasing the input power and completely disappear at input power higher than 100 W. The

decrease of Si-OH groups with input power can be ascribed to the higher ion bombardment energy and dose, which are expected to enhance the OH groups' abstraction as well as the removal of the residual organic groups. Low concentration of silanols is a key factor for the utilization of these coatings as protective layers because the presence of silanols induces the formation of highly porous films, with a consequent higher permeability to water and reactants.
When the plasma phase is investigated by means of optical emission spectroscopy (OES) the trend of the emitting species as a function of the experimental parameters can be drawn. The main species detected are H, O, CH, CO and CO_2^+. It has been found that both by increasing power and O_2 / monomer ratio CH radical (building blocks for the organic content in the coating) drastically decreases.
On the other hand the oxidation products (CO and CO_2^+) increases. This outcome is really interesting since shows how OES well correlates with IR of coatings:
- At high power and O_2 / TEOS no carbon (CH_x) in the plasma phase;
- At high power and O_2 / TEOS no organic functionality in the coating.

Organic functionality can be monitored in line by means of OES by monitoring CH_x in the plasma phase. Remembering that low organic content in the coating means good quality films it can be concluded that the final performance of the coating can be automatically and continuously monitored in situ by means of OES.
The effect of the pulsed plasma has been investigated by means of the application of different Duty Cycles (DC): 10, 15, 25, 50, 100 %, with a on time of 10 ms. Plasma modulation was accomplished by triggering the power supply by means of a home-made pulse generator.
The effect of the duty cycle, in terms of FTIR absorption of the coatings, is shown in the following figure.

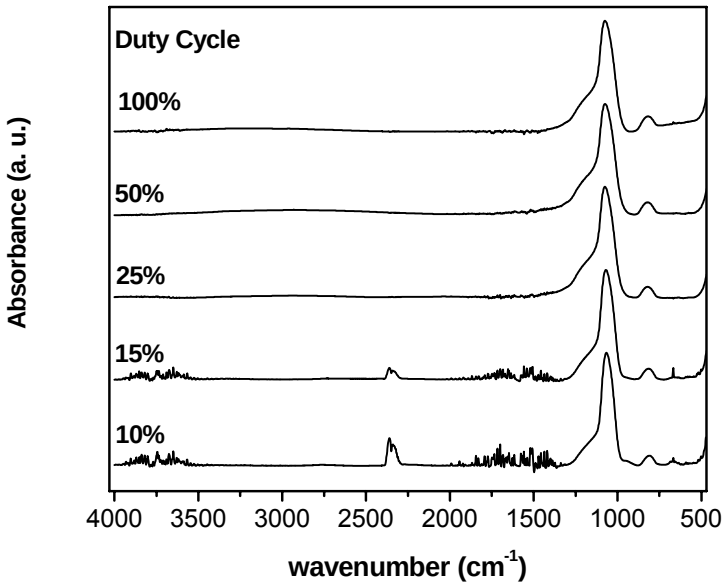

1000 nm SiO_x films (TEOS 4 sccm, O_2 90 sccm, Ar 44 sccm, 250 W, 100 mTorr)

The spectra reveal a typical inorganic SiO_x coating containing the signal due to Si-O stretching at 1070 cm^{-1} and the signal due to Si-O-Si bending at 820 cm^{-1}. Lowering DC leads to some silanol groups, SiOH (900-920 cm^{-1} Si-OH bending), which are generally detrimental for species permeation (in liquid as well as in gas phase). This last finding seems to point out to the importance of sample ion bombardment in the scavenging of -SiOH groups. In fact, at low DC,

when the off time is more relevant and in turn the ion bombardment is reduced, some SiOH groups are identified.
Some attention has been devoted to the evaluation of the deposition rate. The highest value found is 3.6 μm/h in continuous mode.

SiO_xN_y films from ICP and CCP discharges have been studied, particularly with regard to parameters like argon dilution, input power (both film characterization and plasma phase study) and oxygen addition (only as film characterization). Attention has been paid to the OES study of Monomer-Ar-O_2 fed ICP discharges. Moreover, different dimethylaminosilanes precursors have been compared as organosilicon feeds for ICP deposition of SiO_xN_y films. Finally, the effect of the RF source has been investigated by in CC (capacitive coupling) mode. The IC and CC PACVD processes were performed in the same reactor which is capable to be inductively or capacitively coupled, as shown in the scheme below. It is pointed out that, in CC configuration, the substrates are placed on the RF powered electrode so that a substrate biasing occurs during the deposition.

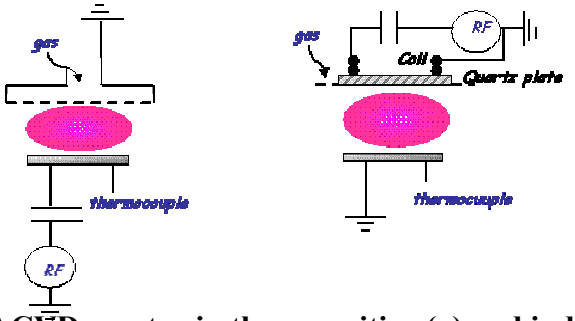

Scheme of the PACVD reactor in the capacitive (a) and inductive coupling (b)

The chemical characterization of SiO_xN_y coatings from IC-plasmas fed with BDMADMS-Ar, has shown that the coating is quite similar to thermal nitride at :
- High power;
- High Ar / Monomer ratio;
- Low pressure.

When O_2 is added to the mixtures, the film passes from a SiN-like structure to a SiO_2-like one, remaining in an inorganic matrix. This transition was shown to be very sharp and almost complete for the stoichiometric O_2-to-monomer ratio of 1.
Interestingly with increasing oxygen content in the film, it was found that nitrogen and not carbon shows the most drastic reduction. Therefore, in order to obtain SiON-like films, under these experimental conditions, low O_2-BDMADMS ratios (0.5-1) and high power (500-700 W) were defined to be suitable.
In order to carry out a plasma phase study of this particular system a detailed Optical Emission Spectroscopy (OES) characterization of all the optically emitting species in plasmas fed by BDMADMS-O_2-Ar (400 W, 8 mTorr) was performed. Emission spectra from 200 to 800 nm were registered by means of an OMA Jobin-Yvon 320. In the tables below, the emitting species, detected in such plasma are listed.

Emitting species	λ (nm)	Transition and threshold energy ε_{th} (eV)
H_2	200-320 453-464 580-650	3Σg-3Σu Primary System G1 Σ+g-B1 Σ+u G→B d3 Πu-a3 Σ+g Fulcher-α → *13.95*
CH	431.4 (0,0), 432.4 (2,2) 388.9 (0,0)	A2Δ-X2Π Å System → *2.9* B2Σ-X2Π 3900 Å System
CN	421.6 (0,1), 388.3 (0,0), 359.0 (1,0)	B2Σ+ - X2Σ+ *(Violet System)* → *3.2*
NH	336.0 (0,0)	A3Π – X3Π *(3360 Å System)* → *3.7*
H	656.3, 486.1, 434.0, 410.2	n(>2) →n=2 *(Balmer line)* → *12.1*
Si	251.4, 288.2	3p2 3P-4s 3P0 ; 3p2 1D – 4s 1P0→ *5.1*
N_2	297.7 (2,0), 315.9 (1,0), 337.1 (0,0), 357.7 (0,1), 296.2 (3,1), 313.6 (2,1), 333.9 (1,1), 380.5 (0,2), 295.3 (4,2), 311.7 (3,2), 330.9 (2,2)	C3 Π-B3 Π Second Positive → *11.1*
CO	283.3 (0,0), 297.7 (0,1), 313.4 (0,2), 330.6 (0,3), 266.5 (1,0) 401.1-646.5 451-608 206-258 252,275	b3∑-a3∏ Third Positive and 5B Bands→**10.4** d3Δ-a3∏ Triplet Bands B1∑-A1∏ Angstrom System a3∏-X1∑ Cameron Bands Kaplan Bands
OH	306.4-306.7-307.8-308.9 (0,0) 281.1-281.6-281.9-282.9 (1,0)	A2∑+-X2∏ 3064 Å System→**4.1**
O	777.2-777.4-777.5	3s 5S°-3p 5P

Emitting species and relative transitions detected in a BDMADMS-Ar-O_2 plasma due to the O_2 introduction

The trends of CN, NH, CO and OH are plotted below. The sharp increase of nitrogen containing species coming from the monomer fragmentation like CN and NH may be correlated to the mentioned reduction of nitrogen in the solid; the increase of oxidation products such as CO and OH is reasonably linked to the decrease of organic carbon moieties in the film. Interestingly, by looking at these trends, it comes out that, for the O_2-to- monomer ratios up to 1-2, the oxidation of silicon to form the SiO_x matrix seems to be highly favoured (so that the recombination with nitrogen radicals is prevented) while the oxidation of organic fragments becomes significant only at higher oxygen dilutions.

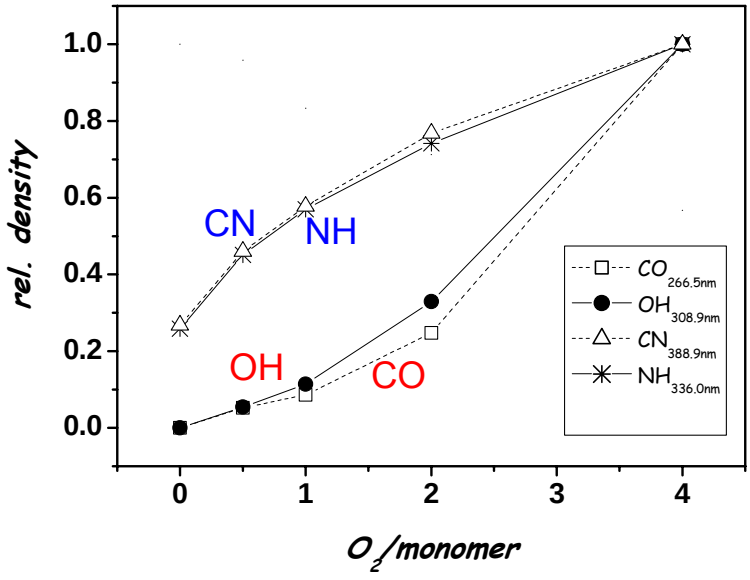

Relative plasma density of significant radicals in BDMADMS-Ar-O_2 plasmas

Besides the addition of reactive gases to the BDMADMS-argon feed mixture, further attention has been paid to the effect of the monomer. In particular, the performances as nitride-like films precursors of three dimetilamminosilanes, BDMADMS included, characterised by a different number of -$N(Me)_2$ groups bonded to silicon, have been compared in order to achieve a better understanding of their role in plasma fragmentation. A table with names, formulas and boiling points of such compounds is reported below.

Molecular structure	Name	Boiling point
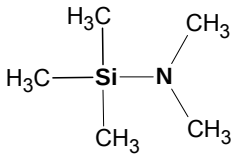	Dimethylaminotrimethylsilane DMATMS ***$SiNC_5H_{15}$***	87°C
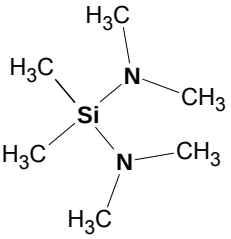	Bis(dimethylamino)dimethylsilane BDMADMS ***$SiN_2C_6H_{18}$***	128°C
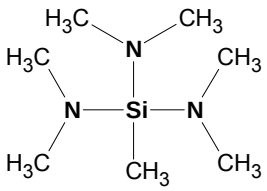	Tris(dimethyilamino)methyilsilane TDMAMS (T) ***$SiN_3C_7H_{21}$***	120°C

Dimethylaminosilane monomers tested as SiN_x precursors

The effect of input power, which had been shown to be crucial parameter in ICP BDMADMS-Ar depositions, was studied for the three precursors at a monomer-to-argon ratio of 0.2, total flow rate of 12 sccm, and pressure of 5 mTorr.
In the next figure, the normalized FT-IR spectra of deposits obtained under the above conditions at different input power (from 100 to 700 W) are reported. The changing of the chemical composition appears very similar, in particular for BDMADMS and TDMAMS: the organic carbon moieties are strongly reduced and the main band becomes closer to the SiN stretching position, effect discussed in detail only for BDMADMS in the 12-months report. For DMATMS, the main band is closer to SiC stretching than SiN.
By comparing, the NCH_3 (2790 cm^{-1}), CH_3 (2960 cm^{-1}), $SiCH_3$ (1265 cm^{-1}) absorption intensities, indicated in the figure, it can be observed that while the $SiCH_3$ is quite persistent and reduced almost with the same slope as CH_3, the NCH_3 absorption disappears vary soon with power. This behaviour suggests that the dimethylamino groups, peculiar of these monomers are particularly involved in fragmentation paths within the plasma.

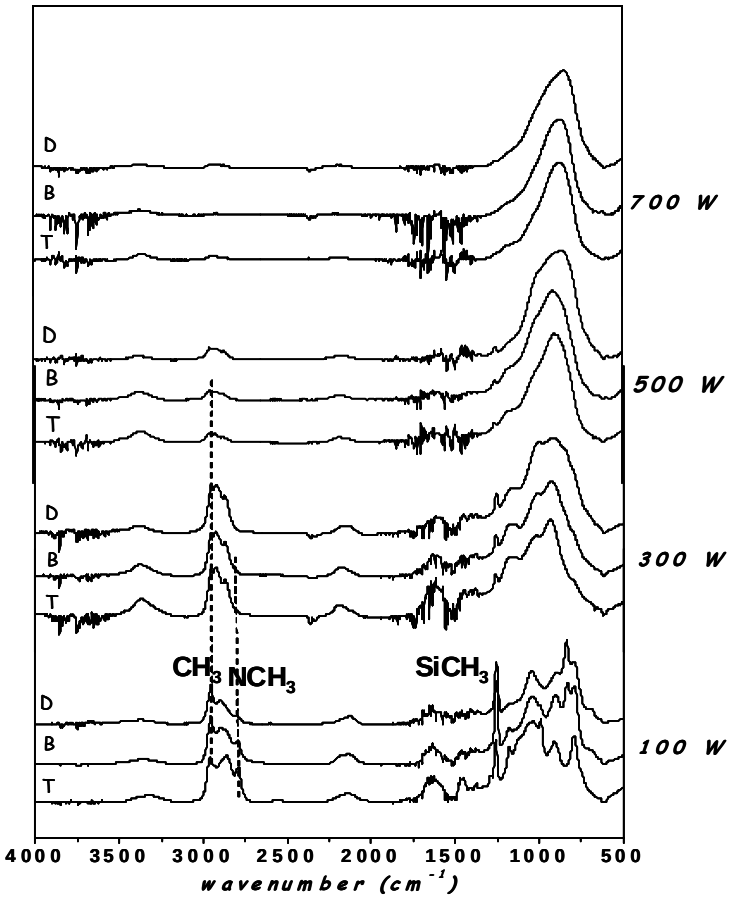

Normalized FT-IR spectra of films obtained from BDMADMS (B), TDMAMS (T), and DMATMS (D) in ICP as a function of input power

In the following figure, the XPS atomic composition is reported for the same coatings. It can be observed that the total carbon is drastically reduced, just in the same way as the organic carbon detected in IR spectra. For the best condition, i.e. 700 W, the carbon content is higher in the DMATMS films.

The N/Si ratio is always less than one, while for the precursor it is equal or higher, result consistent with the hypothesis that the Si-N side of the molecule undergoes a stronger fragmentation.

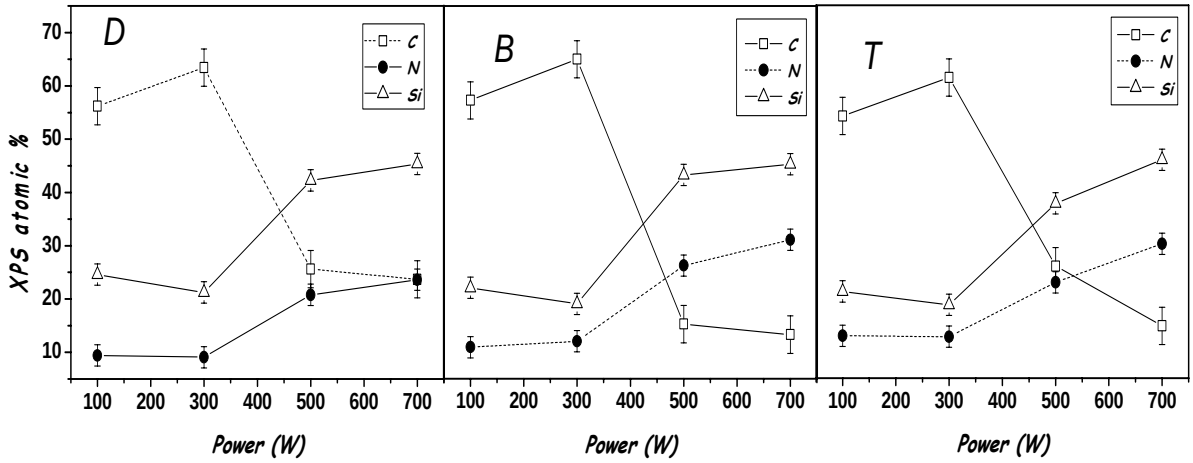

XPS atomic composition of films obtained from BDMADMS (B), TDMAMS (T), and DMATMS (D) in ICP as a function of input power

In figure below, the XPS atomic percentages of films obtained from BDMADMS-Ar mixtures in CC-plasmas at increasing input power are reported (monomer flow rate of 2 sccm, pressure of 30 mTorr). Interestingly a very different scenario is found in such CC-PACVD with respect to ICP : the XPS carbon %, is almost constantly high (50%) and the nitrogen content always very low (10%)with increasing power.

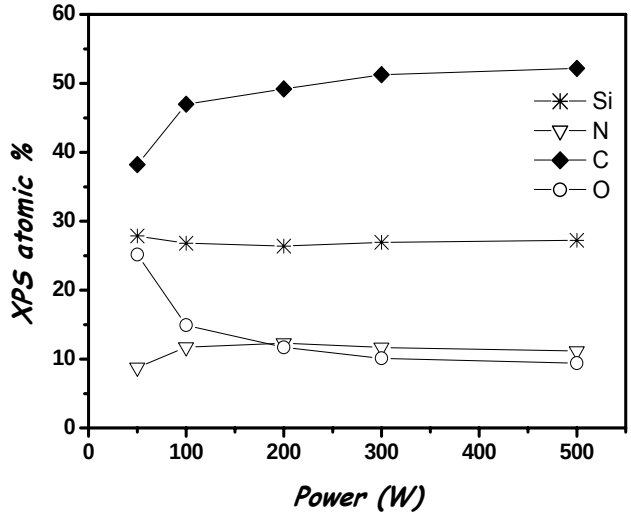

XPS atomic composition of films obtained from BDMADMS in CCP as a function of input power

The normalized FT-IR spectra of the same films, shown in next figure, show a main band peaked at 800 cm^{-1}, SiC stretching position, indicating a matrix basically made of SiC bond. Moreover it is interesting to observe that, in spite of the constantly high total (XPS) carbon content, the organic carbon, absorbing at 2960, is strongly reduced as the power increases, revealing an inorganic SiC network (with N and O as minor components); this network becomes also more and more cross-linked as the power increases as the CH absorption curve shape appears less resolved at higher power values. This is a known effect of the substrate

biasing that occurs in these CC plasmas. All things considered it seems that in CC mode the fragmentation in the plasma, reasonably responsible for the strong carbon depletion seen in ICP depositions plays here a minor role.

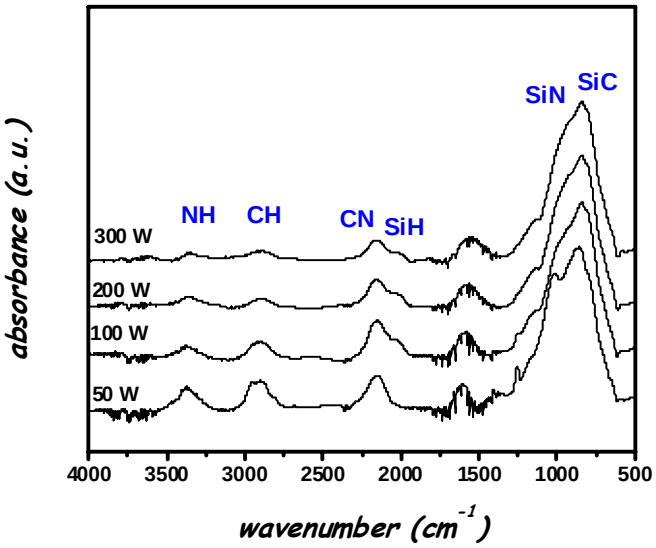

Normalized FT-IR spectra of films obtained from BDMADMS in CCP as a function of input power

Also the addition of oxygen to BDMADMS-Ar plasmas in CC configuration leads to very different results with respect to the IC plasmas. In that case, the transition to oxide appeared highly activated and nearly stoichiometric. In these films, instead, the XPS atomic composition and the FT-IR spectra (figures below) reveal a SiO_2-like structure (O-to-Si ratio about two and complete depletion of carbon and nitrogen) only at very high O_2-to-monomer ratio.

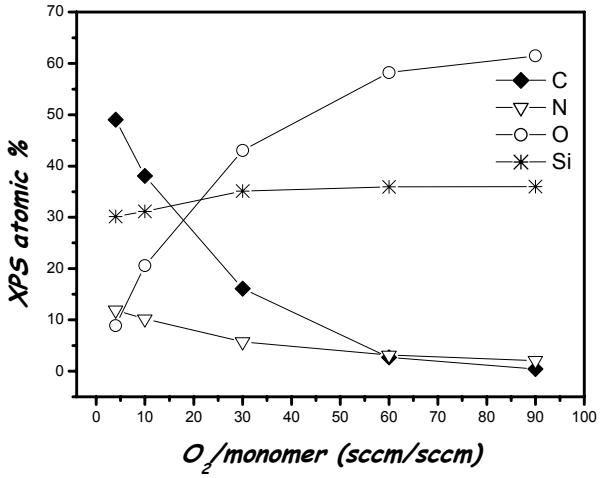

XPS atomic composition of films obtained from BDMADMS-Ar-O_2 mixtures in CCP as a function of O_2 to monomer ratio

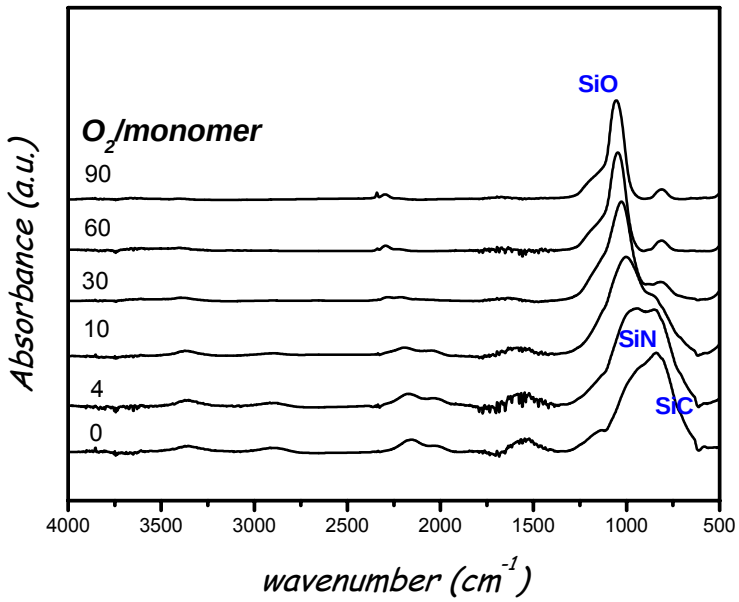

Normalized FT-IR spectra of films obtained from BDMADMS-Ar-O_2 mixtures in CCP as a function of O_2 to monomer ratio

Sub-task 2.1.2. Plasma process modelling (**EPM**)

Concept of distribution

In plasma processing of large area surfaces, a challenge is the scaling up of the plasma process. In the MATECO project, the solution adopted by **EPM** in order to solve this difficulty is to apply the concept of distribution: distribution of the plasma, of course, but also, distribution of the process parameters, such as pumping, precursor gas feeding, heating or cooling, biasing. The distribution of the plasma implies that the plasma production is distributed, i.e. that the electric field is distributed uniformly over the whole plasma source region. This can be easily achieved with DC electric fields (cf. DC magnetrons), but not practicable with RF electric fields with wavelengths of the order of the plasma dimensions. Using microwaves with wavelengths much shorter than the plasma dimensions, the scaling up can be solved via the distribution of plasma production over bi-dimensional (planar source) or tri-dimensional networks of elementary plasma sources excited with microwaves. This concept has been successfully applied to the so-called multi-dipolar plasmas in the low-pressure range (0.1 Pa range) and matrix plasmas in the medium pressure range (100 Pa range)

In such elementary plasma sources, the plasma is produced at the extremity of a microwave applicator. In the medium pressure range, the plasma is produced via the coupling of the microwave electric field with the electrons by collision transfer (collisional absorption). In the low-pressure range, the coupling of the electrons with the microwave electric field is obtained in presence of a magnetic field by resonant transfer at electron cyclotron resonance (ECR). Electron cyclotron resonance is obtained when the frequency of electron gyration in the magnetic field **B** is equal to the microwave frequency f_0:

$$f_0 = e\, B_0 / 2\, \pi\, m_e \qquad (1)$$

At the frequency f_0 = 2.45 GHz, the ECR coupling condition is given by B_0 = 875 gauss. The charge and the mass of the electrons are - e and m_e, respectively.

Description of an elementary plasma source

The microwave applicator that constitutes an elementary plasma source is, in fact, a coaxial microwave feed through. In the medium pressure range, the extremity of the coaxial line is filled up with a dielectric in order to prevent plasma generation inside the feed through. In the low-pressure range, the extremity of the central conductor of the coaxial line supports a magnetic dipole, i.e. a permanent magnet with an axial magnetization, as shown in the following figure.

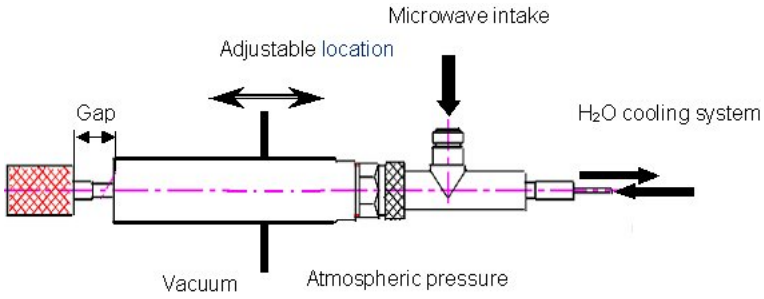

Sketch of an elementary plasma source operating at ECR

In such a design, the microwave electric field accelerates the electrons in the regions where the ECR condition is fulfilled, i.e. on the surface of constant magnetic field intensity where the ECR condition occurs (875 gauss at 2.45 GHz). The fast electrons thus accelerated at ECR then ionise the gas along their path in the magnetic field. The magnetic dipole acts as a tri-dimensional magnetron structure and the trajectories of the fast electrons oscillate within two field lines, between two mirror points, while drifting around the magnetic dipole. The plasma produced along their trajectories around the magnet diffuses away from the plasma source region under the effect of the electric space charge induced by the density gradients.

View of an elementary plasma source implemented on the top flange of the cylindrical chamber

The general view of the plasma produced by such an elementary plasma source is shown in the following figure with the Langmuir probes used for the plasma characterization.

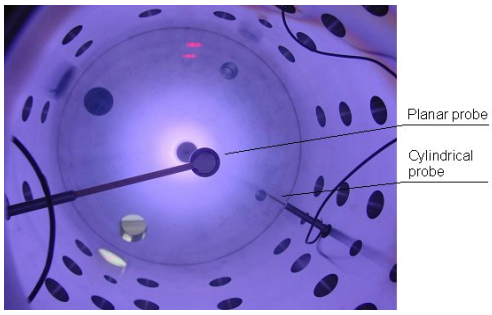

General view of the plasma produced by an elementary dipolar plasma source inside the chamber with the Langmuir probes used as diagnostics means

Short distance front and side views of the plasma are also shown in the following figures.

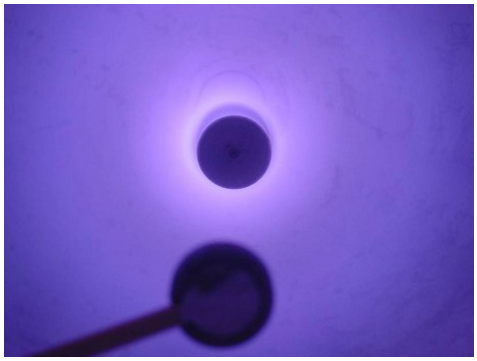

Front view of the plasma produced by an elementary dipolar plasma source(top) with a planar Langmuir probe for plasma characterisation (below)

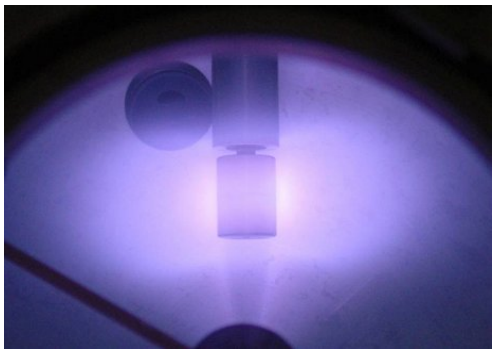

Side view of the plasma produced by an elementary dipolar plasma source

Dipolar plasma source modelling

Despite its simplicity (a permanent magnet, or magnetic dipole, lies at the end of a coaxial line), the functioning of this dipolar plasma source implies the knowledge of:
- Magnetic field configuration;
- Microwave electric field configuration, in presence or not of plasma;
- ECR coupling regions;
- Plasma diffusion in the magnetic field around the source.

The magnetic field produced by the permanent Sm_2Co_{17} does not depend on the presence of plasma, hence its modelling has been made independently.
The microwave electric field component E(t) of the micro-wave power is perfectly known from the magnetron, in rectangular waveguide, and then in a coaxial line up to the rear face of the

permanent magnet. As soon as it goes through the end of the coaxial line its propagation becomes complex. Specialised softwares are able to calculate the electric field components even in uniform plasma by introducing its dielectric tensor. These calculations are very useful for the understanding of the dipolar source functioning.
The coupling between E(t) and the static magnetic field gives the ECR phenomenon. Such a complex mechanism implies a global modelling of plasma generation, including electron heating, diffusion, and trapping in the magnetic field. Even these phenomena are very complex; it is possible to disconnect some of them from each others.
ECR coupling is taken into account by defined zones of constant volume and location where electrons energy is increased. The zones of energy gain are defined as the most probable area of ECR coupling, between the coaxial line and the permanent magnet and near the magnet surface in its equatorial plan. Trajectories of these primary electrons have been hence calculated. In order to obtain an overview of the mechanisms theoretically involved in a simple dipolar source, it is necessary to take into account collisions between the fast electrons and neutrals. The low energy electrons produced by the ionising inelastic collisions with fast (accelerated at ECR) will diffuse afterwards in the magnetic field lines and in the resulting space charge electric field. By the way, a simple model of the dipolar source can be obtained, which is not out of reach.
The following pages present a few examples of the studies performed during the MATECO project.
Magnetic field configuration of a spherical magnet with diametrical magnetisation. In this first example, the magnetic field delivered by a spherical permanent magnet has been calculated analytically.

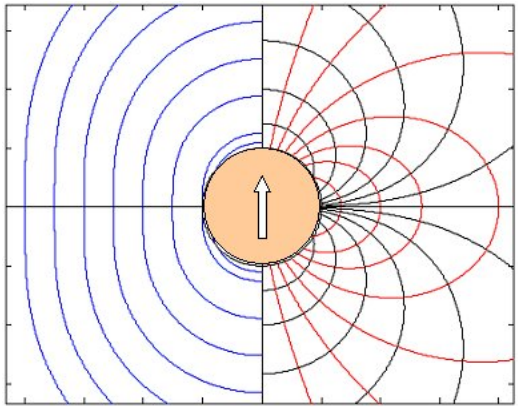

Magnetic field configuration produced by a spherical magnet with diametrical magnetization: dotted red lines are magnetic field lines; black lines are equipotential lines (scalar magnetic potential); blue lines are constant amplitude magnetic field

An important mechanism occurring in such a magnetic field is the trapping of electrons that undergo magnetic forces. The simulation results in the following figure shows the trajectory of an electron trapped in the magnetic field of a spherical magnet, in the absence of space charge electric field and collisions. Its trajectory winds around magnetic field lines of constant amplitude, oscillates between two mirror points near the opposite poles where the velocity parallel to the magnetic field vanishes and change its sense, and drifts around the magnet. Such a structure constitutes a tri-dimensional magnetron structure where the electrons are trapped very efficiently.

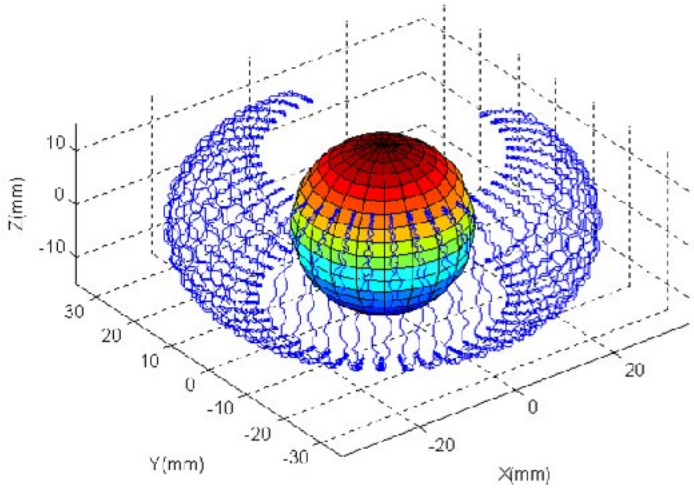

Example of electron trajectory in the magnetic field of a spherical magnet: the energy of the electron is constant (1.5 eV) and the electron does not undergo any collision

Magnetic field lines of cylindrical shape

Unfortunately, the fabrication of a spherical magnet with axial magnetization is difficult and expensive while cylindrical magnets with a central hole for water cooling and handling at the coaxial extremity can be easily machined. The following figures show the magnetic field configurations obtained from specialised software.

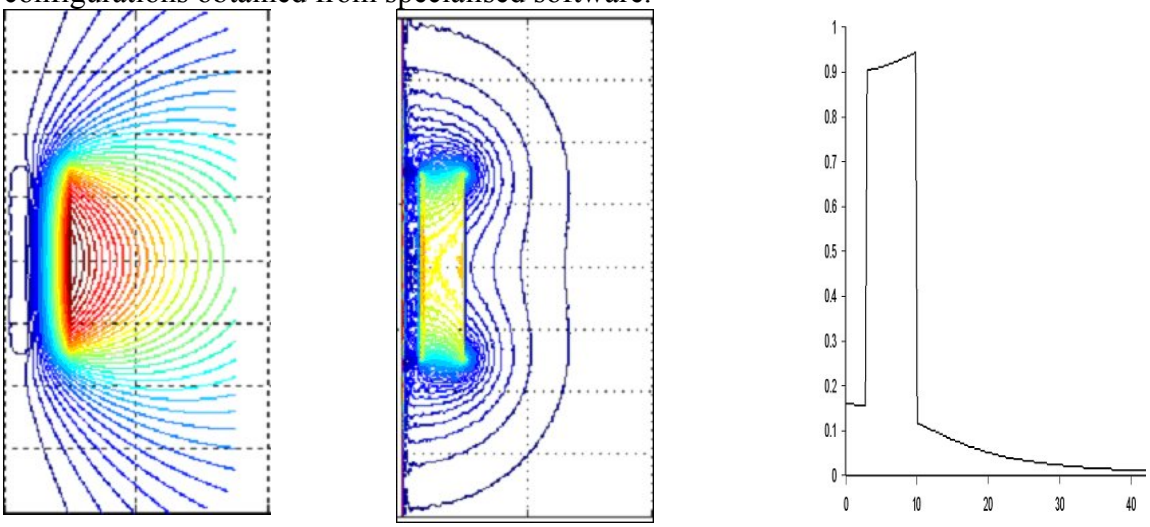

Magnetic field configuration of a cylindrical Sm_2Co_{17} magnet of 30 mm in height, and 20 mm in diameter with a central hole of 6 mm of inner diameter: magnetic field lines (left), lines of constant magnetic field amplitude (middle), profile of magnetic field amplitude in the symmetry plane (right)

Configuration of the microwave electrical field E(t)

Specialised software can calculate both the frequency response of the dipolar structure and the electric field component of the microwave power intake. The frequency response indicates if the microwave power is well transmitted from the source to the vacuum, in the first step, and into plasma of constant density and collision frequency, in the second step.

Near the end of the coaxial line, see figure below, it is possible to notice that **E**(t) is important in the gap (spacing between the end of the coaxial line and the magnet).

f 1 = 2.3812 (0.94)	f 3 = 2.4968 (0.94)
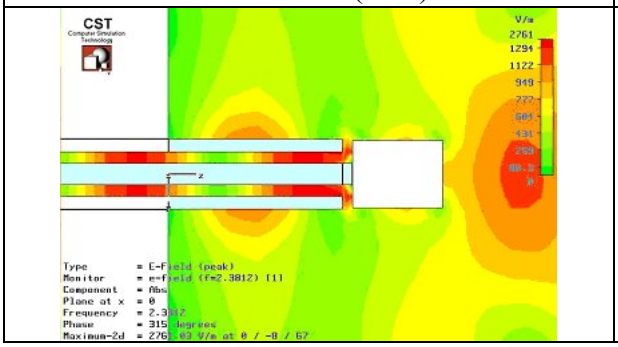	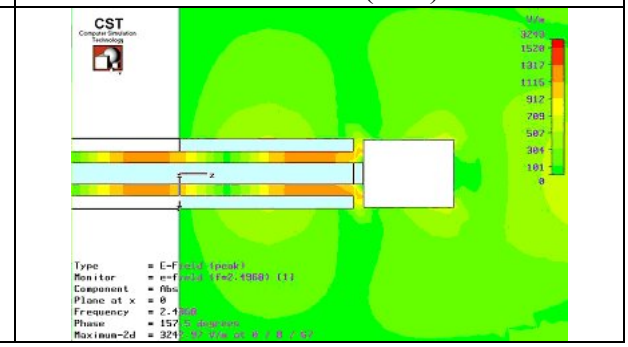

Configuration of the microwave electric field at the end of the coaxial line: electric field amplitude (left); electric field vector (right)

Trajectories of electrons in the magnetic field of a spherical magnet

An important mechanism occurring in such a magnetic field is the trapping of electrons that undergo magnetic forces. The simulation results in the following figure shows the trajectory of an electron trapped in the magnetic field of a spherical magnet, in the absence of space charge electric field and collisions. Its trajectory winds around magnetic field lines of constant amplitude, oscillates between two mirror points near the opposite poles where the velocity parallel to the magnetic field vanishes and change its sense, and drifts around the magnet. Such a structure constitutes a tri-dimensional magnetron structure where the electrons are trapped very efficiently.

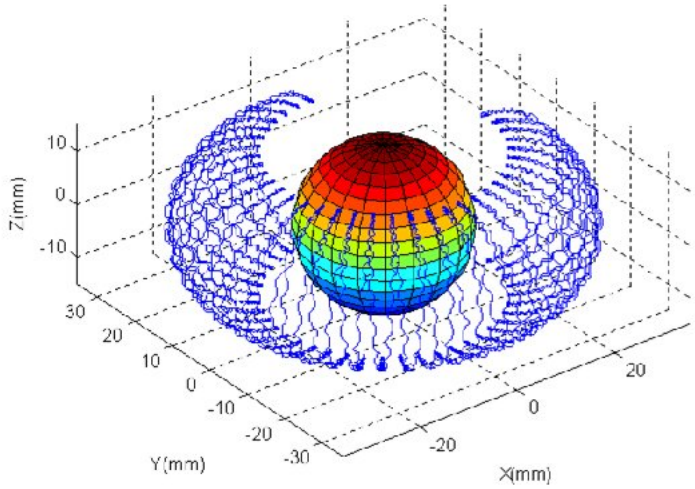

Example of electron trajectory in the magnetic field of a spherical magnet: the energy of the electron is constant (1.5 eV) and the electron does not undergo any collision

Trajectories of electrons in the magnetic field in presence of collisions

Trajectories of the primary electrons have been calculated. However, in order to obtain an overview of the diffusion mechanisms theoretically involved in a simple dipolar source, it is necessary to take into account collisions between the electrons (slow and fast electrons) and neutrals. The fast electrons, as well as the slow electrons produced by the ionising inelastic collisions, will diffuse afterwards in the magnetic field lines and in the resulting space charge electric field (not taken into account in the present modelling). By the way, a simple model of the dipolar source can be obtained, which is not out of reach. The following numerical simulations will present a few characteristic examples showing these diffusion mechanisms.

For such an implementation of the PIC (Particle In Cell) developed model, a Monte Carlo (MC) routine has been used. An hybrid model PIC-MC is necessary as particle trajectories depend on initial velocity and magnetic field lines which are rather different from one point to another around the magnet and collisions between particles occur with given probabilities. Examples of trajectories in presence of collisions are presented below.

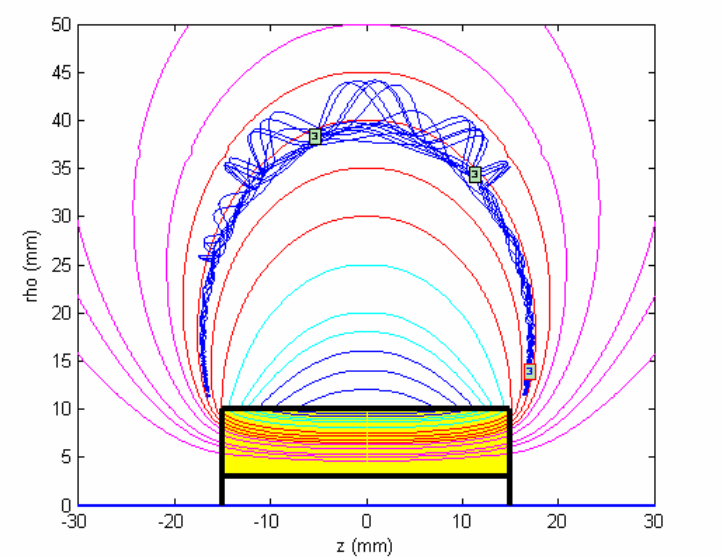

Electron trajectory in the magnetic field of a cylindrical magnet Electron energy is constant (20 eV) and it undergoes elastic collisions (labelled 3)

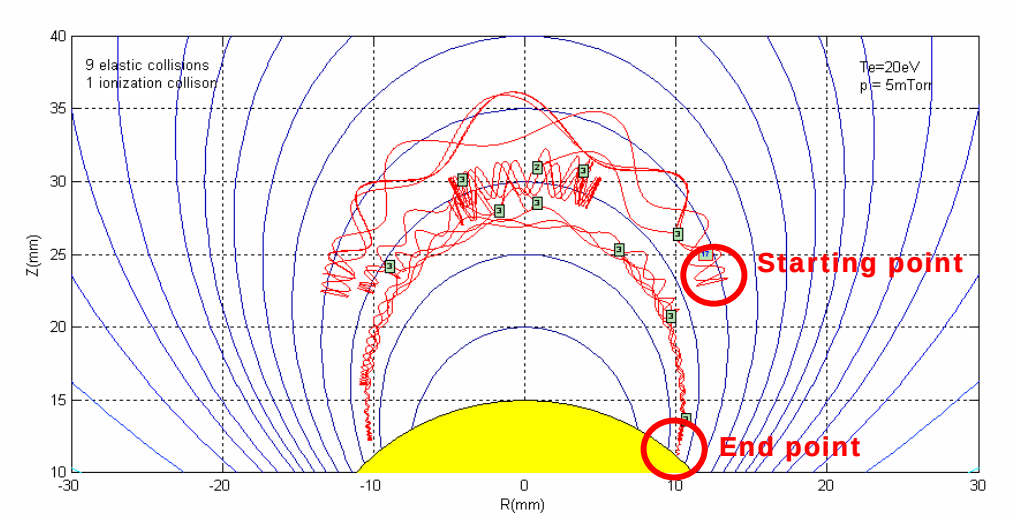

Electron trajectory in the magnetic field of a spherical magnet; Electron energy is constant (20 eV) and it undergoes 1 ionising inelastic (labelled 2) and 9 elastic (labelled 3) collisions. The electron is collected on the magnet surface

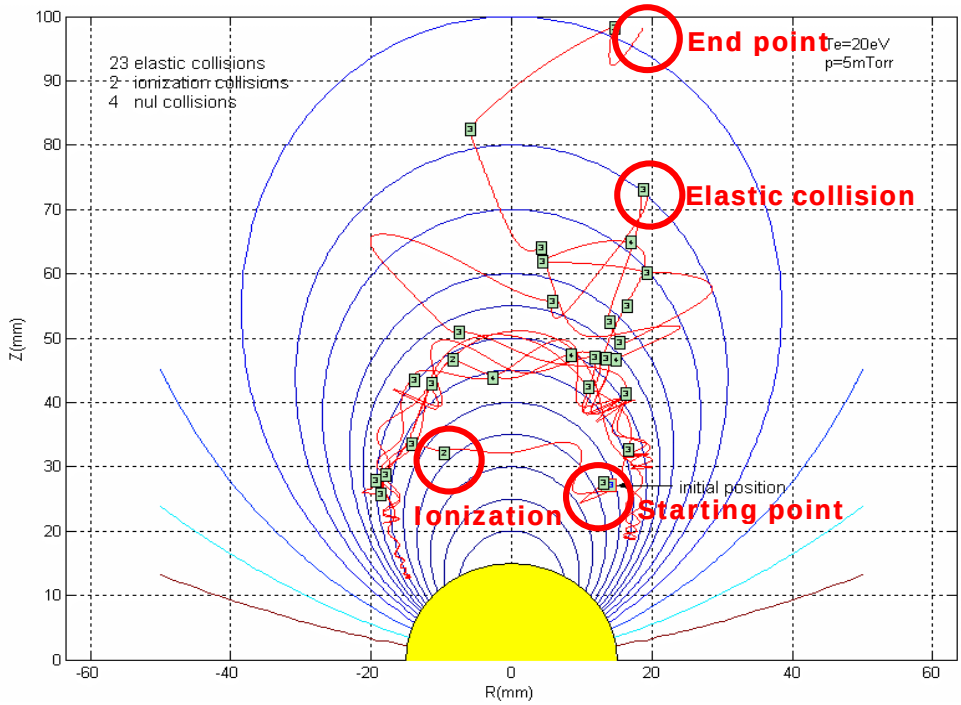

Electron trajectory in the magnetic field of spherical magnet; Electron energy is constant (20 eV) and it undergoes 23 elastic (labelled 3) and 2 ionising inelastic collisions (labelled 2). The electron escapes (diffuses out) the calculation domain

This study shows that collisions tend to scatter fast electrons from their initial magnetic field lines. Therefore, ECR coupling no longer occurs and electron heating vanishes. Hence, taking into account both phenomena (ECR and collisions) will lead to stress the most possible coupling zone between the periodic electrical field and electrons.
Modelling of the dipolar source will further imply to calculate the space charge field created by the variation of plasma density created by fast electrons and neutral collision phenomena. Hence, plasma diffusion outside trapping zone of fast electrons will be described. Another aspect of the modelling concerns the electron heating by the ECR phenomenon. If the static magnetic field is well described by classical model, the periodic electric field E(t) distribution lies on the coupling between the incident microwave field and the created plasma itself. Complexity of such a phenomenon requires much further development of the calculations.

Mechanism of electron heating at ECR

The coupling between the microwave electric field E(t) and the static magnetic field gives the ECR phenomenon. Such a complex mechanism implies a global modelling of plasma generation, including electron heating, diffusion, and trapping in the magnetic field. Even these phenomena are very complex; it is possible to disconnect some of them from each other.
ECR coupling is taken into account by defined zones of constant volume and location where electrons energy is increased. The zones of energy gain are defined as the most probable area of ECR coupling, between the coaxial line and the permanent magnet and near the magnet surface in its equatorial plan.

Simplified electromagnetic configuration. The magnetic field configuration around a cylindrical or spherical magnet, and in particular the lines of constant magnetic field amplitude, are rather complex functions of the spatial coordinates. Therefore, the geometry of the surface where the ECR condition is met, i.e. $\omega_0 = \omega_{ce}$, and the shape of the field lines induce electron

trajectories that cannot be expressed simply as functions of the spatial coordinates. Still more complex is the configuration, around such magnets, of the microwave (EM) electric field delivered at the end of the coaxial line. Under these conditions, the numerical calculations are long and the results difficult to exploit.
For these reasons, a very simplistic magnetic configuration has been adopted in order to reach a better understanding of the ECR heating in a realistic situation. For these reasons, a friendly configuration can be obtained with an infinite cylindrical magnet (z axis) with diametrical magnetization. With such geometry, the surfaces of constant magnetic field are coaxial cylindrical surfaces corresponding to magnetic field amplitude :

$$B_0(r) = B_{0s} (a / r)^2,$$

where B_0 is the magnetic field amplitude at radius r, B_{0s} the magnetic field amplitude at the magnet surface, and a the magnet radius. Another simple feature specific to this geometry is that field lines correspond to the magnetic vector potential $\mathbf{A_z}$.
The invariants In the motion of electrons in this magnetic field are the electron energy 1/2 $m_e v_0^2$ and the generalised momentum defined by :

$$p_z = m_e v_z - e A_z$$

where v_z is the velocity component of the electron along the magnet.
Of course, microwaves can propagate along the cylindrical magnet. The amplitude of the transverse electric field can be simply expressed as:

$$E(r,t) = (E_{0s} / r) \sin(\omega_0 t)$$

where E_{0s} is the amplitude of the electric field at the magnet surface.
The next Figure shows the trajectory of an electron in the magnetic configuration defined above. We can see that the envelope of the motion is defined by two magnetic field lines and that the invariant p_z is perfectly constant during the electron motion.

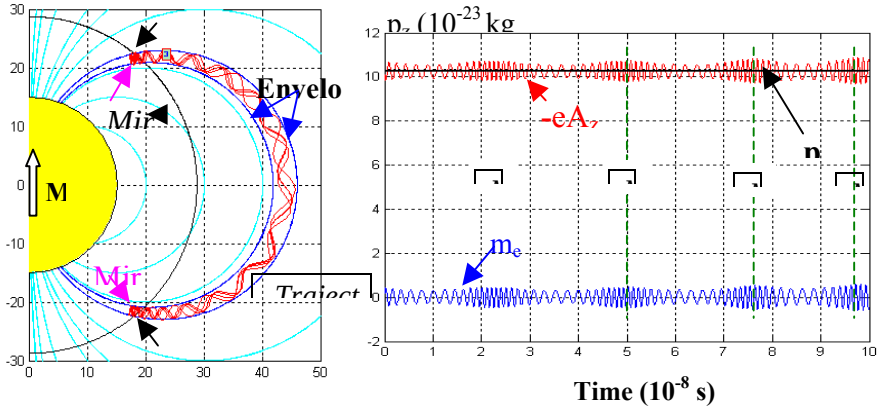

a) **b)**

Trajectory of an electron in the magnetic field of a cylindrical magnet of infinite length along Oz and of diametrical magnetisation (a) and variations in the two components ($m_e v_z$ and eA_z) of the generalised moment $p_z = m_e w_z - eA_z$ (b)

The next Figure shows the variation in the two invariants W_e and p_z in presence of elastic and inelastic collisions. We can observe that the variation in p_z occurs for both types of collisions. In contrast, we observe large variations of W_e for inelastic collisions and no noticeable variation for the elastic collision, since the energy transfer is of the order of the ratio m_e / M, where M is the mass of neutral atoms or molecules.

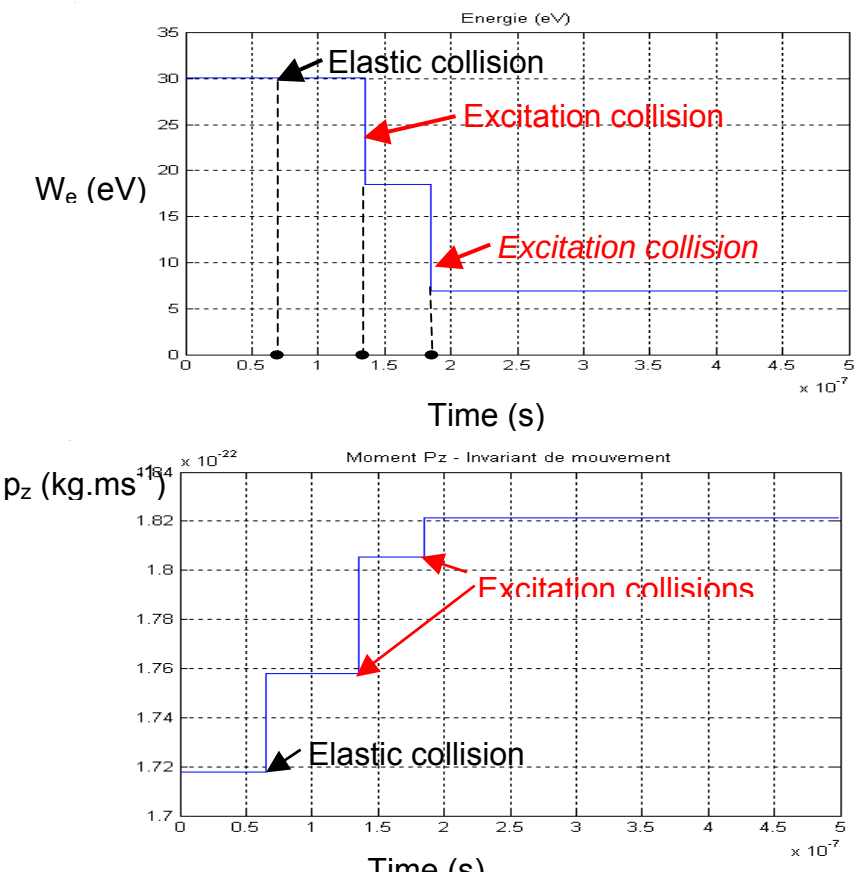

Variation of the kinetic energy W_e and generalised momentum $p_z = m_e w_z - eA_z$ of an electron undergoing elastic and inelastic collisions along its trajectory in the magnetic field of a cylindrical magnet of infinite length along Oz and diametrical magnetisation

Finally, the last Figure shows the evolution of the invariants when the electron trajectory crosses the ECR region. In particular, it can be seen that the mean generalised momentum does not vary since the energy is strongly modified. This numerical simulation shows also that the energy variation can be positive or negative, i.e. the electron can gain or loose energy from the microwave electric field.

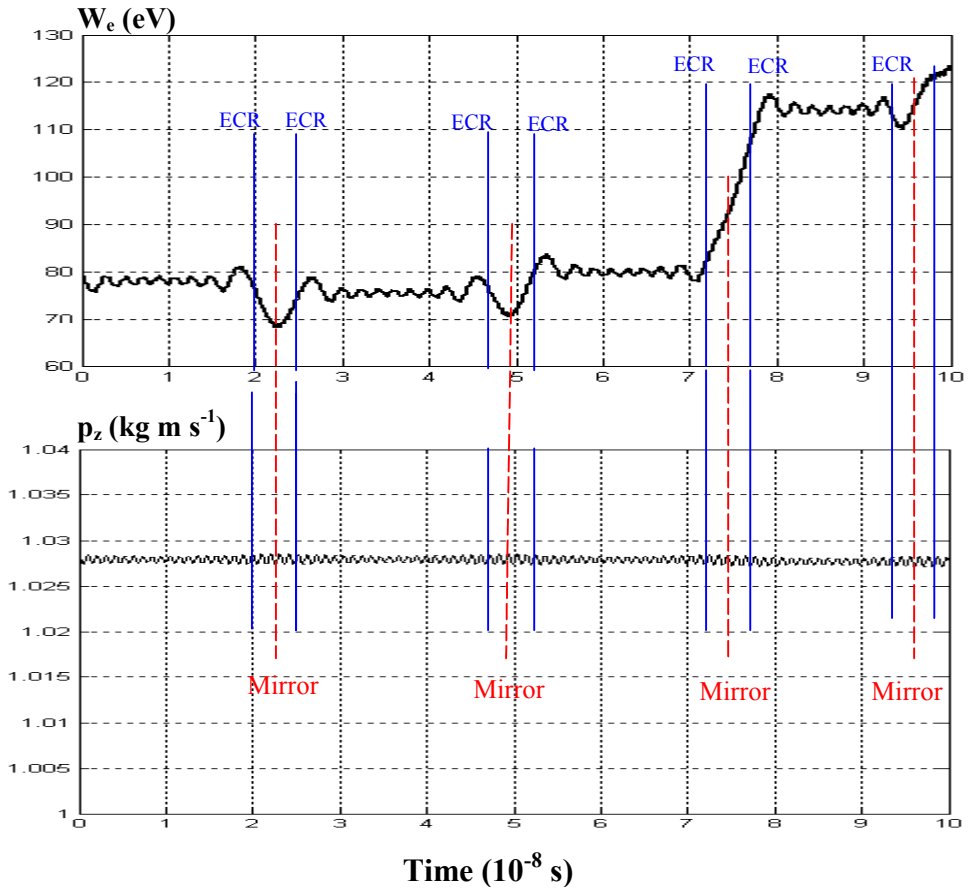

Variation along the trajectory: a) of the kinetic energy W_e; b) and of the generalised momentum ($p_z = m_e w_z - eA_z$) of an electron i) in the magnetic field of an infinite cylindrical magnet with diametrical magnetisation ; ii) and accelerated at ECR (electron cyclotron resonance) by a microwave electric field propagating along the magnet (axis Oz)

1.4.2.2 Task 2.2: Reactor design and testing, PACVD in microwave plasma reactor with DC pulsed biasing (**EPM**, **HEF**)

This work corresponds one of the main objectives of MATECO project in terms of plasma equipments, i.e. to develop new types of microwave plasma reactor. These new types of plasma, called ***multi-dipolar plasma*** and ***matrix plasmas***, are based on the concept of distribution of elementary microwave plasma sources according to bi- or tri-dimensional networks. In this way, plasma scaling up can be obtained without any physical limitation.
In the multi-dipolar plasmas operating in the low pressure range, the plasma produced by the dipolar elementary sources is sustained by microwaves at electron cyclotron resonance with the help of a magnetic field. In the elementary dipolar plasma sources developed in this project, the magnetic field is provided by cylindrical permanent magnets (magnetic dipoles) placed at the end of coaxial microwave applicators (see subtask 2.1.2 above). In the matrix plasmas operating in the medium pressure range, the magnets are removed from the coaxial microwave applicators. The objective of the task was to design such reactors, to make the drawings, and then to fabricate, to implement, and to test the performance of the plasma in terms of plasma density and uniformity as functions of gas nature, gas pressure, or microwave power.

Mutidipolar plasma reactor

Design of the multi-dipolar plasma reactor. The multi-dipolar plasma reactor developed in this study consists in a cylindrical chamber with a peripheral tri-dimensional network of 48 elementary plasma sources distributed on four rings of 12 plasma sources each. A front view of the cylindrical chamber is presented on the drawings shown in the next figure.

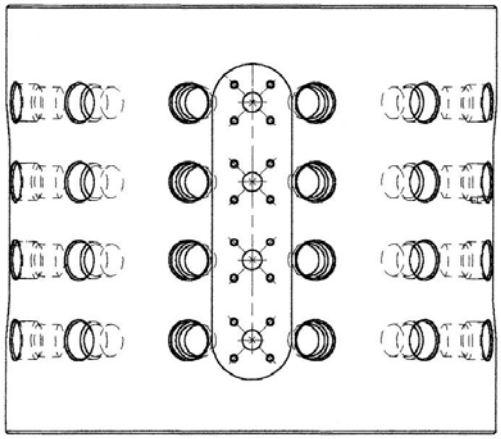

Front view of the cylindrical chamber as designed on the fabrication drawings

The reactor chamber fabricated from this design is shown in next Figure. The chamber, 40 cm high and 40 cm in diameter, is equipped with gas introduction and pumping means, pressure gauges, windows, and plasma characterisation means such as an optical fibre for OES (optical emission spectroscopy) and Langmuir probes for the determination of the electric properties of the plasma. In this Figure, the elementary plasma sources are not yet implemented on the chamber and replaced by as many plugs. In the present configuration, the chamber is used to study a single elementary, dipolar plasma source implemented on the top flange of the chamber. For this reason, a second chamber with 40 dipolar sources distributed on four rings of 10 sources each, has been realised, as shown in the bottom Figure.

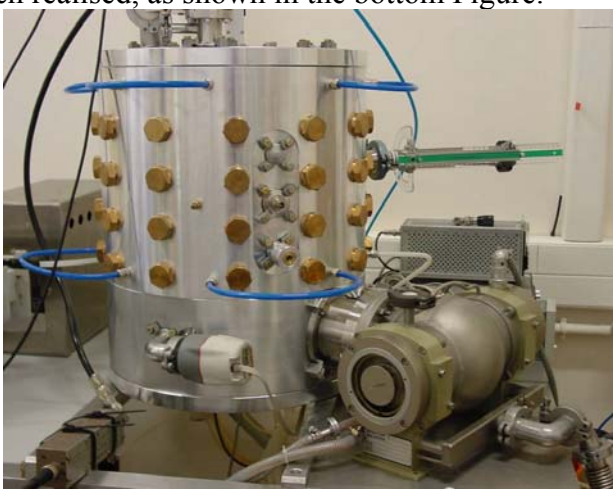

Front view of the cylindrical chamber as designed on the fabrication drawings

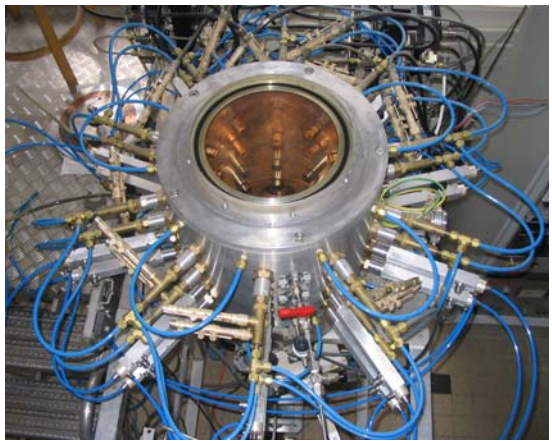

General view of the cylindrical chamber with 40 dipolar sources (4 rings of 10 sources)

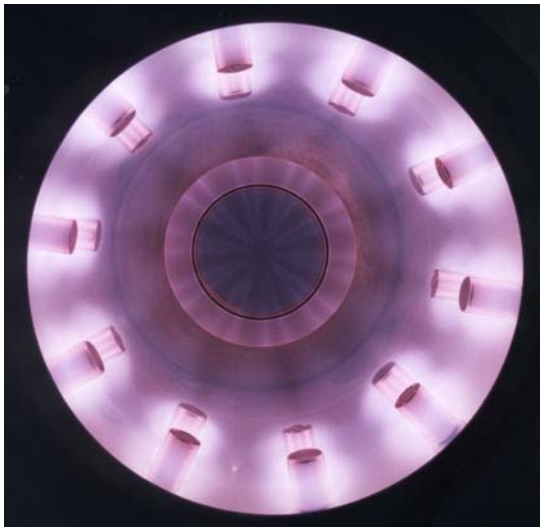

Top view of an argon plasma produced by 2 rings of 10 dipolar sources in the cylindrical chamber

In a first phase, 20 dipolar plasma sources were implemented on two rings at the periphery of the cylindrical chamber. A top view of an argon plasma produced in this chamber is presented above.

Performance of multi-dipolar plasmas. The plasma characteristics, measured by a cylindrical Langmuir probe in the centre of the plasma, are shown in next Figures. The variation in plasma density as a function of the microwave power per elementary dipolar plasma source is plotted at the argon pressure of 0.13 pascal (1 mtorr). The density first increases proportionally to the microwave power and then saturates above 150 W. This saturation can be explained by enhanced microwave absorption along the microwave line at high microwave power due to temperature increase of some components. In any case, it is clear that **milestone M2.2 is not fulfilled** since the **plasma density reaches only 5×10^{11} cm^{-3}** at 150 W per elementary plasma source.
The variation in plasma density as a function of argon pressure is also plotted for a microwave power of 100 W per elementary dipolar source. The plasma density increases when argon pressure increases up to 0.5 Pa (4 mtorr). By comparison with previous results, the plasma density is higher than 5×10^{11} cm^{-3} in the whole pressure range above 0.13 Pa (1 mtorr). This

objective, mentioned in deliverable D4, is already fulfilled in the reduced configuration tested (20 sources instead of 40 sources).

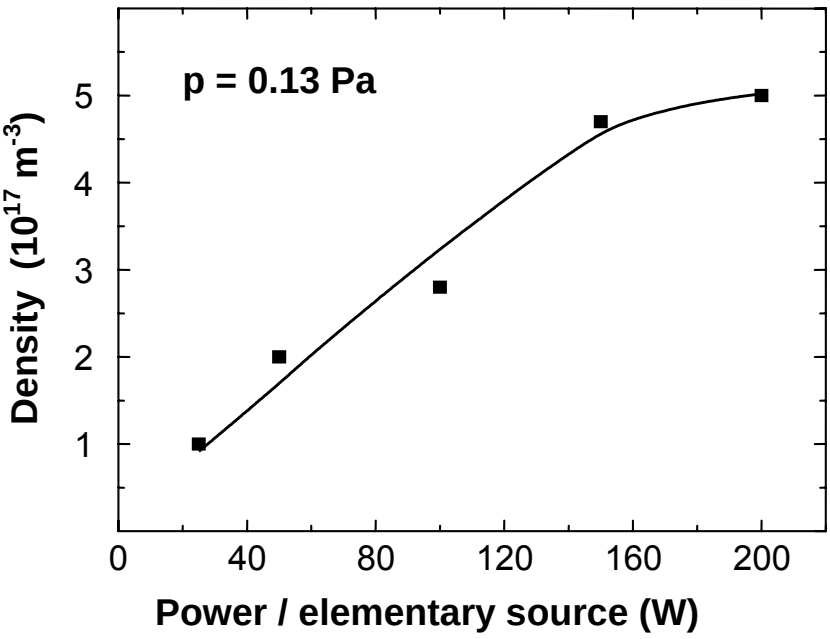

Variations in plasma density as a function of microwave power per elementary dipolar source. The argon pressure is 0.13 Pa (1 mtorr)

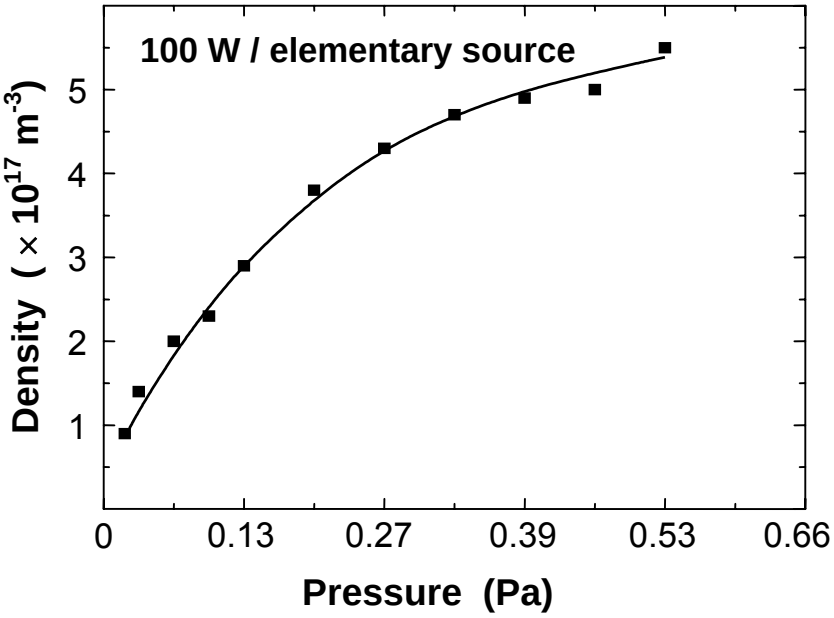

Variations in plasma density as a function of argon pressure; The microwave power per elementary dipolar source is 100 W

In order to increase significantly the plasma density, and to improve the plasma uniformity (not measured with 20 sources), 20 additional elementary sources (2 rings of 10 sources) were implemented on the multi-dipolar plasma reactor. A general view of the reactor with an argon plasma and a top view of the plasma inside the cylindrical chamber are shown in the next

Figures. As in the case of 20 sources, the plasma characteristics have been measured in the centre of the reactor by using a cylindrical Langmuir probe located in the centre of the plasma.
The variation in plasma density as a function of the microwave power per elementary dipolar plasma source is also plotted at the argon pressure of 0.13 Pa (1 mtorr). The behaviour is quite similar as with 20 sources, but, this time, milestone **M2.2 is met** since the **plasma density reaches 10^{12} cm^{-3}** at 150 W of microwave power.
The variation in plasma density as a function of argon pressure is then plotted for a microwave power of 150 W per elementary dipolar source. The plasma density increases when argon pressure increases up to 0.5 Pa (4 mtorr). By comparison with above results, the plasma density is higher than 5×10^{11} cm^{-3} in most of the pressure range investigated.

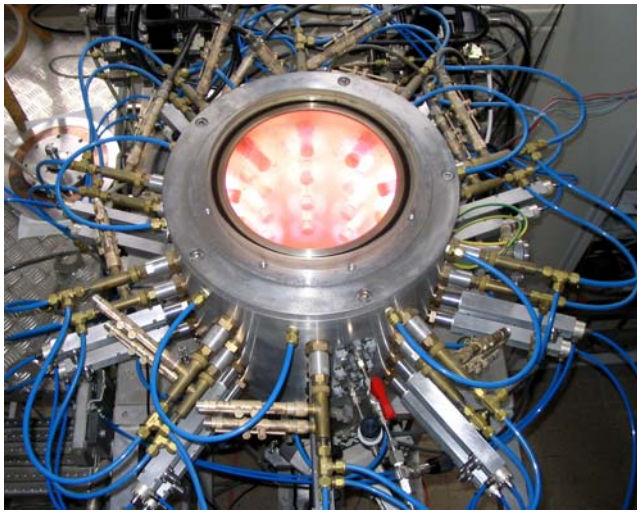

General view of the cylindrical chamber where a nitrogen plasma is produced by 40 dipolar sources (4 rings of 10 sources)

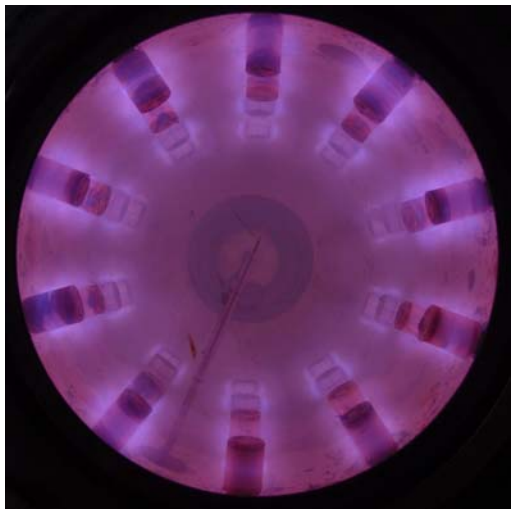

Top view of an argon plasma produced by 40 dipolar sources (4 rings of 10 sources) with a cylindrical Langmuir probe located in the centre of the plasma

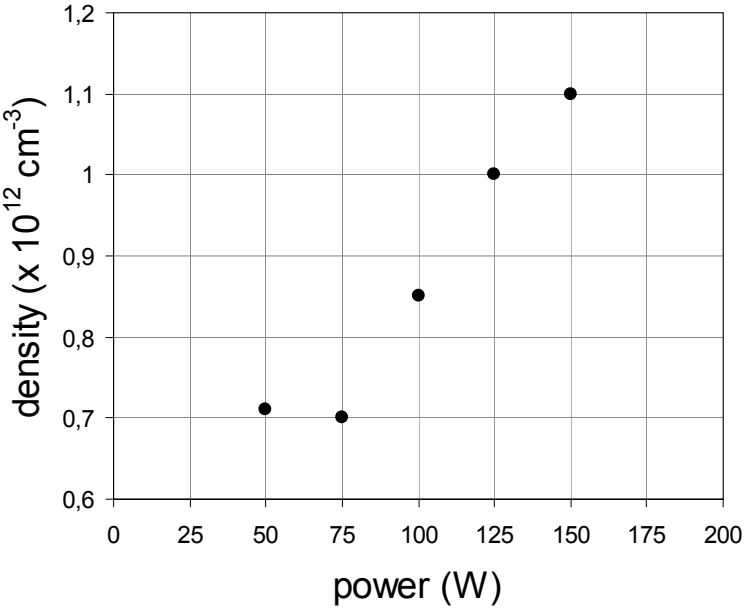

Variations in argon plasma density in the centre of the chamber as a function of microwave power per elementary dipolar source; The argon pressure is 0.13 pascal (1 mtorr)

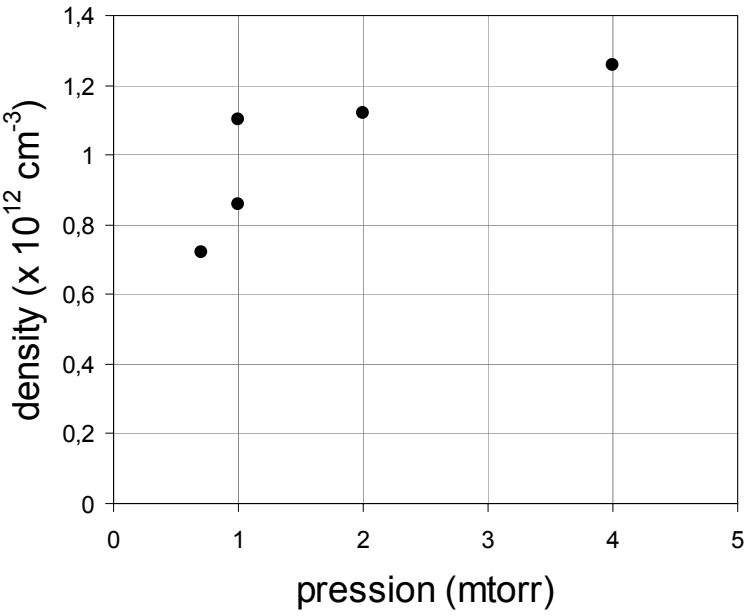

Variations in argon plasma density in the centre of the chamber as a function of argon pressure. The microwave power per elementary dipolar source is 150 W

Matrix plasma reactor

Design of the multi-dipolar plasma reactor. The medium-pressure plasma reactor as been designed as a planar bi-dimensional network of elementary microwave plasma sources. This time, a slice of plasma is produced without magnetic field, via the collisional absorption mechanism. In each elementary plasma source, the plasma is produced at the end of a coaxial

applicator implemented perpendicularly to the plane of the two-dimensional source. The production of a uniform plasma requires that the microwave power is distributed uniformly over the 12 (4 × 3) applicators implemented on this prototype chamber according to a square lattice matrix configuration (lattice mesh of 4 cm). The plasma can be sustained at much higher pressure than in the case of multi-dipolar plasmas sustained at electron cyclotron resonance. With argon, the plasma can operate in the pressure range from 100 mtorr to 10 torr (13 to 1300 Pa). The dimensions of the chamber are 180 mm length, 100 mm width and 30 mm height.
The general views of the plasma reactor are shown in first two Figures. The twelve microwave applicators are implemented on the bottom of the reactor. The chamber cooling, gas inputs, and pumping apertures are distributed over the whole surface in order to favour uniform plasma processing. On the second picture, one can observe the end of the 12 quartz, i.e. the ends of the antennae.

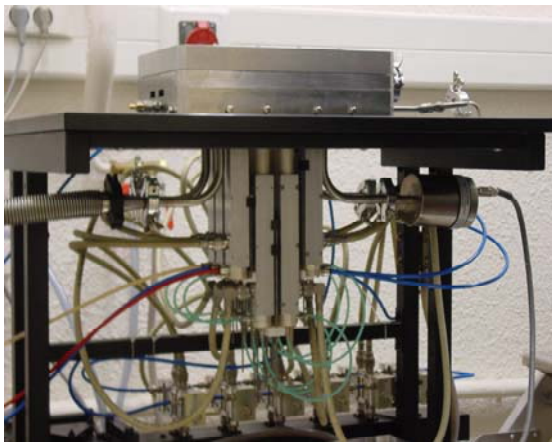

General view of the reactor.

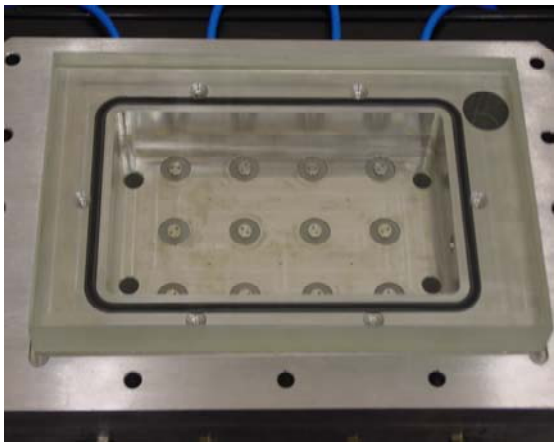

The chamber of the reactor.

Breakdown and sustaining conditions. The microwave power required to achieve the argon breakdown and to sustain the plasma as a function of argon pressure are shown in the figure below. These results indicate that argon plasmas can be sustained at pressures ranging from 7.5 to 750 Pa and that argon breakdown can be obtained above 27 Pa. The minimum microwave powers for argon breakdown and to sustain the plasma correspond to an argon pressure between 75 and 100 Pa, with microwave powers of 450 W and 280 W, respectively.

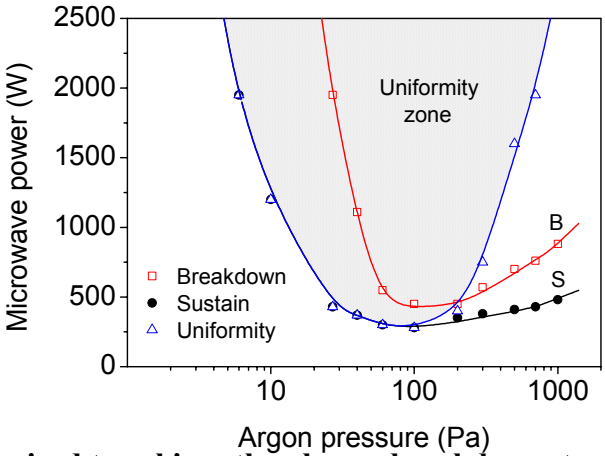

Microwave power required to achieve the plasma breakdown, to sustain the plasma, and to obtain a visually uniform plasma as a function of argon pressure

Visual uniformity. In the low microwave power range and high-pressure range, a localised plasma with azimuthal symmetry can be observed around each coaxial applicator. When increasing the microwave power, the localized plasmas expand and then meet together to produce a sheet of uniform plasma (see photographs below). The area of this uniform sheet is about 200 cm^2 (184 mm × 108 mm) for 12 (4 × 3) microwave applicators.

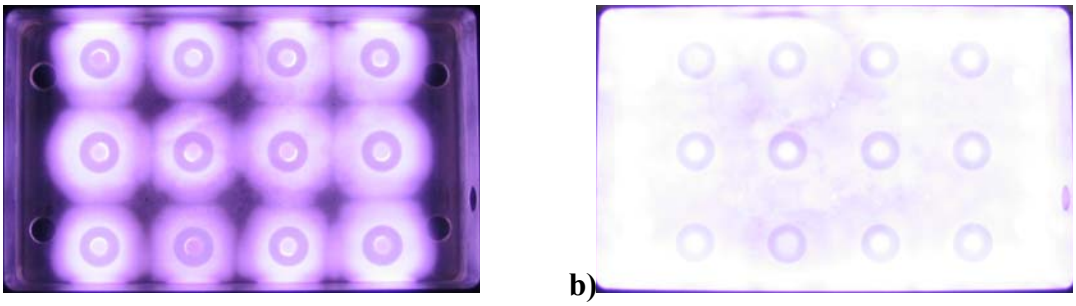

Top view of the planar matrix plasma: (a) at low microwave power, a localised plasma with azimuthal symmetry can be observed around each coaxial applicator; (b) at high microwave power, the localized plasmas expand and then meet together to produce a sheet of uniform plasma

The minimum microwave power needed to obtain visually uniform plasma is plotted in the first figure as a function of argon pressure. The plasma is visually uniform over all the microwave power range when the pressure is lower than 100 Pa. When increasing the argon pressure to 700 Pa, 1950 W microwave power is needed to reach visually uniform plasma. Therefore, with the microwave power available (1950 W maximum), plasmas cannot be uniform at pressures higher than 700 Pa.

The source geometry is presented in Figure (a) below and a schematic cross section of the planar matrix plasma between two lines of elementary sources is shown in (b). The characterisation means used to measure the plasma parameters are movable Langmuir probes.

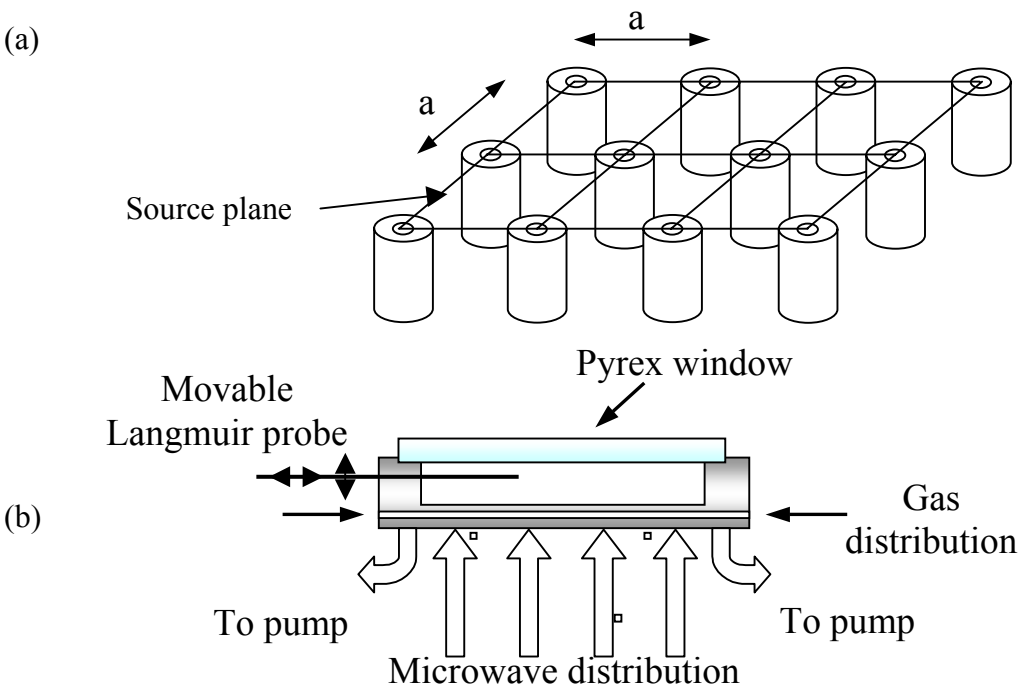

(a) Source geometry with a square lattice mesh a = 4 cm; (b) Schematic cross section of the planar matrix plasma between two lines of elementary sources

Experimental results

Characterization of electric parameters. Variations in plasma density n have been plotted as a function of the distance h from the source plane for argon pressures of 60 Pa and 145 Pa, as shown in the next Figure. For both pressures, measurements were performed above a coaxial applicator and between two coaxial applicators in order to determine the domain of local uniformity at a microwave power of 1200 W (100 W per applicator). When the distance from the source plane is higher than 15 mm, the plasma becomes locally uniform for both pressures to form a planar sheet of plasma. This distance of 15 mm is less than half the lattice mesh of the matrix network. It can be also observed that the plasma density is higher close to the source plane when the argon pressure is 60 Pa. The domain of local uniformity as a function of the distance being defined by the above measurements, we have chosen to measure the long-range plasma uniformity at a distance of 20 mm from the source plane.

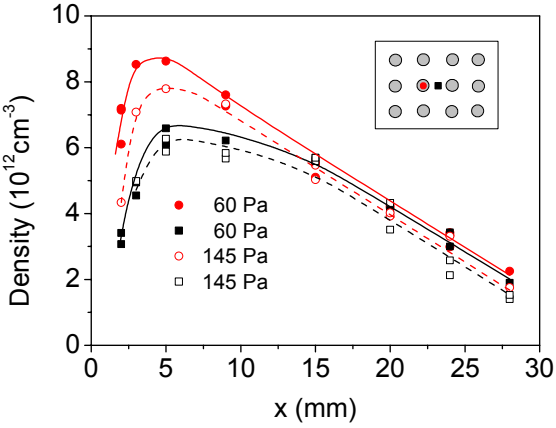

Variations in plasma density n as a function of the distance h from the source plane for a microwave power of 1200 W (100 W per applicator) and two argon pressures: 60 Pa (full circles and squares) and 145 Pa (empty circles and squares); Circles and squares represent measurements performed above the applicator and between two applicators, respectively

Variations in plasma density along the planar chamber are shown in the next Figure for argon pressure and microwave power of 60 Pa and 1200 W, respectively. This plot shows that the plasma uniformity is rather good. The mean plasma density is 4.1 × 10^{12} cm^{-3} and decreases sharply near the edge of the chamber, after the last row of applicators. In the central part of the plasma inside the peripheral applicators, the plasma exhibits an excellent uniformity with a standard deviation Δn such than Δn/n is less than ± 3.5 %.

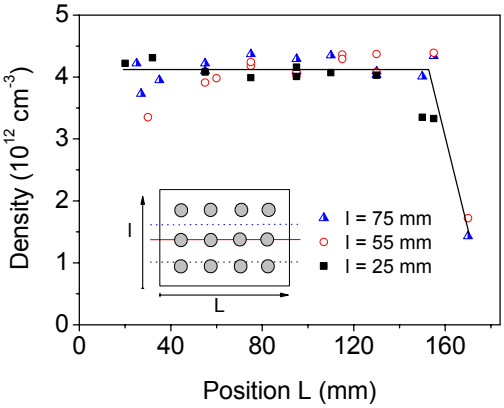

Variations in plasma density n along the planar chamber at the distance h = 20 mm from the source plane. Argon pressure and microwave power are 60 Pa and 1200 W

In the central region of plasma uniformity, the plasma density is shown as a function of the microwave power distributed over the 12 applicators for several pressures, as shown in the Figure below. At constant pressure, the plasma density increases linearly with the microwave power. For example, at 100 Pa, the ion density increases from 0.5×10^{12} to 7.3×10^{12} cm^{-3} when the microwave power increases from 500 W to 1800 W.

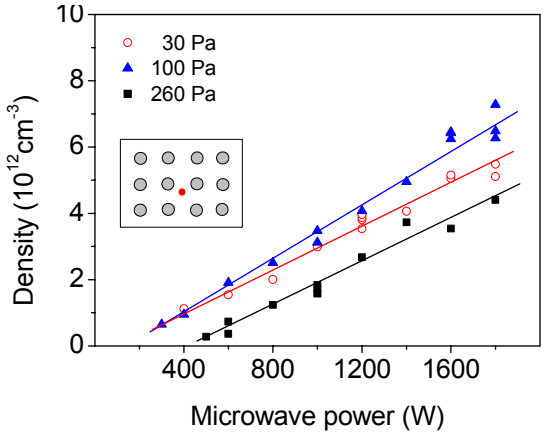

Variations in plasma density as a function of the microwave power for several argon pressures

The plasma density variation with argon pressure is presented in the next Figure for several microwave powers. An important feature is that the maximum density (at a distance h = 20 mm from the source plane) is obtained for an argon pressure between 75 and 100 Pa.

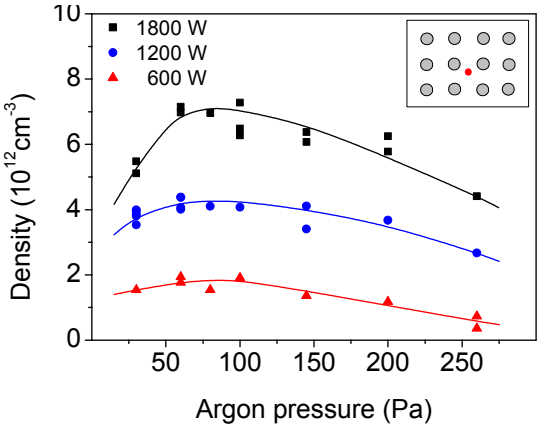

Variations in plasma density as a function of argon pressure for several microwave powers

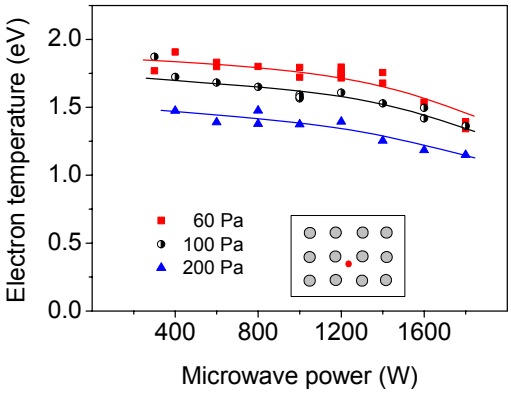

Variations in electron temperature T_e as a function of the microwave power for several argon pressures

Variations in electron temperature as a function of the distance from the source plane, above an applicator and between two applicators, are then presented in the next Figure for an argon pressure of 60 Pa and a microwave power of 1200 W. The electron temperature T_e is almost constant in the volume of the plasma (for the x values between 5 and 30 mm, beyond the abscissa of maximum of plasma density) with a value around 1.8 eV. Between 0 and 5 mm, i.e. close to the source plane where the microwave electric field is applied, the electron temperature increases sharply towards the source plane and reaches about 4.5 eV at the distance x = 2 mm.

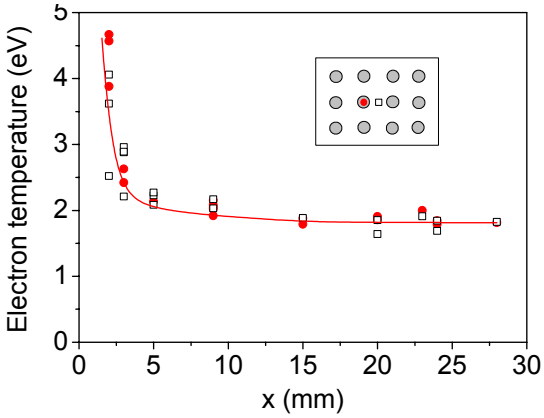

Variations in electron temperature T_e above an applicator (red circles) and between two applicators (empty black squares) as a function of the distance from the source plane. The microwave power is 1200 W and the argon pressure is 60 Pa.

1.4.2.3 Task 2.3. Development of coating processes (**EPM**, **HEF R&D**, **UNIBA**, **ICMSE**, **EADS**)

Sub-task 2.3.1 Coupling of PACVD microwave plasma and DC pulsed biasing (**EPM**, **HEF R&D**)

Deposition in matrix plasmas (EPM)

This work was performed in order to estimate the capabilities of matrix plasmas in terms of deposition rate and uniformity using TMS as the precursor gas and oxygen or nitrogen in order to test the incorporation of oxygen or nitrogen in the layer. The layer composition will be obtained after characterisation by **ICMSE**. In Task 2.2, the characteristics of argon plasmas obtained in the matrix plasmas were extensively studied. In the case of PACVD deposition of SiCOH films, it is clear that the plasmas produced from TMS / O_2 mixtures may behave very differently. In fact, the behaviour of TMS plasmas was very similar to that of argon plasmas. In contrast, as shown in the two Figures below, the behaviour of oxygen plasmas quickly appeared very different from argon plasma behaviour. Therefore, before plasma deposition study, an investigation of the characteristics of oxygen plasmas was undertaken. For this reason, the results below includes three parts, the first one on the experimental study of oxygen plasmas, the second one on deposition of SiCOH films, and the last one on deposition of SiCNH films.

Characterisation of oxygen plasmas (EPM). As shown in the two photographs of oxygen plasmas, the plasmas do not appear uniform even at the highest microwave powers. In fact, as can be seen on the oblique view of the second Figure, a luminous stream appears at the end of each applicator. This phenomenon is more visible at higher microwave powers, when the plasma density becomes important. Such plasma streams can be attributed to negative ions O^-

and O_2^- trapped in front of the applicators. In fact, ambipolar diffusion will accelerate the positive ions and decelerate the electrons and negative ions to maintain plasma neutrality. Thus, negative ions remain trapped near their creation region.

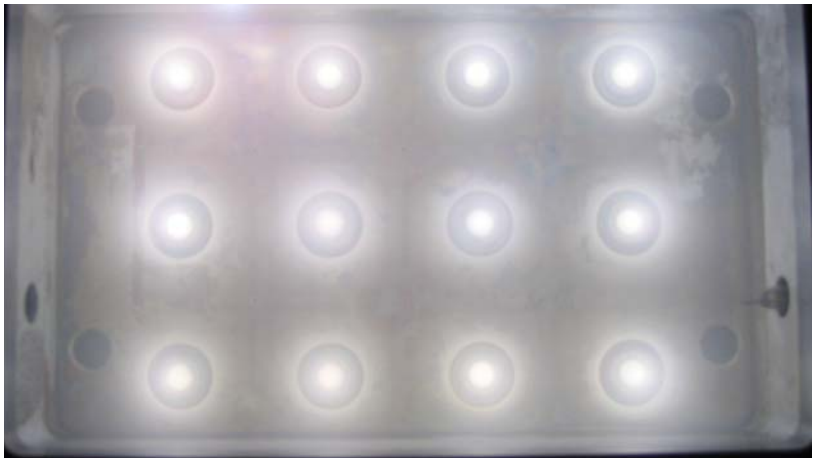

Top view of an oxygen plasma (P = 1950 W, p_{O2} = 7 Pa.)

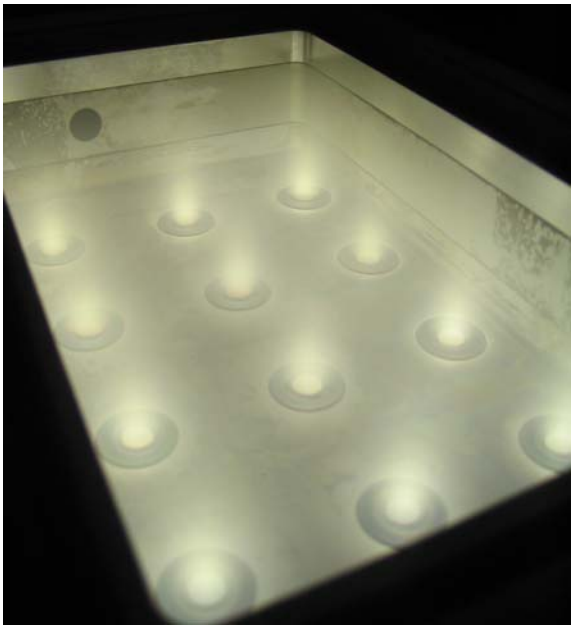

Oblique view of an oxygen plasma (P = 1200 W, p_{O2} = 19 Pa)

It must be noticed that the plasma density varies between 10^{11} and 10^{12} cm^{-3}, i.e. nearly one decade less than the density of argon plasmas.

Deposition of SiCOH films (EPM). In order to deposit SiCOH films it is mandatory to incorporate oxygen and therefore to generate plasmas from TMS - O_2 gas mixtures, where TMS (tetramethylsilane) is the organic precursor of silicon and carbon. The next figure shows a general view of an oxygen plasma, as described above. The bottom figure shows a top view of a plasma produced from an O_2 – TMS gas mixture.

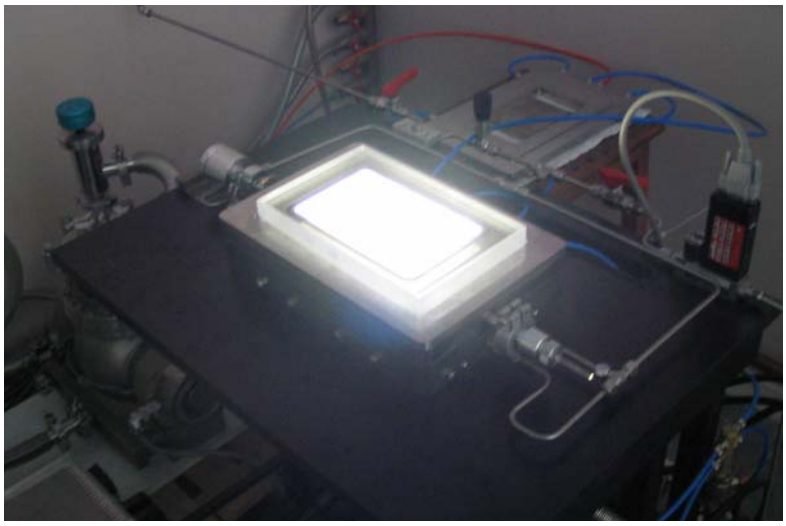

Photo of an oxygen plasma (P = 1950 W, p_{O2} = 7 Pa).

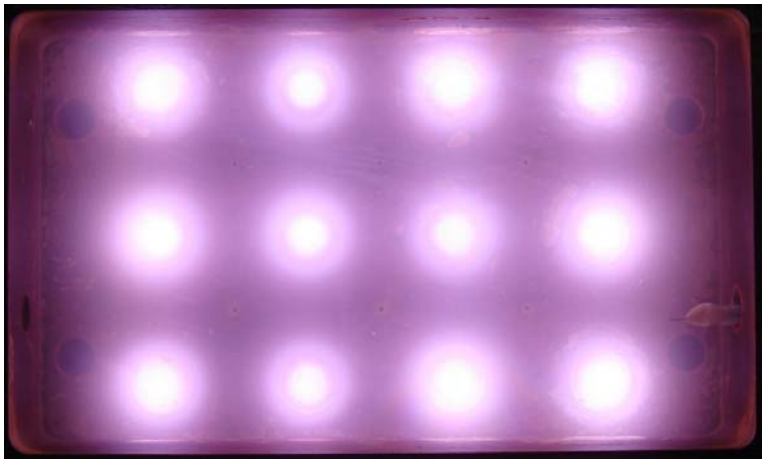

Top view of an O_2 - TMS plasma.

During the deposition process, the silicon wafers and the substrates are placed on a substrate-holder located between two rectangular windows seen on the next figure.

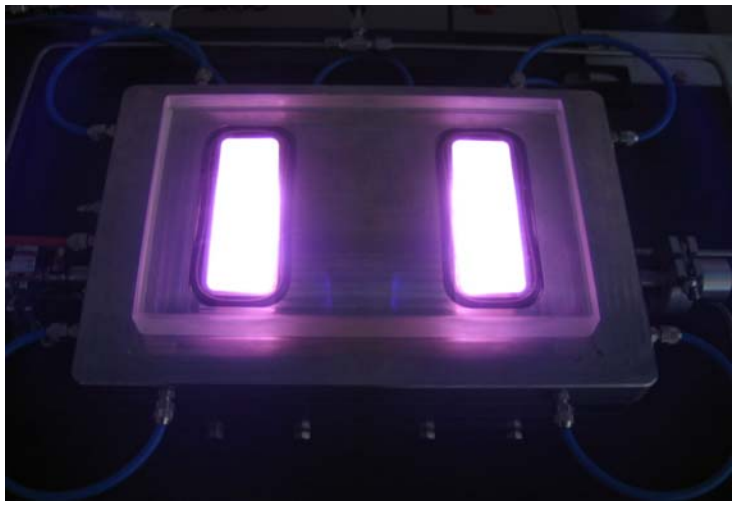

Photo of the reactor during PACVD of SiCOH films from an O_2 – TMS plasma

The next figure shows the deposition rate as a function of microwave power for a gas mixture 1/3 O_2 - 2/3 TMS at a total pressure of 23 Pa. As can be seen, the deposition rate is of the order of 1µm / min (up to 75 µm / hour), i.e. practically **one decade higher than required in milestone M2.1**. This result justifies, if necessary, the interest to operate at intermediate pressures in PACVD processing.

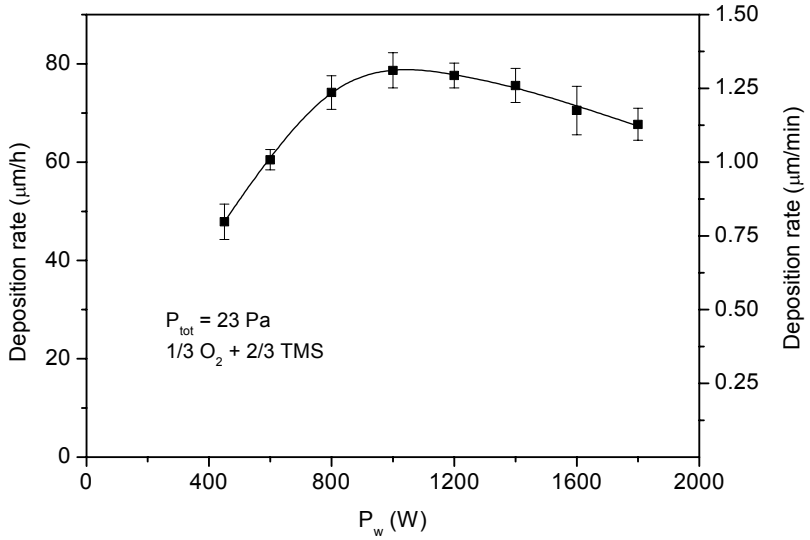

Deposition rate as a function of microwave power in a O_2 – TMS plasma.

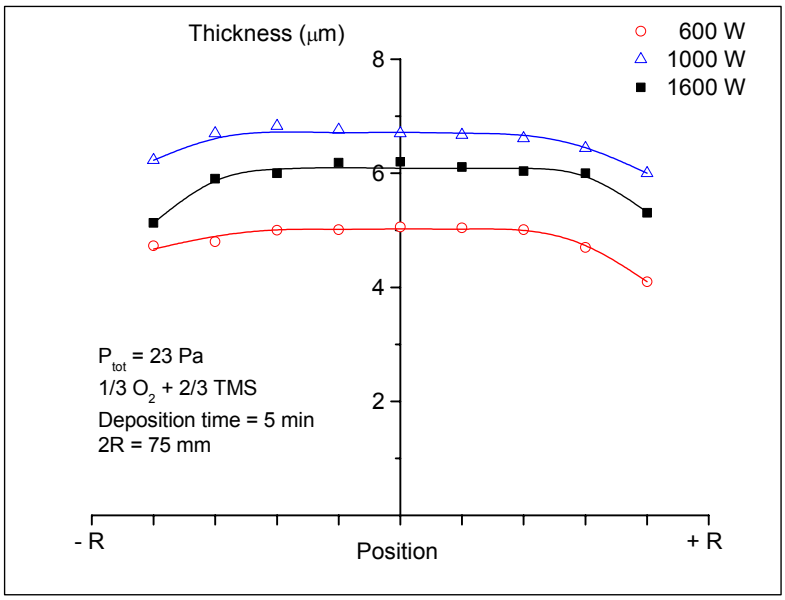

Thickness uniformity of SiCOH films deposited from O_2 – TMS plasmas.

The above figure shows the uniformity of the thickness of deposited layers, and we can notice that the uniformity is quite good in the central part of the wafer, and this, for any operating conditions. Photos of deposited films of thickness between 4 and 7 µm are presented in the next figure. The colour does not change significantly with microwave power or total pressure in the power and pressure ranges investigated.

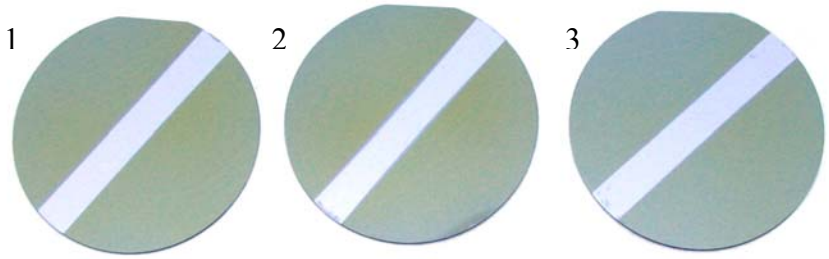

p_{O2} = 7,7 Pa	p_{O2} = 7,7 Pa	p_{O2} = 10 Pa
p_{TMS} = 15,3 Pa	p_{TMS} = 15,3 Pa	p_{TMS} = 20 Pa
P = 800 W	P = 1200 W	P = 1000 W

Photos SiCOH films deposited from1/3 O_2 – 2/3 TMS gas mixtures;Film thicknesses are between 4 and 7 µm

Deposition of SiCNH films (EPM). The two next figures show the deposition rate of SiCNH films as functions of microwave power and partial pressure of nitrogen. As for SiCOH films, the deposition rate is of the order of 1 µm / min, i.e. a deposition rate of high interest for industrial applications. However, an interesting behaviour is the decrease in deposition rate when increasing the nitrogen partial pressure, at a constant TMS partial pressure.

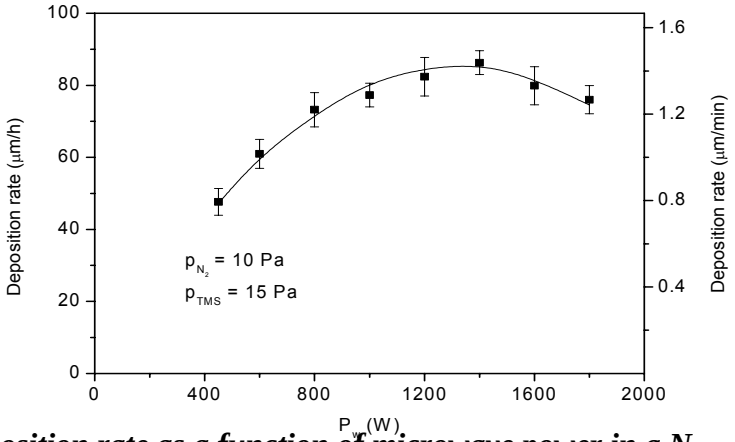

Deposition rate as a function of microwave power in a N_2 – TMS plasma.

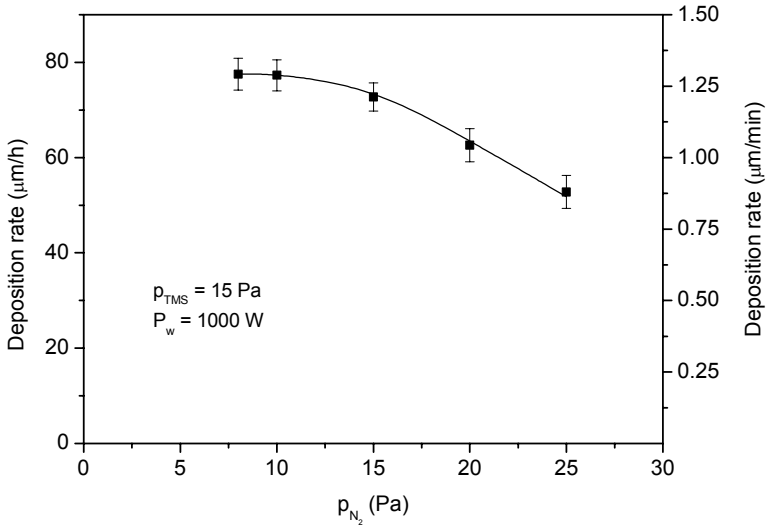

Deposition rate as a function of nitrogen partial pressure in a N_2 – TMS plasma

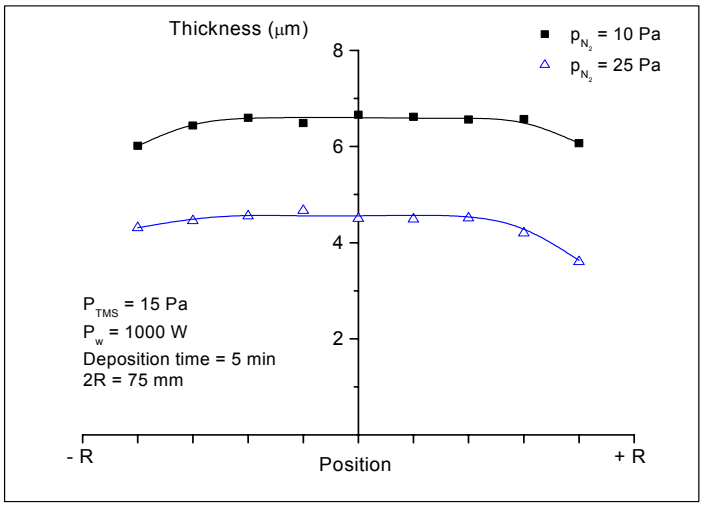

Thickness uniformity of SiCNH films deposited from N_2 – TMS plasmas.

The above figure shows the thickness uniformity of the SiCNH films, as measured from sample 2 below obtained at a given TMS partial pressure. When the partial pressure of nitrogen increases, the colour of the films varies from a grey-blue colour to a golden colour. Also, microwave power seems to influence the colour of the film, suggesting a modification in film composition. XPS analysis will provide indication on nitrogen incorporation in the SiCNH films.

Chemical composition of SiCOH and SiCNH films (ICMSE)

Sample	Power	P N_2	Atomic %				ratio	ratio
	W	Pa	Si	C	O	N	Si/C	Si/O
3,5	**1000**	**0**	50,1	23,3	26,7	0,0	2,1	1,9
4,5	**450**	**0**	49,8	25,1	25,1	0,0	2,0	2,0
6,5	**1000**	**25**	62,7	12,0	23,8	1,5	5,2	2,6
7,1	**600**	**10**	67,2	13,5	17,7	1,6	5,0	3,8
6,1	**1000**	**10**	67,6	10,8	20,2	1,4	6,3	3,3
7,2	**1600**	**10**	61,6	10,6	25,7	2,1	5,8	2,4

Chemical composition of EPM samples prepared by matrix MW-PACVD

ICMSE has analysed some samples of SiCOH and SiCNH prepared by EPM using a matrix microwave plasma assisted CVD and O_2 + TMS *vs.* N_2 + TMS mixtures as gas precursors. The objectives were to obtain information about the matrix plasma reactor and the influence of synthesis conditions on the coating characteristics. The synthesis conditions are listed in the next table together with the chemical composition obtained by XPS after 2 min of Ar ion bombardment for cleaning the surface sample (see also enclosed graph).

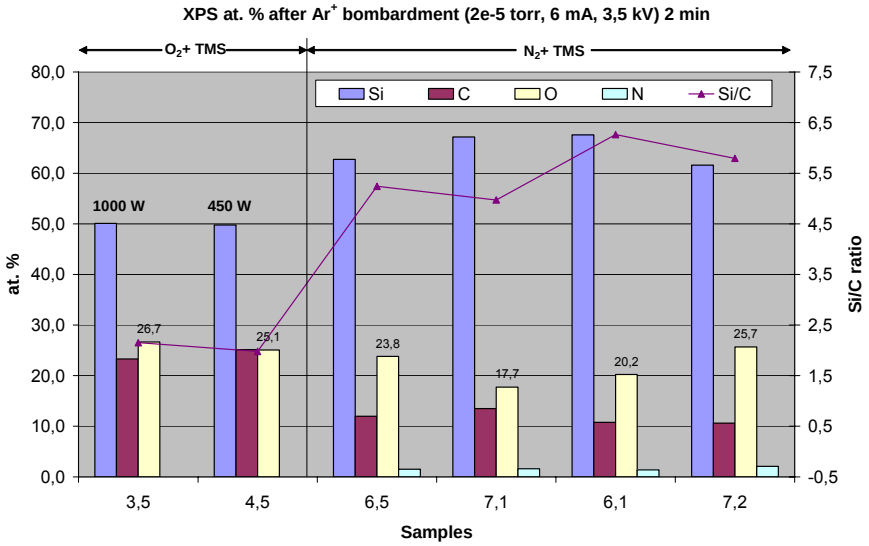

Chemical composition for SiCOH and SiCNH fims prepared under different plasma conditions

These are the main conclusions obtained:

a) Influence of the synthesis procedure O_2 + TMS vs. N_2 + TMS

The first conclusion is the higher Si incorporation in the samples prepared with nitrogen, and smaller C at. % (half of the first series). This can be seen in the Figure 1 by plotting the Si/C ratio.

The incorporation of N in the film composition is very low (< 2 %) probably due to the high stability of the N_2 molecule. Other N-precursors as NH_3 or volatile N-containing organic compounds should be used.

The oxygen content does not change too much if O_2 is used or not, as gas precursor, the values range from 18 to 27 %. The O_2 background pressure in the chamber and the known tendency of silicon atoms to trap water vapour molecules should be the responsible of that. Also, it must be taken into account the high surface sensitive character of XPS technique.

b) Influence of the power

O_2 + TMS: practically identical results (450 and 1000 W).

N_2 + TMS: slight increase of the nitrogen content (1.4 to 2.1 %). Maybe, the most significant feature is the increment of the oxygen content (contamination) with the increase in plasma input power. In the next figure, the Si/C and Si/O ratios are plotted versus the microwave power for partial pressures of N_2 and TMS of 10 and 15 Pa, respectively. It is observed that the Si/C ratio exhibits a maximum between 600 and 1600 W what demonstrates the influence of the plasma power conditions on the chemical conditions. This maximum may be correlated with the optimum found in the film deposition rate around 1400 W.

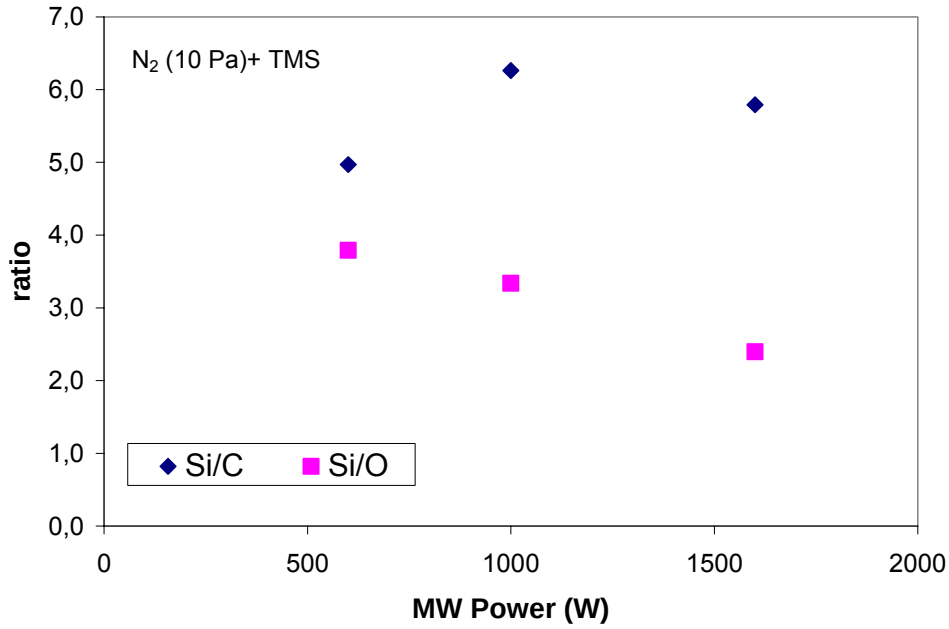

Values of the Si/C and Si/O ratios as a function of the microwave power (synthesis conditions PN_2 = 10 Pa and PTMS = 15 Pa)

c) Influence of N_2 pressure (N_2 + TMS series)

There is no difference in N content using 10 or 25 Pa of N_2, the values are always around 1.5 %.

In summary, it appears that the plasma power is influencing more the chemical composition than precursor pressures. Higher power lead higher O and N (very small) contents. Another N-precursor should be used to introduce N satisfactorily into the film including Si-N and/or C-N bonds.

Coupling of PACVD microwave plasma and DC pulsed biasing (HEF)

The evaluation of the new process technology was carried out on DLC processes, as such coating material is rather well known when elaborated using classical diode PACVD processes. The influence of the microwave power, reactive gas flow and bias voltage was studied. These 3 parameters are the most influent ones.

Experiments have shown that the deposition rate is directly proportional to the acetylene flow (= pressure), keeping the other parameters constant. This first results immediately illustrates the difference with conventional PACVD process, i.e. the processes where the plasma is generated by the part biasing. With conventional processes, the increase of gas pressure generally increases the deposition rate but not in a proportional way as the increase of pressure also changes the ion energy and the power of the plasma. With the ECR sources, the change of pressure does not change the power in the plasma which is independent.

The increase of microwave power does not change the deposition rate above a threshold value of power, while bias current is increased proportionally. It can be explained by a full dissociation of the gas in the environment of the ECR sources at low power. Additional power cannot create more dissociation but can create additional ions.

Finally, the most important parameter that influences the properties of DLC is the bias voltage which defines the energy of the ion bombarding the growing film. The new PACVD technology allows elaborating a much wider field of coating materials, especially less hard

coatings which show a higher toughness. At low ion energy, coatings with hardness around 400 kg mm^{-2} are achieved. The increase of ion energy induces a strong increase of hardness and Young Modulus which tend to reach a maximum for ion energies comprised between 300 and 400 eV. The graph below shows these evolutions and the domain that can be accessed by conventional PACVD.

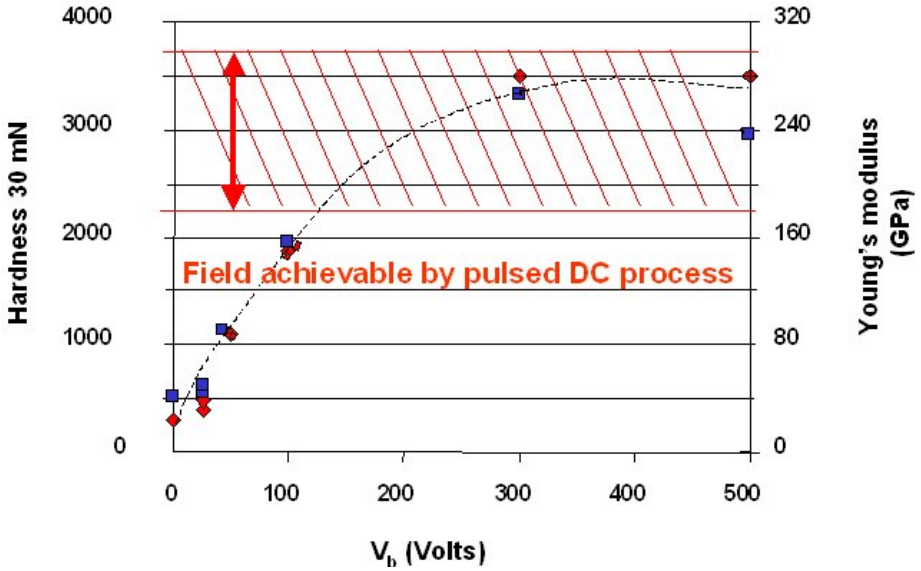

As mention previously, the field of material properties obtained by the new technology is wider. The picture below shows a drop of water on a DLC elaborated at - 40 V pulsed DC. This coatings is water repellent, the water contact angle is around 110°.

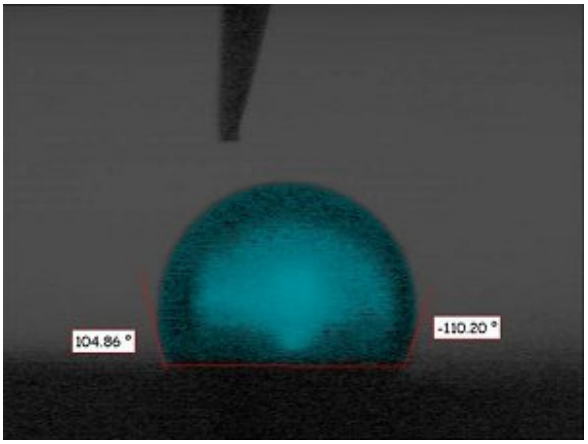

It is interesting to mention that some coatings were deposited in static mode in front the ECR sources. The deposition rates have reached up to 12 µm/h. This value is higher than the target in milestone 2 (7 µm/h). The deposition rate in rotation mode is lower and depends on the quantity of parts on the substrate holder, it is generally comprised between 1 and 2 µm/h. The deposition temperature can be adjusted by decreasing bias voltage and microwave power, but it also means to change the properties of the coatings.

Sub task 2.3.2 Pulsed DC PACVD alone

In this part, HEF has studied some corrosion protective coatings deposited in pulse DC PACVD. The plasma is generated by applying a high pulsed DC negative voltage on the substrate holder. The most important parameter identified is the ratio of NH_3 to TMS flow. Increasing the ammonia flow, induce a decrease in hardness and Young modulus as illustrated in the following graph.

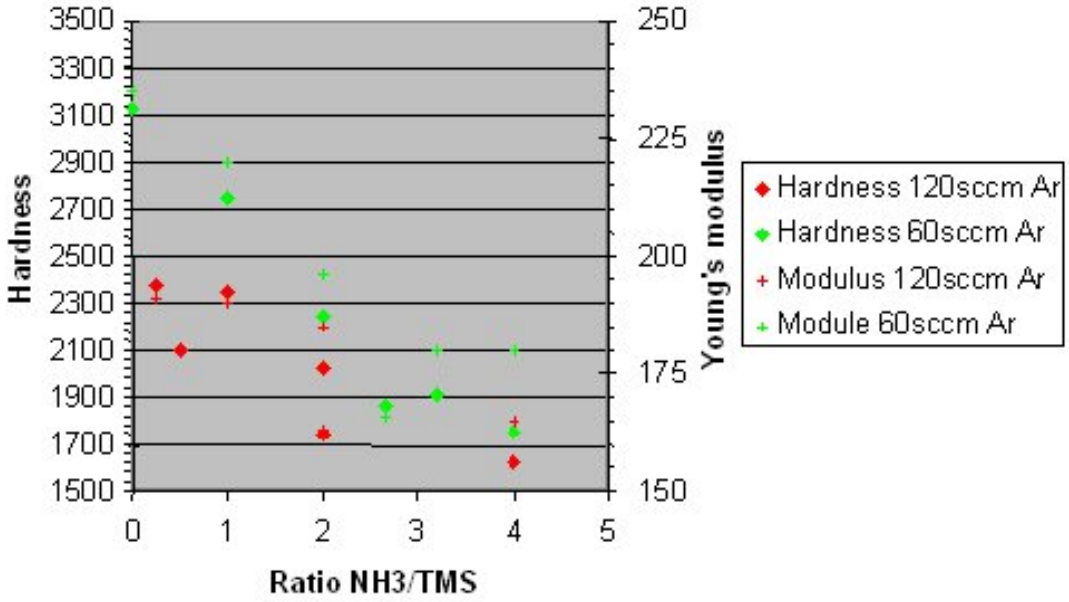

The low nitrogen containing coatings have hardness close to the one of DLC, while the softest have hardness close to CrN. These coatings were deposited on high speed steel samples. They were characterised in salt spray test. The next graph shows the corrosion protection of different coatings as a function of the nitrogen content in the films.

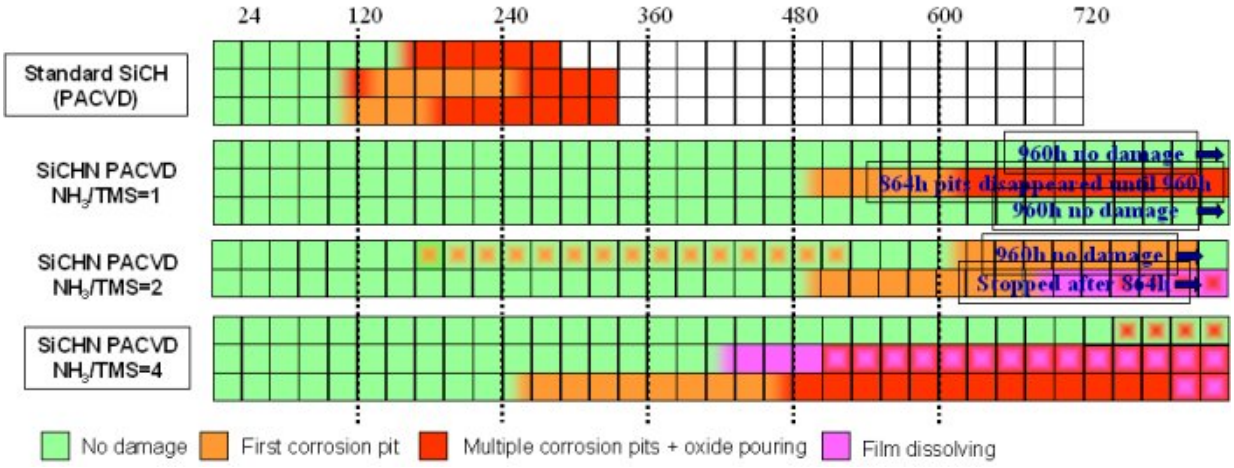

It is interesting to note that coatings deposited without nitrogen can provide small protection efficiency. The addition of nitrogen in the coating allows a drastic improvement of corrosion protection. The first corrosion pit appeared after 480 h for 1 of the 3 samples elaborated at NH_3/TMS = 1 and no corrosion was observed on two other samples up to 960 h. It seems that further increasing nitrogen content reduces the corrosion protection efficiency. A patent was

applied by HEF. It covers the SiCHN coatings showing the best corrosion protection efficiency.
A second family of coatings was also studied. They are elaborated using mixtures of oxygen and organo-silicon precursors (TMS, HMDSO). The interest of the SiO_x coatings concerns both corrosion protection and optical transparency. The corrosion protection by the SiO_x coatings

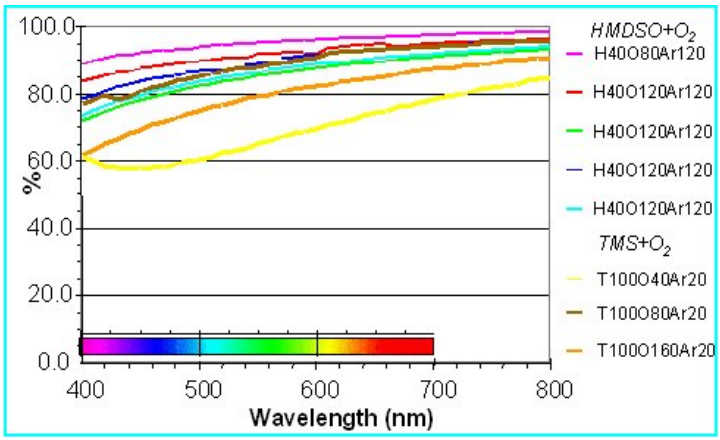

deposited by HEF has not reach the level of corrosion protection by coatings elaborated by UNIBA. The first pits were observed after only 24 h. It can be easily explained by the very small thickness of the coatings deposited by HEF. The thickness was minimized to prevent interference fringes to appear. The coatings were also characterised by optical transparency. The best coatings had transparencies over 90% as it is illustrated below.
A lack of oxygen gives some coatings which are less transparent. This is the case of the coatings deposited by using TMS which is more carbon rich than HMDSO. The second important parameter concerns the film thickness. As they are deposited on metals to protect them, the reflection of light on their surfaces induces the formation of light interferences and coloration appears which depends on thickness and refractive index.

Sub-task 2.3.3. PACVD RF and RF pulsed biasing (**UNIBA**, **ICMSE**, **EADS**, **POLITO**)

Two different Plasma-CVD reactors were used at EADS for the deposition experiments. For the deposition of the Si-O-N-C coatings the reactors had to be modified. In particular new gas supplies for the N-containing gases were built up.

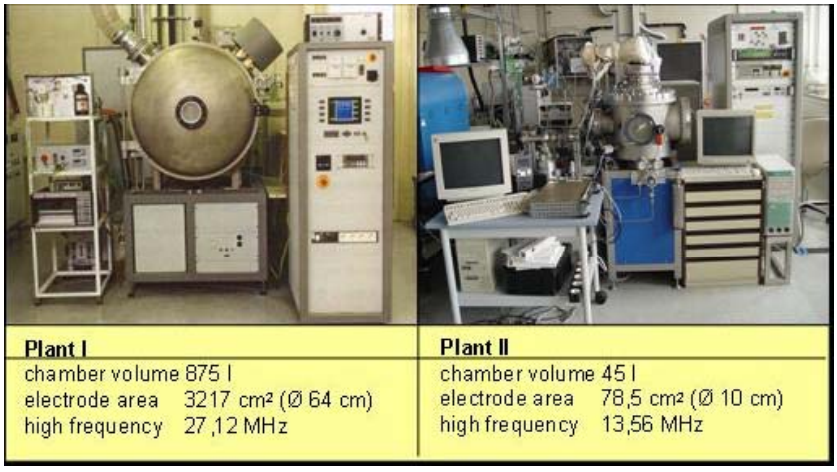

Plasma deposition plants at EADS

Three different precursor gases were used for the coating depositions:
- Hexamethyldisiloxane (HMDSO);
- Hexamethyldisilazane (HMDSN);
- Bis-dimethylamino-dimethylsilane (BDMADMS);

while additional nitrogen sources N_2 and NH_3 were investigated. With oxygen the residual carbon content of the coatings was reduced and therefore the oxidic character of the coatings increased. Parameters varied in the deposition processes have been gas flow, plasma power and substrate temperature.

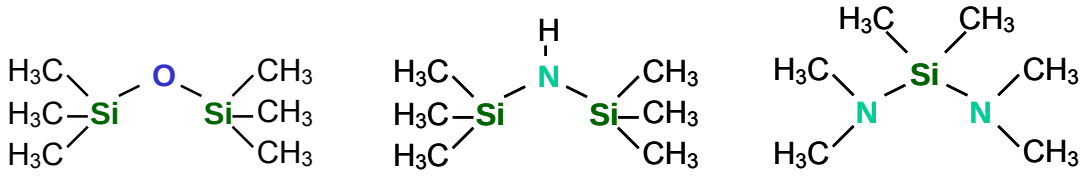

Molecular structures of HMDSO (left) HMDSN (middle) and BDMADMS (right)

Summarising the results, it can be said that the addition of N_2 does not add nitrogen to the coatings, independently of the other plasma parameters. This is only possible when NH_3 is used as an additional nitrogen source. Maximum N contents reached at EADS in the parameter range investigated were in the range of 20 at %.
In case of HMDSO as precursor and if oxygen is used as additional gas, higher plasma powers increase the oxidic character of the coatings. The same is true for higher substrate temperatures.

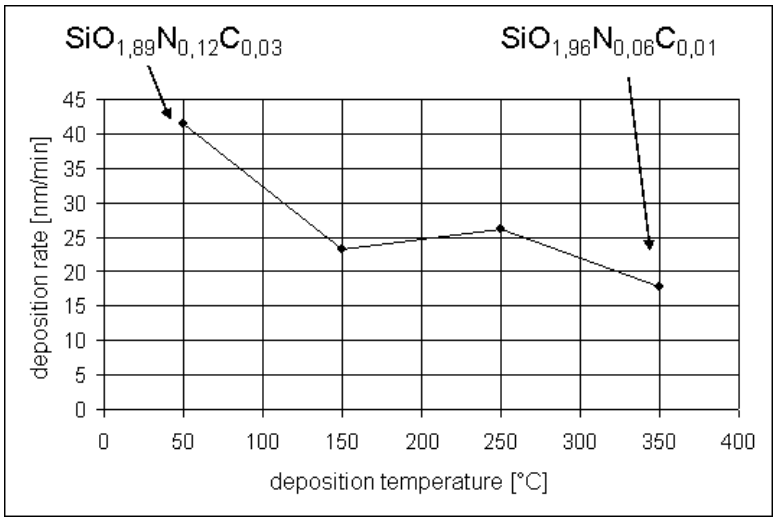

Influence of deposition temperature on deposition rate (plant II, HMDSN + N_2 + O_2)

With increasing $T_{Substrate}$ besides a decrease in deposition rate an increase in the oxygen content in the coating can be detected when HMDSN is used as precursor gas and oxygen is used as reactive gas.
The same decrease in deposition rate at higher substrate temperatures can be found with BDMADMS as precursor.

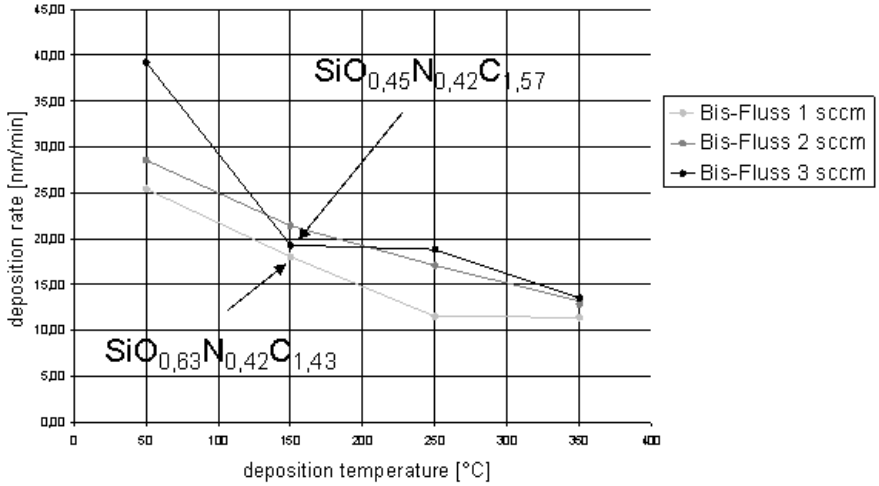

Influence of deposition temperature on deposition rate (plant II, BDMADMS)

1.4.2.4 Task 2.4. Development of cleaning process (**EPM**)

For confidential reasons, the reactor cleaning process proposed and developed in the MATECO project is not available at the moment since a patent has been applied on 2006. After validation and extension of the patent, discussions will be opened in order to negotiate licences.

1.4.3 WP Leader Assessment and Conclusions

Assessment

At the end of the MATECO project, the milestones and deliverables related to WP 2 have been fulfilled beyond expected and the work performed by the partners involved in the different tasks and sub-tasks have been done in due time with positive results, in terms of process understanding, plasma and process performance, plasma and process modelling, reactor cleaning and characterization of layers in terms of corrosion protection.

The partners in this workpackage were complementary, such that they have covered all the scientific and technical aspects involved in WP 2. At the end of the project, all tasks are finished, and all of them with successful results. In particular, the development of a reactor cleaning process represents a challenge, since, until now, no satisfactorily and friendly processes were available at the industrial level.

In WP 2, two theses were finished and successfully defended at the very end of MATECO project. A solution to the key problem of reactor cleaning at industrial level has been proposed and patented and some of the scientific results obtained in WP 2 have already been presented in various conferences or published in international journals.

Conclusions

The studies performed in WP 2 were of high importance for achieving a better knowledge of mechanisms of plasma production, plasma deposition as a function of plasma parameters.

In particular, the results obtained by **UNIBA** and **POLITO** in Task 2.1.1 can be favourably used for the in-situ control of Si-based film deposition. The deposition kinetics and physico-chemical properties of the deposited films have been investigated as functions of plasma operating and deposition parameters (RF power, coupling mode, pressure, gas composition, precursor gases). The FTIR analyses provide well correlated results and OES allows in situ

control of film deposition, so that process transfer in any reactor will be facilitated. Task 2.1.2 by **EPM** concerns the modelling of the plasma production in dipolar elementary plasma sources excited by microwaves at ECR. The mechanisms proposed have been modelled via numerical simulation and validated from different characterization techniques such as Langmuir probes, OES, and microwave diagnostics.
In task 2.2, a new concept of plasma source based on the distribution of microwaves on coaxial applicators has been applied by **EPM**. In the low pressure range, dipolar elementary plasma sources, as studied in Task 2.1.2, have been distributed uniformly around a cylindrical reactor. Plasma densities obtained in argon are higher than 10^{12} cm^{-3} at pressures above 1 mtorr (0.13 Pa). This type of source, which can be scaled up without limitation to very large dimensions, has been implemented with success on DC pulsed reactors of **HEF**.
In the medium pressure range, a new kind of plasmas, the so-called matrix plasmas, have also been developed by **EPM**. These plasmas are also based on the distribution of microwaves on magnetic free coaxial applicators on bi- or tri-dimensional networks. The planar source, which has been designed in the present study, has been tested and characterised in order to obtain a good understanding of plasma production mechanisms. These matrix plasma sources can generate a sheet of uniform plasma of densities between 10^{12} and 10^{13} cm^{-3} over a wide range of argon pressure, from 7.5 to 750 Pa. This type of source, which can be scaled up without limitation to very large dimensions, has been applied to processes such as PACVD deposition.
Tack 2.3 deals with deposition performance of Si-based films, particularly in terms of deposition rate obtained in different plasma reactors and with various gas precursors, driven either by **EADS** for RF capacitive discharges, or by **HEF** and **EPM** for DC pulsed discharges and microwave plasmas. In particular, the objective of deposition rates higher than 7 µm / h has been easily reached by **HEF** on static substrates and by **EPM** in matrix plasmas where the deposition rates passed 1 µm / min (> 60 µm / h) under any operating conditions, and this, together with a rather good uniformity. However, as shown by **HEF**, such high deposition rates generally produce sharp increases in substrate temperature not compatible with deposition on polymers. Physico-chemical characteristics of the films were analysed by **UNIBA** and **POLITO** while other film properties (adhesion, roughness, optical properties, micro-hardness, morphology …) as functions of operating parameters were determined and reported by **HEF**.

1.5. WP 3: Materials for corrosion resistance coating (WP Leader: UNIBA)

WP Leader	UNIBA
Participants	EADS – POLITO – ICMSE - TEFAL

1.5.1 Objectives

The main objective of WP 3 is to study the influence of the chemical composition of the SiOCN coating on their basic properties (morphology, structure, electrical, optical, mechanical, etc).

1.5.2 Progress towards objectives

1.5.2.1 Task 3.1: Definition of materials for coating requirements for achieving suitable properties and requirements and specifications of end-users (**EADS**, **HEF**, **CRF** and **TEFAL**)

EADS has given the specification for the coatings to be developed in this project. The aeronautic parts to be coated are bolts. These high precision components are prone to fretting corrosion due to vibrations. The requirements have been deduced from the special forces acting on the bolts.
With the input of the end-users (EADS, HEF, TEFAL, CRF) the Deliverable 3.1 entitled: "Report on the material requirements for achieving suitable properties and requirements and specifications of end-users" has been written and distributed in July 2004.

1.5.2.2 Task 3.2: Preparation of substrates for coating (**EADS** and **HEF**)

The following substrates were considered for the project.

End user	Material	Type of sample
EADS	TA6V Steel	Flat samples, fretting test samples, bolts
CRF	100Cr6	Shims
TEFAL	Stainless steel AISI304 AISI 436 Al alloy 5005	Flat samples Household devices elements
HEF	X85WmoCrV 6-5-4-2 42CrMo4 Ag coated polysulfone	Flat samples Gas spring axes, flat samples Flat samples

Metal substrates were prepared as defined in WP 1, to eliminate small roughness favourable to corrosion initiation
EADS has prepared and distributed low carbon steel and TiAl6V4 samples of different sizes (2D and 3D) to the partners for coating.

EADS 3D samples (diameter 28 mm, height 12 mm)

The roughnesses and the coefficients of friction, measured against a steel ball, of plane substrates can be seen from the following table.

	Low carbon steel (final cutted)	TiAl6V4 (final cutted)	TiAl6V4 (sheet material)
Roughness Ra [µm]	0,2	0,7	0,4
Roughness Rz [µm]	1,6	3,5	2,7
Coefficient of friction	0,5	0,4	0,4

Ball on disc test apparatus

To evaluate the best pre-treatment parameters in oxygen plasma a test series with different pre-treatment times was performed. As an indication of the surface cleaning and activation the water contact angle was measured immediately after the removal of the substrates from the plasma chamber.
Already short treatment times result in a significant decrease of the water contact angle. After 1 min values of 20° for steel and 10° for titanium can be measured. Longer pre-treatment times only give a small further reduction of the contact angle.

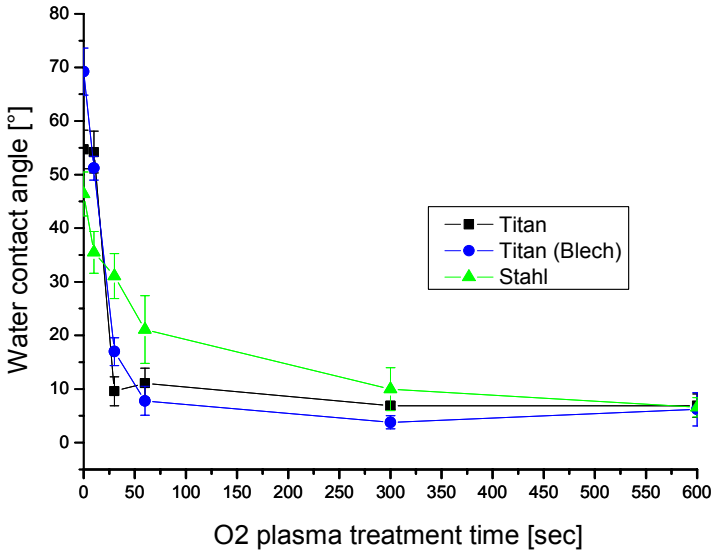

Influence of pre-treatment time in oxygen plasma on water contact angle

Therefore at EADS a 1 min oxygen plasma pre-treatment was selected before coatings the metallic substrates with the $SiO_xN_yC_z$ layers.

1.5.2.3 Task 3.3: Preparation and characterisation of a first set of materials (**UNIBA**, **ICMSE**, **POLITO** and **EADS)**

Sub-task 3.3.1 "Synthesis of the materials for coatings" (**UNIBA**, **POLITO**, **EADS**, **ICMSE**)

The aim of this subtask is to deposit inorganic, non-conductive and dense coatings of different nature, basically SiO_x and SiOxNy, and to understand the influence of the chemical composition with the intrinsic properties of the final material. The coatings has been deposited by UNIBA while POLITO perform the EIS measurements for the assessment of their corrosion protective properties.
The effects of the following process parameters have been tested for improving the corrosion protection of the alloys considered in MATECO by means of SiO_2-like coatings:
- Precursor nature;
- O_2/monomer flow rate ratio;
- RF Power;
- Pulsing vs continuous plasma.

When different monomers are considered as film precursors a good corrosion protection (Rct values higher than 10^6 ohm cm^2 is obtained onto low carbon steel). When considering the effect of the RF power it has been found that (see figure below) higher inputs are beneficial to coatings performance. This can be ascribed to the higher inorganic and dense character of the coating as revealed by the chemical characterization carried out in WP2.

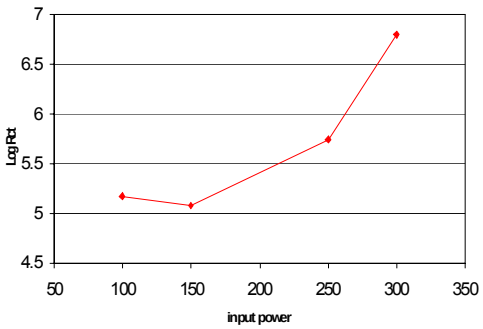

RF Power effect onto R_{ct} value in SiO_x coating deposition from TEOS / Ar / O_2 glow discharges (100 mTorr, 1µm); Rct value after 1h immersion

The effect of the plasma pulsing was investigated by the application of different Duty Cycles (DC): 10, 15, 25, 50, 100%, with a on time of 10 ms and 250 W input power for a SiO_x coating deposited from TEOS/Ar/O_2 fed plasma . In the following figures it is shown that passing from continuous to pulsed plasma an increase of the protective properties can be observed. This could be explained by the formation of less defect in the coating due to surface mobility of the impinging radicals during the off time.

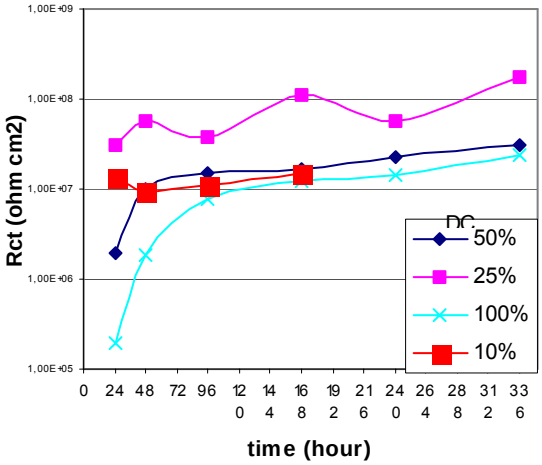

Effect of % DC onto R_{ct} value for 1 µm SiO_x coating deposition as a function of immersion time with Al 5005 as substrate

Properties of SiOxNy coatings

SiOxNy coatings have been deposited onto the substrate considered for MATECO. In particular the results obtained onto Steel 304 are reported in the figure below, for coatings obtained from bis-dimethylamino-dimethylsilane and Ar as buffer gas. Also for this kind of coatings a similar behaviour of R_{ct} with the plasma power has been found.

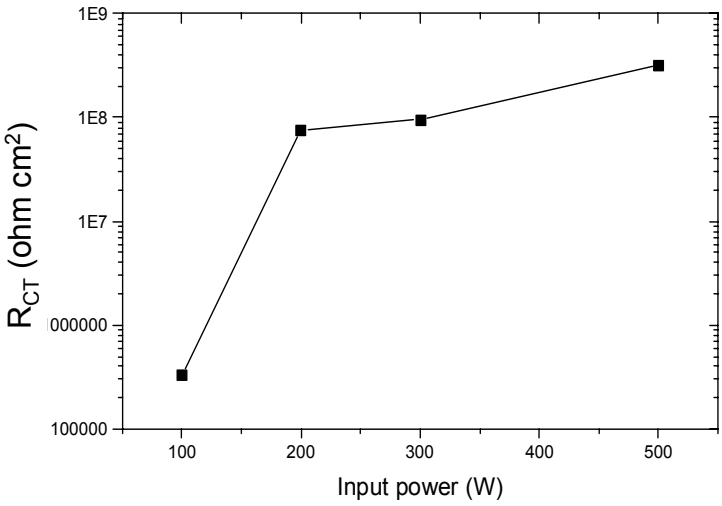

Effect of RF power onto R_{ct} value for SiN_xO_y, coated 304 stainless steel. CCP, Monomer 4sccm, Ar 50sccm, 30mtorr, 2µm

In order to study the degradation of CCP SiOxNy films, samples prepared at different RF power and gas feed composition were immersed in a NaCl 0.1M solution for 1h, 20h, 168h.
At lower input power (100W) a degradation of the film can be observed as a consequence of the immersion in the NaCl solution. In particular SiH (C≡N) IR absorption bands decreases, while the contribution of Si-O bands (Si-O-Si at 1060cm^{-1} and Si-OH broad band at 3300cm^{-1}) increases. This can be ascribed to hydrolysis reaction of the coating with the solution. An

increase of the input power (300W) even if O2 is added or if the gas feed flow rate is increased lead to a more stable coating since no changes in the FTIR spectra can be evidenced even after 168h immersion in the NaCl solution. The main difference between the low and high power coating can be in the crosslinking: it is very likely that the one deposited at 300W is more crosslinked as a result of an higher ion bombardment.

Comparison of SiO_2-like vs SiO_xN_y coatings

In next table the best R_{ct} values obtained on the different metal alloys with coatings produced with different chemistries and plasma apparatus configuration have been reported. 2µm thick coatings have been considered, except for the pulsed plasma deposited films (1 µm). The following observation can be addressed:

- The SiO_x plasma coating (2µm) can grant about 3 order magnitude increase in the Rct values;
- SiOxNy coatings are less effective with respect to the silica layers;
- SiOxNy coatings are more effective when deposited by capacitive coupled plasma (CCP);
- Surprisingly SiOx coatings deposited by means of pulsed plasma can reach Rct values as high as 3×10^7 ohm cm^2 with a half thickness (1 µm), when considering Al alloys;
- The main drawback of SiOxNy coatings deposited in the inductive coupled plasma is their susceptibility to delamination.

Substrates	**R_{CT} Bare substrate (ohm cm^2)**	**R_{CT} Coated samples (ohm cm^2)**			
		SiO_x	**Pulsed SiO_x (1µm) *CCP***	**SiO_xN_y *ICP***	**SiO_xN_y *CCP***
Al 5005	9.5×10^3	2.3×10^6	3×10^7	2.3×10^4	3.5×10^6
TiAl6V4	2.4×10^5	3.1×10^9		2.7×10^5 (24h)	
INOX 436	4.8×10^5	2×10^8			
INOX 304	1.9×10^6	2×10^9		10^7	3.2×10^8
42CrMo4	150	4.7×10^6		1.6×10^5	5.4×10^5

Comparison of best RCT values of coated metals determined after 1h immersion in NaCl. Thickness is 2µm if not specified. SiOx coatings are deposited with TEOS(O_2/Ar at 250 W, 100mtorr. ICP SiO_xN_y have been deposited with bisdimethyl amino dimethylsilane/Ar at 500W, 10 mTorr. CCP SiO_xN_y bisdimethyl amino dimethylsilane/Ar at 500W, 30 mTorr

The morphological characterisation of the coatings performed by POLITO by means of field emission scanning electron microscopy (FESEM) allowed to put in evidence the high compact and homogeneous film morphology of the SiO_x pulsed film.

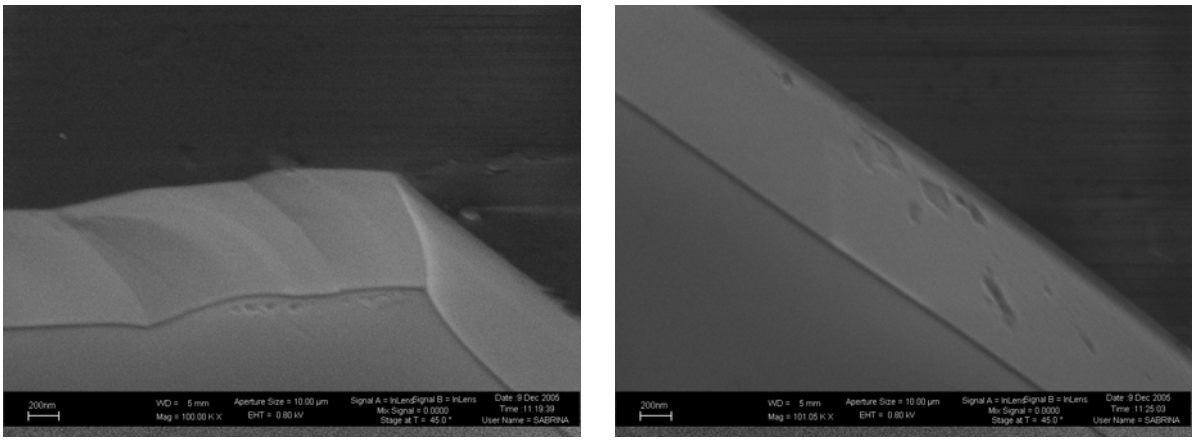

(a) (b)

FESEM images of SiO_x pulsed coatings deposited at: (a) 10% DC and (b) 50% DC

In particular, SiO_x film deposited by increasing the % DC shown a less dense structure characterised by the presence of porosities, which can facilitate the penetration of aggressive agents until the metal surface.
Coatings were synthesized with a number of different parameters as described in Sub-task 2.3.3. For an easier comparison of the coatings the process times typically were chosen in a way that coatings with a thickness of about 1 µm resulted.
Due to this small coating thickness the topography of the coatings represents the initial roughness of the substrates (see table above). A scanning electron microscope picture shows the waviness of an example coating on steel resulting from final cutting topography of the substrate.

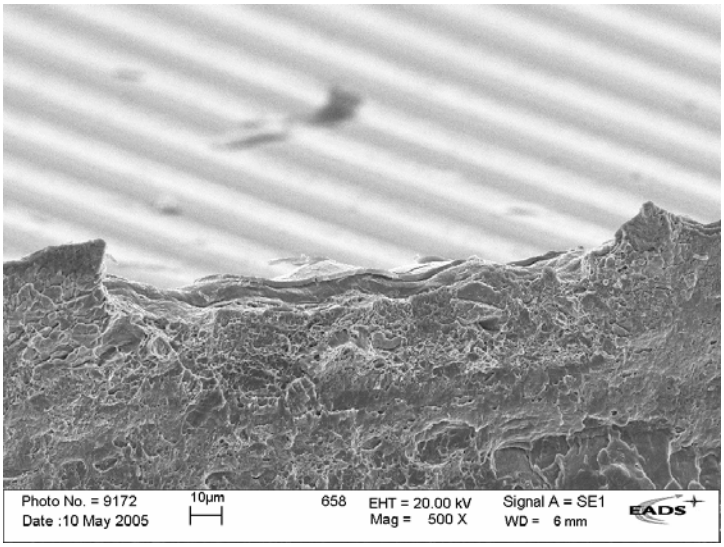

SEM picture of 1 µm thick $SiO_xN_yC_z$ coating on final cutted low carbon steel

All coatings deposited show a very homogeneous, amorphous structure as can be seen from the following SEM pictures.

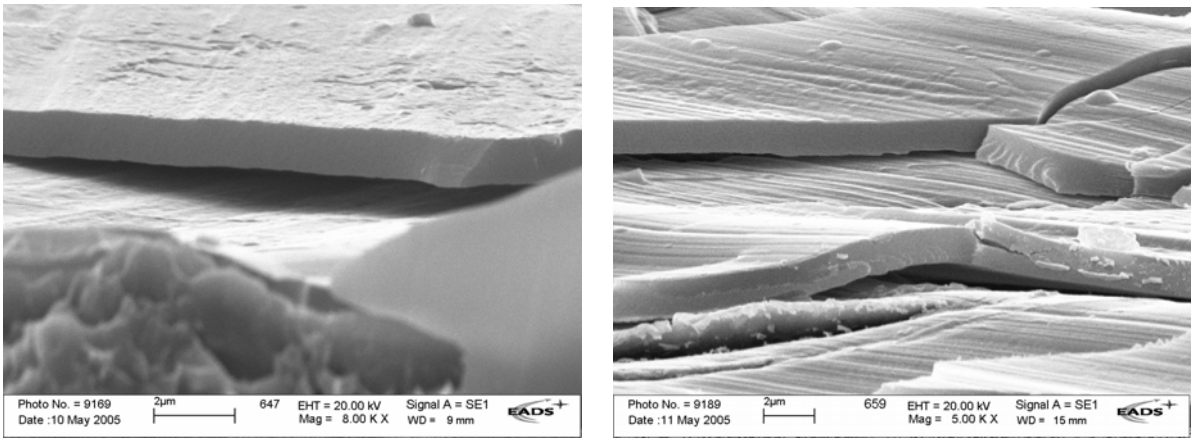

SEM pictures of 1 µm thick SiO_xC_y coating (left) and $SiO_xN_yC_z$ coating (right) on final cutted low carbon steel

Basic tribological properties (hardness, coefficient of friction, wear resistance) of SiO_xC_y coatings and SiO_xN_y coatings both on steel and titanium have been tested.
For the SiO_xC_y coatings higher hardnesses can be measured for coatings deposited at higher plasma powers (647 ± 29 N/mm^2 at 0,12 W/cm^2 ; 814 ± 20 N/mm^2 at 0,18 W/cm^2).
The same it true also for the $SiO_xN_yC_z$ coatings. An increase in plasma power from 0,12 W/cm^2 to 0,15 W/cm^2 results in an increase in hardness from 433 ± 16 N / mm^2 to 694 ± 26 N/mm^2.
Coatings from HMDSN plasma without oxygen have very low hardnesses in the range of 150 N/mm^2. This results from the very high carbon content of these coatings. Adding oxygen to the coating process nearly triples the coating hardness.
Surprisingly the friction of the coatings seems independent on the coating parameters. For all tested coatings coefficients of friction of about 0,5 were measured in ball-on-disc testing at EADS (6mm titanium ball; Force 1 N).
This coefficient of friction is nearly the same as for the uncoated substrates.
To evaluate the adhesion of the coatings to the substrate different tests were conducted.
The cross cut test gives good adhesion values with GT 1 in nearly all cases of final cutted substrates. The best adhesion with GT 0 can be achieved on the TiAl6V4 sheets.
In the Rockwell adhesion test only on TiAl6V4 sheets acceptable adhesion values can be measured.

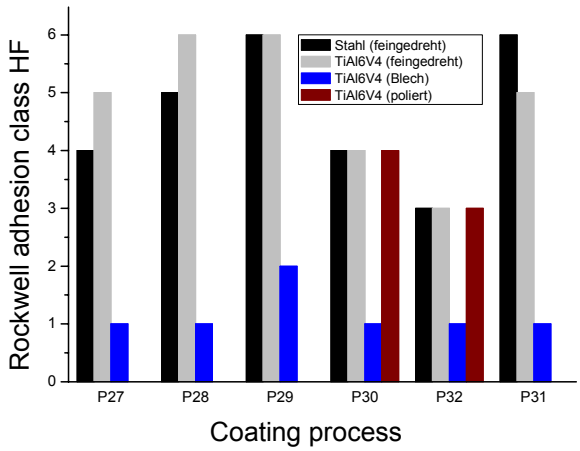

Adhesion values from Rockwell adhesion test

Concerning the wear resistance, better values (meaning wear tracks that are less deep after certain cylcles in the ball-on-disc) can be found when the coatings are deposited at higher plasma powers. This result corresponds with the higher hardness values found for the coatings at higher powers.
An increase in deposition temperature from 50°C to 150°C significantly increases the wear resistance of the coatings for all precursors investigated. In the case of BDMADMS as precursor despite smaller coating thicknesses resulting from the higher substrate temperatures much flatter wear tracks can be found when temperatures above 150°C are adjusted.

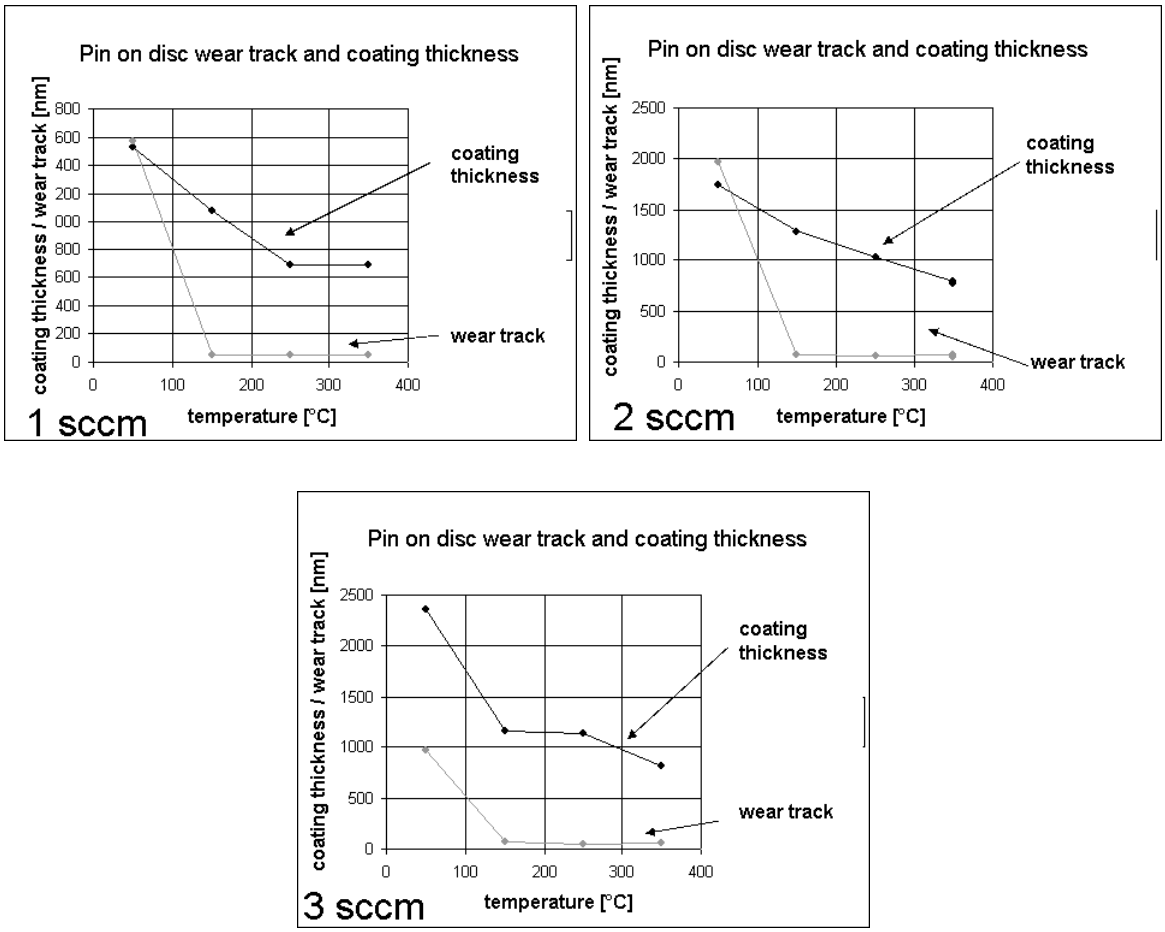

Influence of $T_{Substrate}$ and BDMADMS flow (1, 2, 3 sccm) on ball on disc wear tracks

Sub-task 3.3.2: Characterisation of the synthesised materials (**ICMSE**)

ICMSE has participated in this subtask by doing microstructural characterization (a) and chemical composition (b) and bonding nature (c) of the prepared films. The goal was to achieve information about the influence of the growth parameters (type of precursor, type of reactor, synthesis conditions, etc.) and thus to establish correlations with the final properties (mechanical, anti-corrosion, adhesion…). Many different techniques were employed to assess this kind of information, (i.e. XPS-Depth profiling, X-ray induce AES, GD-OES, SEM/TEM/EELS).
The list of studied samples is the following:
- SiCH (HEF);
- SiCHN (HEF);
- SiCNO (EADS, UNIBA, EPM);

- SiO_x (UNIBA).

The influence of various parameters was studied in order to help the coating elaborator about the best conditions to achieve the best film characteristics and properties. In the next we have selected some significant examples of the most relevant contributions given by ICMSE in these aspects.

Morphological characterization

ICMSE has carried out morphological characterizations of the coatings by SEM / EDX technique and TEM observation of the substrate/film interface. A detailed description of the TEM cross-sections analysis after different pre-treatments is shown in WP1. Roughness measurements and SEM observations were valuable measurements to evaluate the surface finishing of the samples and determination of impurities. In the next figure two SEM pictures are shown for SiCH (classical underlayer) and SiCHN prepared by HEF. The surface of the two types of coating seems very smooth with nearly no defects. EDX analysis highlights a rather low quantity of Argon present inside the SiCH films (< 2 %).

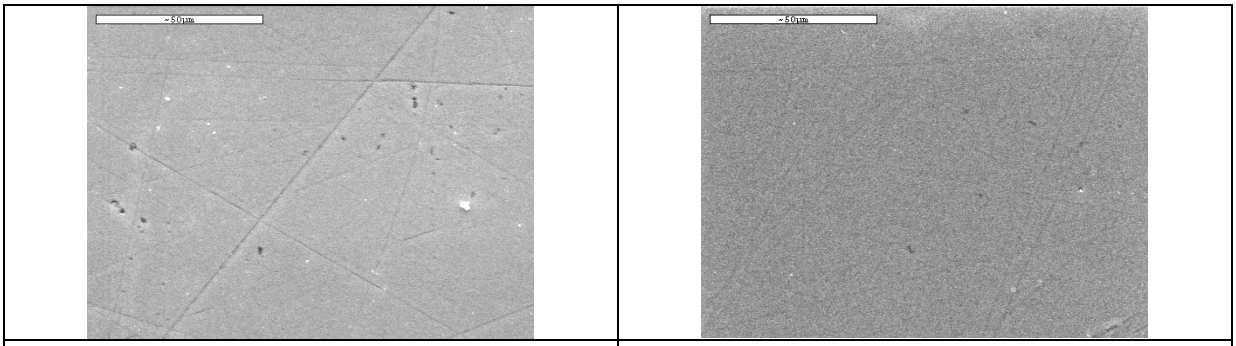

SiCH film	SiCHN film

SEM micrographs of SiCH and SiCHN thin films by DC PECVD

SEM / EDX characterisations have been also performed on microwaves (SiCHMO 502 and 510) coatings in order to compare their morphology with those of the films deposited by classical PECVD. The micrographs below show comparatively the morphology of SiCH and SiCHN types of films.

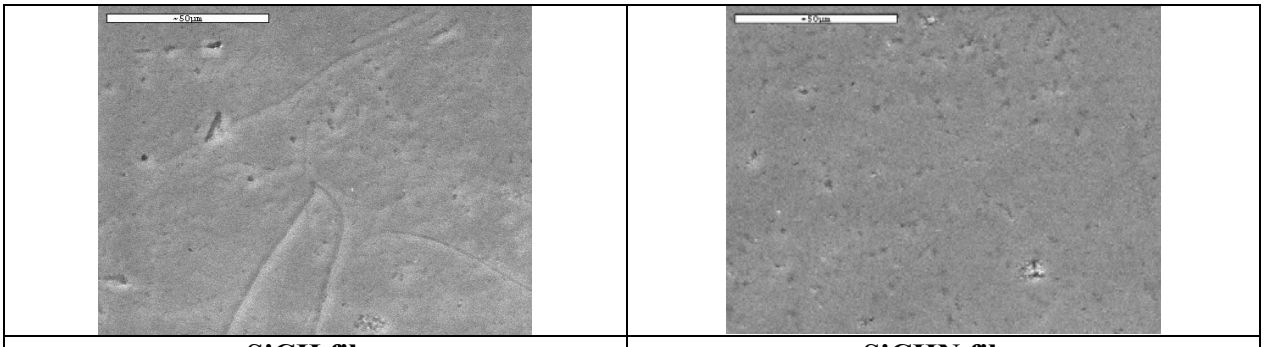

SiCH film	SiCHN film

SEM micrographs of SiCH and SiCHN thin films deposited by microwave PECVD

We observe that the films are also homogeneous when they are deposited by ECR microwave PECVD which is confirmed by profilometry measurements. The roughness of the substrate and

both films are very similar: R_a ~ 0.05 µm, R_z ~ 0.6 µm and R_t ~ 0.9 µm. The "defects" we can see are provided by the tribo-finished surface (see Task 1.3.1).

Chemical composition

XPS Depth profiling has been used to investigate the **surface chemical composition**. *In situ* Ar^+ sputtering of the sample (2.10^{-5} mtorr, 6 mA, 3.5 kV) and XPS spectra were recorded at 0, 60, 120, 240 and 900 seconds. In the graphs below are shown the results for the same films of previous section.

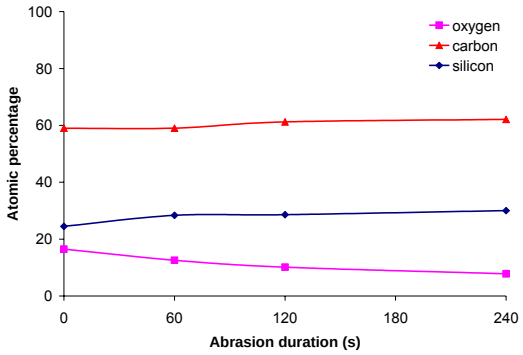

SiCH film

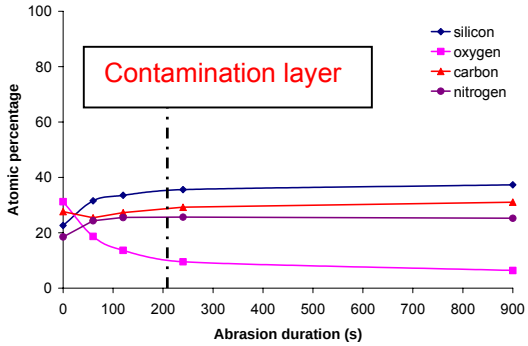

SiCHN film

Chemical composition of SiCH and SiCHN films versus the abrasion duration before XPS analysis

The quantification of SiCH coatings gives an atomic ratio of about 60 % for carbon, 30 % for silicon and 10 % for oxygen in all the cleaning conditions. For the initial state this percentage reaches a 16 % value due to the air exposure and the presence of an O-rich top-layer. Concerning the SiCHN layer, the quantification by area integration gives approximately these average ratios: 33 % Si, 27 % C, 25 % N and an oxygen ratio varying from 31 % to 6 % depending on the Ar^+ sputtering conditions (from 0 to 900 seconds).

We have obtained exactly the same quantitative and qualitative results for two samples prepared in different batches what highlights the good reproducibility of the PECVD process. It is also noteworthy that film composition remains steady across the analysed section emphasizing the good chemical homogeneity of the film. To give an idea of the stoichiometry of the film, we could write the formula: $Si_{1.2}CNO_{0.5}$.

The surface oxide layer was estimated to be thinner than 10 nm. This sublayer was almost removed after 120 s of Ar^+ etching (2.10^{-5} mtorr, 6 mA, 3.5 kV). Similar pre-treatment was used for all the remaining analysis done in the project in order to eliminate the contamination layer and thus to study the bulk chemical composition of the materials.

XPS analyses performed on SiO_x films in order to determine their chemical structure. showed that the composition of SiO_x thin films is independent of the type of substrates and is rather homogeneous in depth. The atomic ratio is about 75 % for oxygen and 25 % for silica whatever the sputtering conditions. Complementary analysis carried out on a SiO_2 standard sent by **UNIBA** in order to check the atomic ratios measured for the SiO_2-like films put in evidence that a correction factor must be applied to the elemental atomic concentrations. Finally silica-based films deposited by UNIBA present a Si/O ratio of 2.07 after correction. This value is slightly higher than 2 as usually observed for SiO_x-like films deposited by PECVD.

ICMSE has also performed some experiments using GD - OES (Glow Discharge - Optical Emission Spectroscopy) on SiCHN coatings. This technique results very suitable to analyse the variation of the film chemical composition (expressed in element weight %) as a function of

the material analysed depth along entire thickness very fastly. Quantitative analysis required the estimation of the elemental sputtering rates and film density. This process implies the selection of appropriated standards of certificated chemical composition, measurements on same experimental conditions and determination of the eroded mass by means of profilometry. These measurements have been found very difficult due to the lack of appropriated standards for light elements (Si, C, N, O) and the high insulating character of the coatings.
We can observe that the approximated thickness of the SiCHN film is about 3.5 µm and the chemical composition seems to be constant along the film thickness.

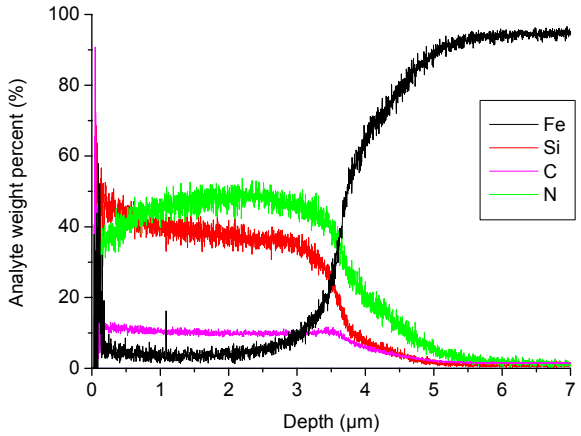

Depth profiling analyses of Fe, Si, C and N elements of SiCHN film deposited on 42MoCr4 steel substrates

The XPS analysis has also been very significant to elucidate the **influence of synthesis parameters**, for instance: TMS/C_2H_2 ratio, the plasma technology (DC or MW PECVD), Ar dilution, etc. In the next table, we present the results obtained for SiCH samples as representative example:

Samples SiCH	TMS/C_2H_2/Ar	at. % Si	at. % O	at. % C	C/O	Si/O	Si/C
SiCH502	*150/0/60*	**25.0**	**9.5**	**65.5**	**6.9**	**2.6**	**0.4**
SiCH505	*150/0/60*	**28.0**	**5.3**	**66.7**	**12.7**	**5.3**	**0.4**
SiCH503	*200/100/60*	**17.7**	**8.3**	**74.0**	**8.9**	**2.1**	**0.2**
SiCH504	*100/200/60*	**9.**	**4.7**	**85.9**	**18.1**	**2.0**	**0.1**
MO SiCH502	*150/0/20*	**21.3**	**6.2**	**72.4**	**11.7**	**3.4**	**0.3**

Chemical composition and ratios C/O, Si/O and Si/C of the SiCH films

In DC PECVD, we remark that the Si/O ratio seems to be constant whatever the gas feed composition and as expected, the Si/C ratio can be controlled by TMS and C_2H_2 mass flow. Concerning the film deposited in MW PECVD, we observe an increase of the C/O and Si/O ratio probably due to the higher deposition rate in the microwaves conditions. MW PECVD conditions for SiCH films reduce significantly the oxygen content into the films.

Chemical bonding nature

The chemical nature of the silica-based films has been investigated by means of XPS and X-AES spectroscopic analysis on the different coatings. This analysis results fundamental to correlate the chemical composition (stoichiometry and bonding nature) with the corrosion

protection afforded by the coatings. Particularly we have studied the modified Auger parameter (α´) which is defined by the sum of the kinetic energy of the Si KLL Auger transition and the Si 2p photoelectron peak. This parameter has the advantage that its value is independent of photon energy and charge effects and present a characteristic value depending on the bonding nature.

$$\alpha' = \alpha + h\nu = KE\ (Auger) + BE\ (photoelectron)$$

By estimating this parameter for the broad family of Si-C-N-O based-compounds prepared in the project we were able to identify the predominant bonding type in each case. In the graph below we have plotted the Auger parameter for different coatings prepared by different partners and the main type of Si bonding present in the films thanks to the α´ value.

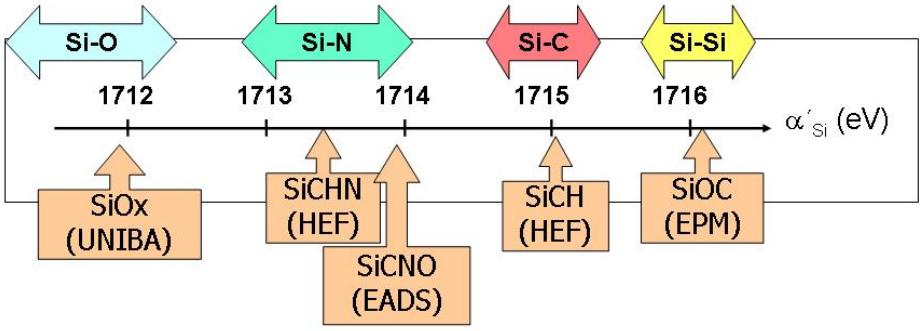

Family of Si-C-N-O materials prepared in MATECO project and acharacteristic Si-bonding as determinded accordingly by means of the modified Auger parameter

In the enclosed graphs can be noticed the variation in positions of Si 2p and Si KLL Auger peaks for these representative types of coatings, values used for the determination of α´.

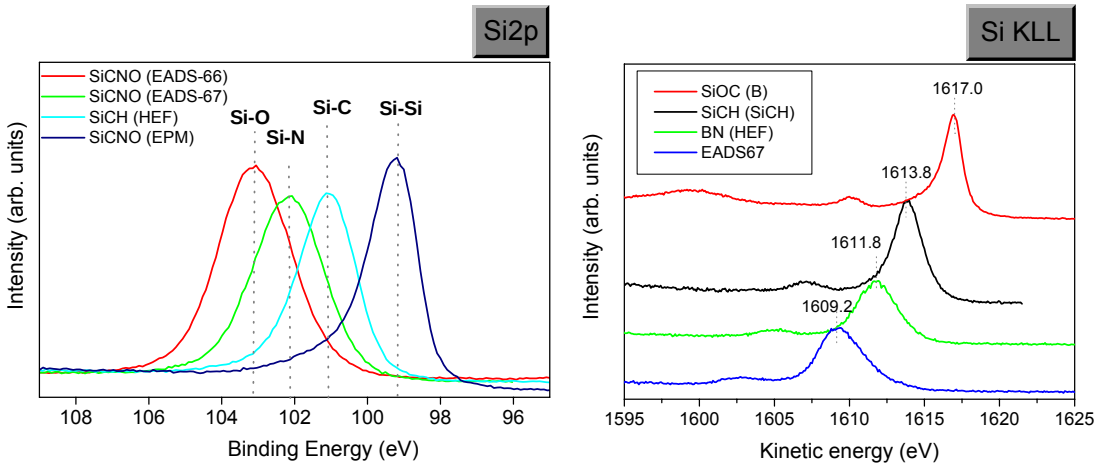

XPS Si 2p and Si KLL peaks for representative type of SiCNO films prepared in MATECO

The use of the modified Auger parameter has also enabled to determine ***the influence of the synthesis condition***s on the bonding characteristics within a set of samples prepared by the

same coater. In the enclosed table, it is summarized the synthesis conditions for SiCHN films prepared by HEF.

Samples (TMS/NH_3/Ar)	KE Auger (eV)	BE Si (eV)	Parameter α'_{Si} (eV)
*100/200/**0***	1611.9	102.2	***1714.1***
*100/200/**60***	1611.8	102.2	***1714.0***
50**/200/**120	1611.5	102.4	***1713.9***
***100**/200/120*	1611.6	102.4	***1714.0***
***200**/**200**/120*	1612.7	101.5	***1714.2***
*200/**50**/120*	1612.8	101.9	***1714.7***
MW** 200/50/**20	1613.1	101.5	***1714.6***

More Si-N

More Si-C

Kinetic energy of the Si Auger transitions, binding energy of the Si2p peak and Si modified Auger parameter for the studied SiCHN films

After surface cleaning with Ar^+ sputtering, the Si_{2p} peak of SiCHN coating is situated at 101.5 - 102.2 eV and is attributed according to the literature to Si atoms bonded to N atoms. The Si_{2p} peak is clearly not due to Si – C bonds because silicon carbide bonds appear around 100 eV. All the Auger transitions are located at 1611.5 - 1613.1 eV and can be attributed according to the literature to Si-N bonds which confirm once more the predominance of Si-N bonds into the films. However, an increased Si-C character can be predicted in agreement with the increment of the Auger parameter from 1714.0 eV to 1714.7 (value of α´ for Si – C contributions is around 1 715 eV).
These values also confirm that the influence of the TMS and argon mass flows on the atomic chemical composition is quite low (typical values ~ 1714eV). The NH_3 precursor seems to present the most important effect on α'_{Si} and thus on the chemical structure of the films. Decreasing its flow from 200 to 100 or 50 sccm, the modified Auger parameter increases up to 1714.6 – 1714.7 eV (closer to Si-C type of bonding). The microwaves process do not seem to affect considerably the chemical composition of the films deposited in the same conditions with classical PECVD process as shown by the modified Auger parameter (1714.6 - 1714.7 eV).

1.5.3 WP Leader Assessment and Conclusions

WP3 has allowed a good understanding of the plasma deposited coatings performance in terms of corrosion protection. In particular it has been found that SiOx coatings are better than SiOxNy ones in corrosion protection. On the other hand coatings deposited in this project are very homogeneous and smooth. Finally it has been well understood that to get nitrogen included in a SiN environment it is necessary to start from N containing monomers, with the eventual addition of NH_3, more than N_2.

1.6. WP 4: Coating understanding, architecture and characterisation (WP Leader: HEF)

WP Leader **HEF**
Participants **HEF – UNIBA – CRF – EADS – POLITO –INSA –TEFAL - ICMSE**

1.6.1 Objectives

The objective of this workpackage was to study the influence of the combined, multifunctional coatings on their basic properties (morphology, structure, electrical, optical, mechanical etc…).

1.6.2 Progress towards objectives

Several architecture were investigated. It has included multilayers, graded layers. The research work has rapidly focussed on the simplest coating structures which consist of two layers.
The base layer was deposited for corrosion protection purpose and for adhesion purpose both with the substrate and the top layer. The top layer nature was chosen according to the surface functionality required.
For mechanical purpose, DLC top coating was chosen to improve both wear resistance and friction decrease. It has been shown that a DLC top layer had a good adhesion to SiCHN corrosion protective coatings while it was not possible to achieve good mechanical properties by using SiO_x as the base layer. The research work has shown that the combination of two coatings could interfere in some case and modify the corrosion protection behaviour.
SiO_x coatings have been found to be the best solution for corrosion protection. Indeed, the research work carried out on the corrosion behaviour have shown that the corrosion protection efficiency was linked to the electrical conductivity of the coating. Then SiO_x has the most efficient protection ability because of its very low conductivity. The SiCHN protection ability is not as efficient as SiO_x but it is much higher than conventional coatings like SiCH used for the adhesion of DLC. The SiCHN coating have been identified as semiconductors and their electrical properties were found to depend on their composition.
The Easy to Clean (ETC) is a more difficult subject. It was shown that it was necessary to add fluorine to the coatings to reduce their surface energy then improve the ETC. However, the ETC performances were not sufficient enough for the foreseen industrial application. It is suspected that roughness considerations and chemical inertness have to be also considered.

1.6.2.1 Task 4.2: Coating elaboration (**HEF**, **UNIBA** and **EADS**)

The main result obtained by UNIBA has consisted in the production of multilayers based on Teflon like coatings (CF_x) over SiO_x layer. In the next table the results for stainless steel are reported. It can be seen that even if there are no big differences after 24h of immersion in NaCl in Rct values, the bilayer coatings are much stable at long immersion time. This can be ascribed to a hydrophobic effect.

Substrate	R_{ct} (Ω*cm²) 24h	R_{ct} (Ω*cm²) 240h	WCA (°)
Virgin Inox304	$6.8*10^5$		
2µm SiO_x coating	$2.4*10^9$	$2.7*10^8$	15 ± 2
1µm SiO_x coating + 50W 1µm CF_x	$3.6*10^9$	$1.7*10^9$	104 ± 6
1µm SiO_x coating + 100W 1µm CF_x	$1.9*10^9$	$4.6*10^9$	
1µm SiO_x coating + 200W 1µm CF_x	$6.8*10^9$	$8.0*10^9$	

EADS has prepared a set of samples with different plasma parameters for characterization and coating understanding.
Among all the architecture tested, HEF R&D has deposited multilayer structure by varying periodically the gas flow mixtures. Strong and soft transition between layers were investigated. The pictures below show calotest on multilayers including or not gradient at the interfaces. The coatings selected is a SiCHN composition allowing corrosion protection and a DLC.

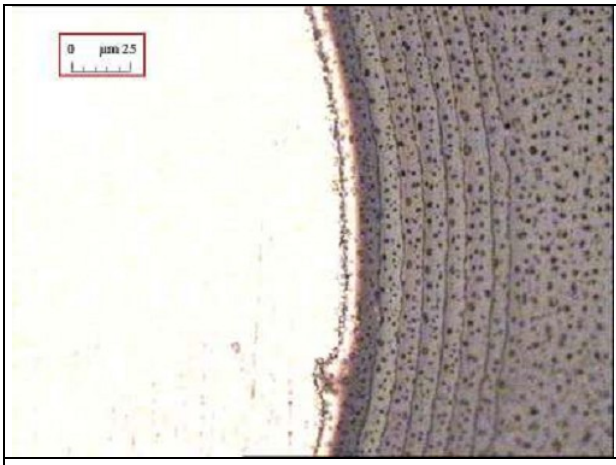

Sharp transition

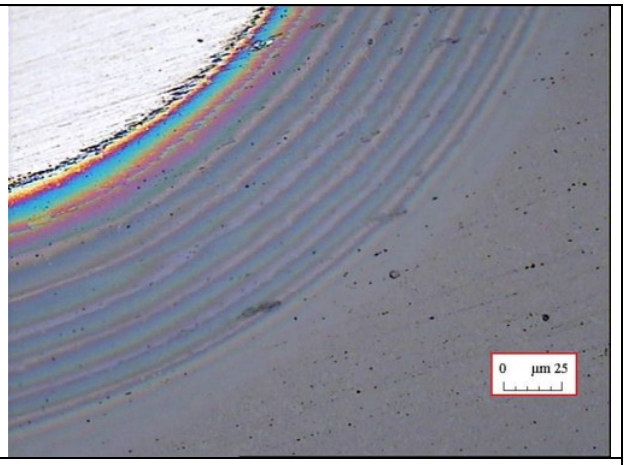

Smooth transition

On the mechanical point of view, graded transitions show a better behaviour, however corrosion test have shown pitting at 96 h which was less than bi-layers. The work was then continued on coatings consisting of a Si base layers with a DLC top coat which was in some case modified by F incorporation for ETC.

1.6.2.2 Task 4.3: Characterisation of samples (**POLITO**, **HEF**, **ICMSE**, **UNIBA**, **EADS**, **CRF** and **TEFAL**)

ICMSE has received many different samples for determination of the microstructure, morphology and chemical characterization at the micro- and nano-scale in this task regarding the best structures and characteristics that fulfil the multifunctionality requested for selected applications. The characterization of the Si-N based materials is reviewed in WP3 while here we will focus on the DLC top-coat used in the applications requesting good tribological and anti-corrosion properties. A special attention was devoted to investigate the substrate-coating

interface (sub-task 4.3.5). Here enclosed a list of different materials studied alone or in the form of multifunctional architecture.

Film	Provider	Characterizations performed
DLC (DC)	HEF	XPS Depth profiling X-AES SEM GD-OES Roughness TEM/EELS
DLC (MW)	HEF	
DLC-F	HEF	
SiOx	UNIBA	
SiCH underlayer	HEF	
SiCHN	HEF	
SiCNO	UNIBA	
SiCNO	EADS	
SiOCN	EPM	

List of received samples, coating provider and characterization performed at ICMSE

Subtask 4.3.1 Morphological characterisation (**POLITO**, **ICMSE**, **EADS**, **CRF**)

Aluminium layer and SiOx top-layer

ICMSE has performed roughness measurements of the uncoated and coated polysulfone (PS) parts.

Roughness (μm)	Uncoated PS	PS + Al coating	PS + Al + SiO_x coatings
R_a	0.030	0.010	0.022
R_z	0.250	0.160	0.248
R_t	0.660	0.295	0.348

Roughness of PS substrates uncoated, coated with an aluminium layer and coated with a duplex film (aluminium and SiOx layers)

In each case, the roughness values are rather low. We observed no difference between the roughness of PS parts and those coated with aluminium and SiO_x films. Moreover, as revealed in Task 1.3.3, the SiO_x films present a homogeneous surface. EDX analyses also confirm that the SiO_x coatings do not present defects as seen for the aluminium layer deposited onto the polysulfone substrates (see Task 1.3.3).

DLC films with SiCH underlayer

a) Morphology

The coatings have been analysed by SEM technique and profilometry in order to obtain information about their morphology. XPS analyses have been also performed in order to determine their chemical nature and composition. The SEM analysis has shown that the DLC films deposited by PECVD present a homogeneous surface (see figure). The roughness of the samples has been measured by profilometry. The results are given in the next figure using R_z parameter. This is the best parameter to give an overview of the defects of the measured surface

(pores, particles, …). This roughness seems to be increased after the DLC deposition that is to say DLC films could present pores and particles on their surface.

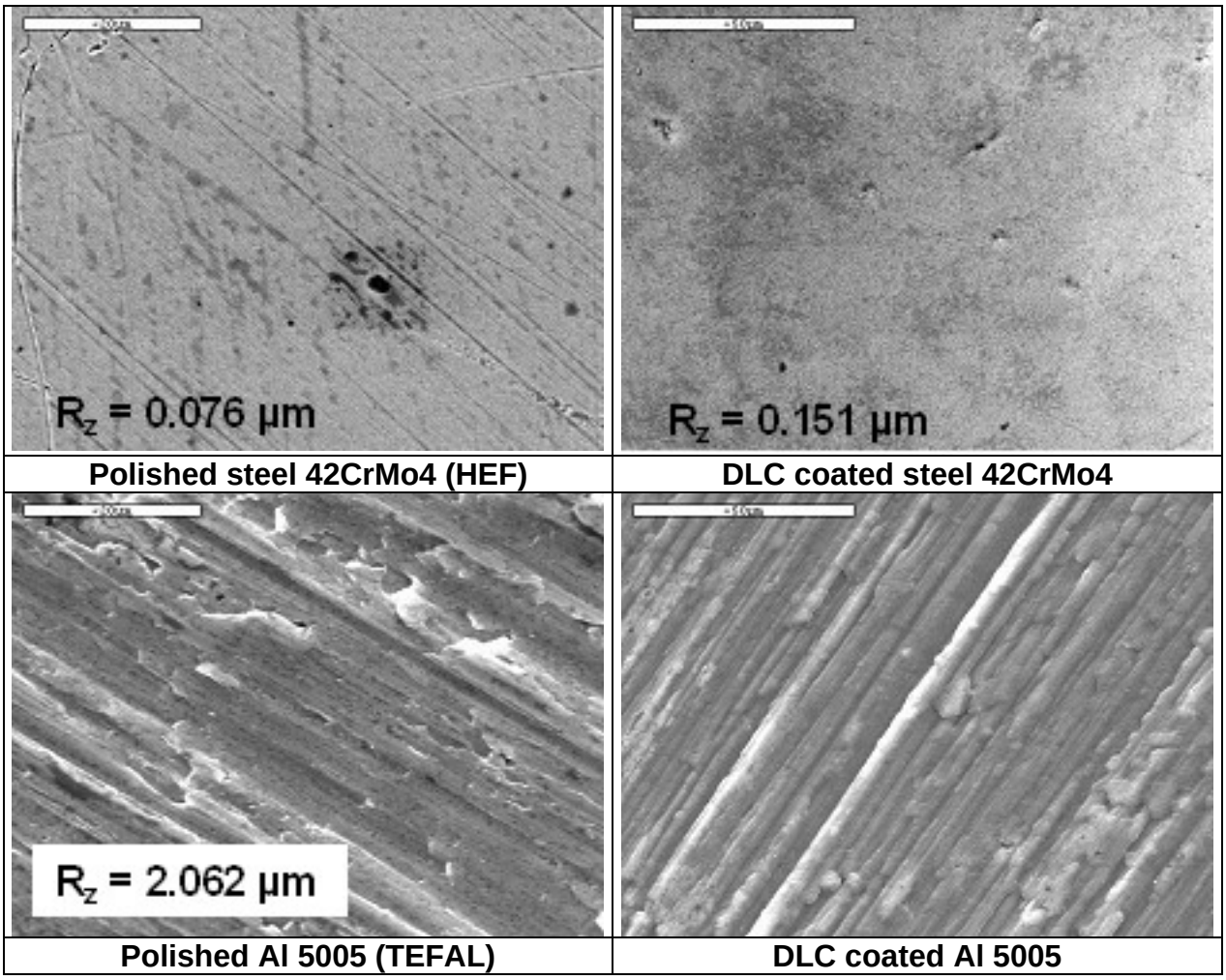

SEM micrographs of steel 42CrMo4 and aluminium 5005 substrates before and after "classical" DLC thin film deposition

b) Chemical bonding

XPS analyses have been performed on DLC coatings deposited onto steel 42CrMo4 and steel 304 substrates provides respectively by HEF and TEFAL. The quantification of the DLC films (without previous Ar^+ ions sputtering) gives an atomic ratio of about 90% for carbon and 10% for oxygen. We have obtained exactly the same quantitative and qualitative results for both kinds of substrate what highlights the good reproducibility of the PECVD process. The observed C_{1s} photoelectron peak is typical of DLC films and in order to obtain more information concerning the carbon hybridisations, we have also recorded the valence band and the C Auger transitions (C_{KLL}) for each sample.

Concerning the valence band (see next figure), we observe three peaks:

- A peak situated at around 26-27 eV attributed to the O_{2s} energy level and resulting from the presence of oxygen adsorbed on the surface of the samples;
- A broad peak C_{2s} located at 18-20 eV attributed to a valence band with an exclusive s character typical of carbon sp^2 hybridisation;
- A peak C_{s-p} located at 10-12 eV attributed to a valence band with a mixed s-p character typical of carbon sp^3 hybridisation.

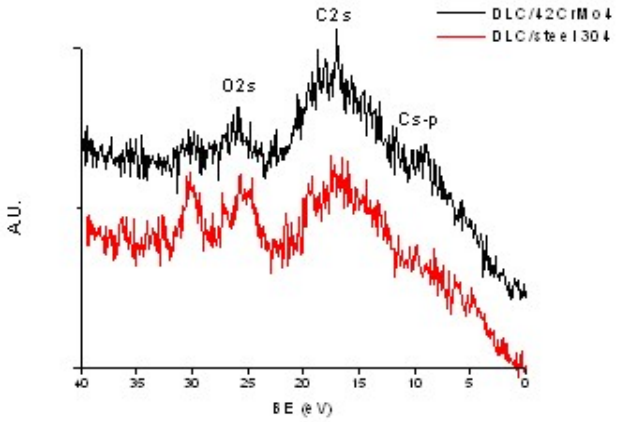

Valence band of DLC film deposited on steel 42CrMo4 (black curve) and steel 304 (red curve) substrates

These observations suggest that the DLC films present a majority of carbon sp^2 hybridisations that is to say a graphite character.

ICMSE has also characterised DLC films deposited by classical DC or MW PACVD in order to determine the carbon hybridisations and to correlate them with their properties. In particular a decrease of the hardness values was observed when using the MW process. The XPS results are very similar for each sample that is why we only depict one characteristic spectrum for each category of DLC thin films. We have studied the derivative of the carbon Auger contribution and the D parameter in particular. This parameter is defined as the difference between the two minima of the derivative and give us an estimation of the average sp^3/sp^2 character of the film network.

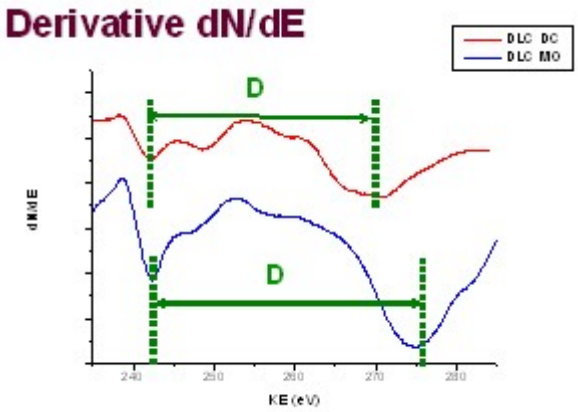

Derivative dN/dE of the carbon Auger spectrum for one DC and one MW PACVD DLC film

Samples	D parameter (eV)	Hardness (Hv)
Graphite	20.4	<1000
Diamond	14.2	8000
DC DLC	17-18	3500
MW DLC	22	2300

D parameter and hardness for some samples

The D parameter for graphite and diamond are 20.4 and 14.2 eV respectively. Concerning the DLC films deposited by DC and MW PACVD process, this parameter is found to be about 17-18 and 22 eV and the hardness H = 3500 Hv and 2300 Hv respectively (see table above). The hardness for MW DLC coating is lower than the one for DC DLC film. We can conclude that the sp^2 character (graphite character) in MW DLC is more predominant than in classical DLC what could explain the reduction in hardness. Moreover, we have studied the valence band of both films.

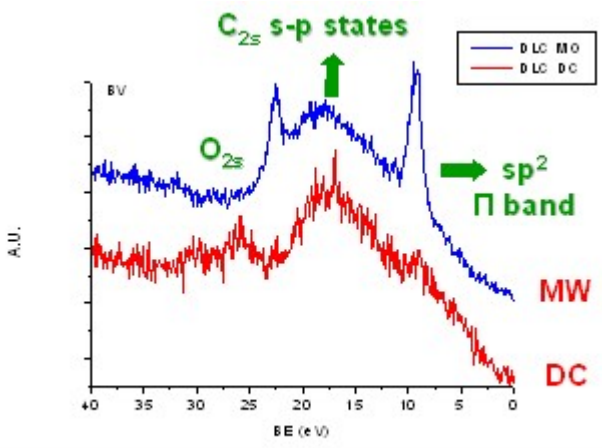

Valence band for one DC and one MW PACVD DLC film

We clearly observe a well-defined and sharp peak on the valence band of the MW DLC film at around 8 eV. This peak is attributed to the electrons present in the π band that is to say characteristic of sp^2 contribution. The valence bands spectra confirm thus the enhancement of the sp^2 character of DLC deposited by MW PACVD.

F-doped DLC

ICMSE has characterised the MW PECVD DLC films doped with fluorine atoms deposited by **HEF R&D** by XPS and friction tests. Synthesis conditions and mechanical properties of the fluorinated films are summarized in the table below.

	SiCH step		DLC step		CF_4 step		Thickness (µm)	Hardness (15mN)
	MW power	Vb	MW power	Vb	MW power	Vb		
DLCfMO502	Pulsed DC PACVD	300V			450W	0V	0.4	1700
DLCfMO503	Pulsed DC PACVD	300V	450W	150V	450W	0V	3.1	1650
DLCfMO504	450W	300V			450W	0V	3.9	3890
DLCfMO505	450W	300V	450W	150V	450W	0V	4.7	2120
DLCfMO506	450W	300V	450W	150V	450W	0V	2.1	2130
			5min step 8times		3min step 8times			

List of samples received by ICMSE for XPS and tribological characterisations

Observation of ball cratering tests, especially DLCfMO502 and DLCfMO504 reveals that during the CF_4 introduction step, there is no film formation. Fluorine is indeed incorporated into the film, but the process used is rather grafting on the surface than layer growth. Therefore

films 502 and 504 can be considered as F doped SiCH whereas films 503, 505 and 506 are F doped DLC.
To validate the presence of fluorine, XPS analysis have been carried out by **ICMSE** on these samples after Ar^+ ion sputtering (2.10^{-5} mtorr, 6 mA, 2 kV) during 0, 15, 30 and 60 seconds in order to obtain the chemical composition by depth profiling.
The results are presented in the following table.

Samples	Coatings	F/C (0s)	F/C (30s)	F/C (60s)
DLCfMO504	*SiCH / CF4*	0.85	0.07	0.04
DLCfMO505	*SiCH / DLC / CF4*	0.49	0.13	0.06
DLCfMO506	*SiCH / (DLC/CF4) multilayers*	0.80	0.30	0.12

Chemical composition of fluorinated samples after Ar^+ ions sputtering

Evidences of C-F bonds have been found because of the presence of a contribution situated at 290.6 eV in the C1s peak. The evolution of the chemical composition (see the following figure) in function of the sputtering time duration demonstrates that after 60s, there are no more fluorine atoms. F atoms seem to be grafted to the coating surface along 1-2 nm in thickness because the sputtering rate is about 2 $nm.min^{-1}$. The XPS results are in total agreement with those of HEF R&D.

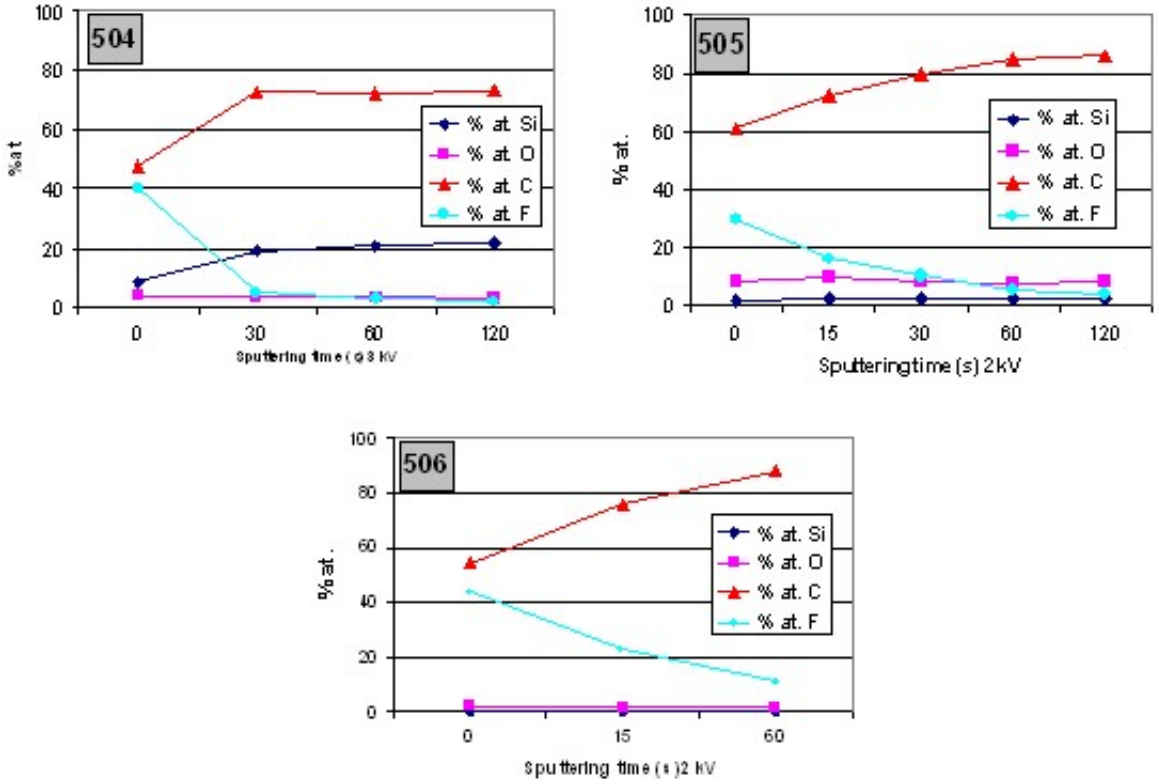

Evolution of chemical composition of silicon, oxygen, carbon and fluorine atoms in function of the sputtering time duration

For roughness measurements EADS has coated polished silicon wafers to exclude topography influence of the substrate. All Plasma-CVD SiOxNyCz coatings measured have very low roughness with R_A values in the range from 0.004 µm to 0.007 µm and R_Z values in the range from 0.1 µm to 0.4 µm.
From the tests performed is seems that coatings with HMDSN as precursor are smoother than coatings from BDMADMS plasmas. This is even true when the BDMADMS coatings are deposited with lower monomer gas flows, at lower process pressure and higher substrate temperatures.

Subtask 4.3.2 Electrochemical characterisation (**POLITO**, **CRF**)

POLITO characterised the following samples from the electrochemical and morphological point of view in order to compare the corrosion behaviour of the coatings developed in the project:
- SiCHN/DLC layers deposited by pulsed DC and MW by HEF samples;
- SiN_xO_y/SiO_x multilayers deposited by UNIBA in the experimental conditions optimised in the task 3.3.1.

Specimens from HEF:

Batch	DLC bias	SiCHN bias	TMS flow	NH_3 flow	Ar flow	R_{ct} (Ω·cm^2) 24h
DLC520	500 Vp	500 Vp	100	200	120	$3.79 \cdot 10^5$
DLC521	500 Vp	500 Vp	100	200	120	$3.43 \cdot 10^5$
DLCMO558	150 Vp	300 Vp	100	200	20	$3.04 \cdot 10^5$
DLCMO559	**150 Vp**	**150 Vp**	**100**	**200**	**20**	$\mathbf{1.56 \cdot 10^6}$
DLCMO563	150 Vp	300Vp	200	100	20	$2.21 \cdot 10^6$

SiCHN/DLC coatings deposited by pulsed DC and MW show very promising protective properties. The deposition of the SiCHN layer allows to reduce the defectivity degree of the DLC film and, consequently, to increase the corrosion protective properties of the developed coating.
As already discussed in the previous report, he double-layers coating appear very compact and homogeneous in comparison to the DLC layer characterised by the presence of many droplets that can be considered sites where the localised corrosion attack starts.

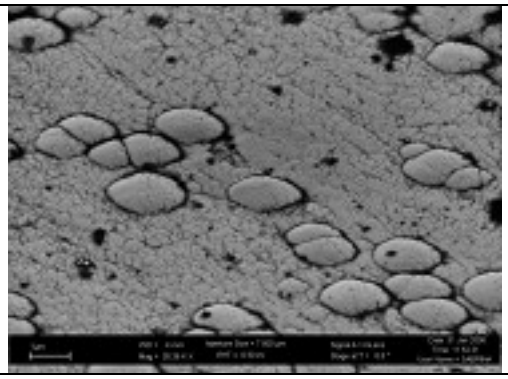

DLC film

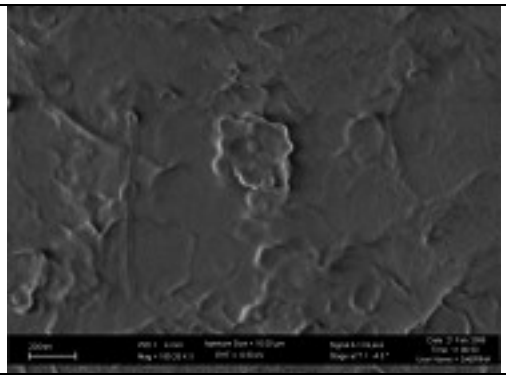

SiCHN/DLC film

FESEM images of DLC and SiCHN/DLC coated 42CrMo4 steel samples

The EIS measurements performed as a function of the immersion time in the chloride solution allow to conclude that The best corrosion performance has been obtained for coating deposited with an high NH_3/TMS ratio at low bias voltage.

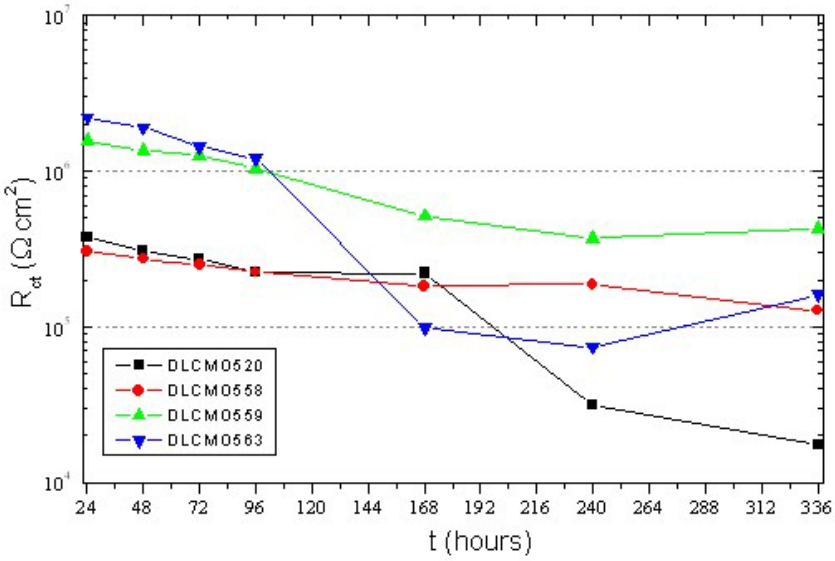

Trend of the R_{ct} values as a function of the immersion time in the NaCl 0.1M solution for SiCHN/DLC coated 42CrMo4 steel samples

Salts spray tests allowed to confirm the EIS results. The first noticeable corrosion attacks on the DLCMO559 steel sample appear after 144h.

DLCMO559 – 144h

DLC – 24h

POLITO performed also the electrochemical characterisation of SiN_xO_y/SiO_x multilayers deposited by UNIBA. The following table reports the value of the charge transfer resistance, R_{ct}, recorded after 24 h of immersion in the NaCl 0.1M solution for the different PECVD coatings.

Substrate	R_{ct} ($\Omega \cdot cm^2$)*	Coating	Thickness (μm)	R_{ct} ($\Omega \cdot cm^2$)*
AISI 304	$1.96 \cdot 10^6$	SiO_x	2.0	$2.41 \cdot 10^9$
		SiN_xO_y	2.0	$3.24 \cdot 10^8$
		SiN_xO_y/SiO_x	2.4	$5.10 \cdot 10^8$
A15005	$9.50 \cdot 10^3$	SiO_x	2.0	$1.06 \cdot 10^7$
		SiN_xO_y	1.70	$1.55 \cdot 10^6$
		SiN_xO_y/SiO_x	1.80	$1.93 \cdot 10^5$

As it is possible to observe the higher R_{ct} values have been recorded for SiO_x monolayer. The multilayer deposited onto Al shows less protective properties in comparison to the monolayer, while onto steel substrate the bilayer and the SiO_x film show a comparable electrochemical behaviour.

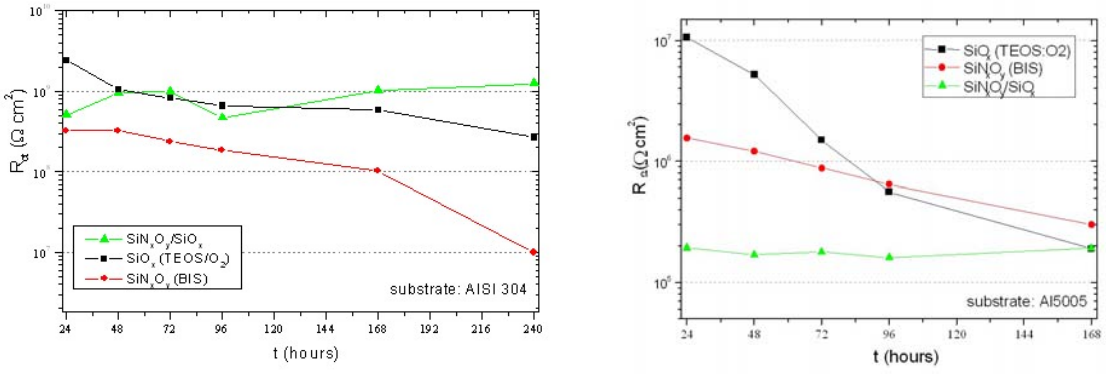

The morphological analysis of the SiN_xO_y/SiO_x double-layers deposited by UNIBA and characterized from the electrochemical point of view in the sub-task 4.3.2 has been performed by POLITO by means of FESEM microscopy.

The FESEM images of the SiN_xO_y/SiO_x double-layers are reported below.

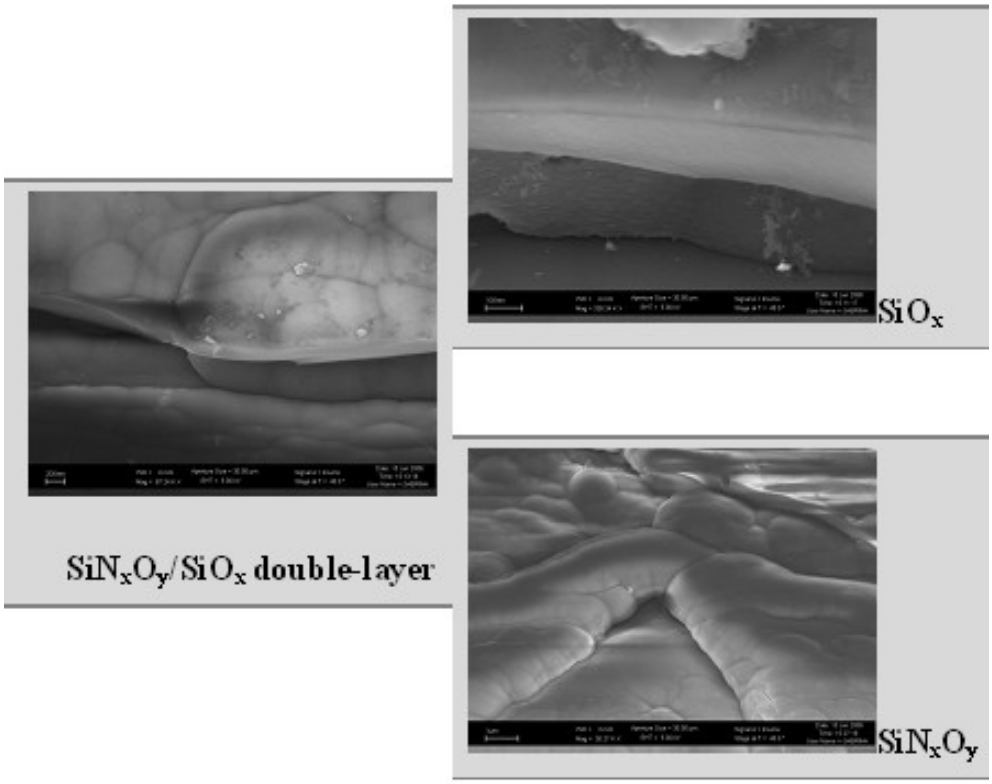

FESEM images of the SiN_xO_y/ SiO_x double-layer

The SiN_xO_y is characterized by a high conformability to the surface roughness, while the SiO_x shows the typical amorphous structure. The FESEM characterisation performed on the coated Al substrates after the EIS measurements show that poor corrosion protective properties of the double-layer in comparison to the SiO_x monlayered coatings can be correlated to the poor adhesion between the two layers and consequently to the delamination of the SiO_x layer due to the interaction with the electrolyte.

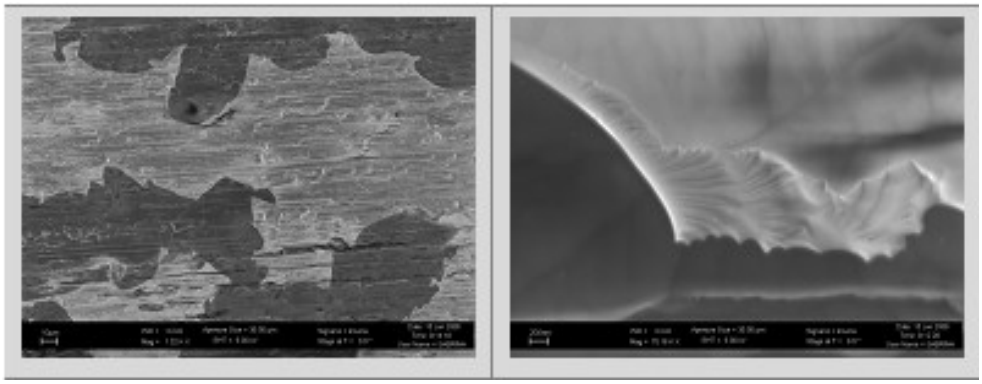

FESEM images of Al substrate coated with SiN_xO_y/ SiO_x double-layer after the corrosion test

In the case of SiO_x/CF_x double-layers the EIS measurements allowed to evaluate the effect of the input power and of the chemical composition of the plasma phase (C_4F_8/Ar ratio) on the protective effectiveness of the CF_x top layer.

The following table summarises the value of the charge transfer resistance, R_{ct}, obtained after 24h of immersion in the chloride-containing solution for the CF_x film deposited in the different conditions.

Substrate	Pre-treatment	Monomer (sccm)	O_2(sccm)	Ar(sccm)	C_4F_8/Ar	Pressure (mTorr)	Power (watt)	R_{ct} (ohm cm^2) 24 h
Inox430	O_2	TEOS (4)	90	44		100	250	3,16E+09
	without	C4F8(10)	0	10	1	200	50	
Inox430	O_2	TEOS (4)	90	44		100	250	1,87E+09
	without	C4F8(10)	0	10	1	200	100	
Inox430	O_2	TEOS (4)	90	44		100	250	6,76E+09
	without	C4F8(10)	0	10	1	200	200	
Inox430	O_2	TEOS (4)	90	44		100	250	4,13E+09
	without	C4F8(15)	0	5	3	200	100	

R_{ct} values recorded on C double layers after 24h of immersion n NaCl 0.1M aerated solution

It is possible to conclude that SiO_x/CF_x double-layers are characterised by good protective properties against corrosion, as confirmed by the high Rct values higher than $1.00 \cdot 10^9 \Omega cm^2$.

An increase in the stability of the top layer has been observed for CF_x coatings deposited at high input power (200W) in C_4F_8 rich plasma, as confirmed by the trend of the R_{ct} values as a function of the immersion time in the aggressive environment (see figures below).

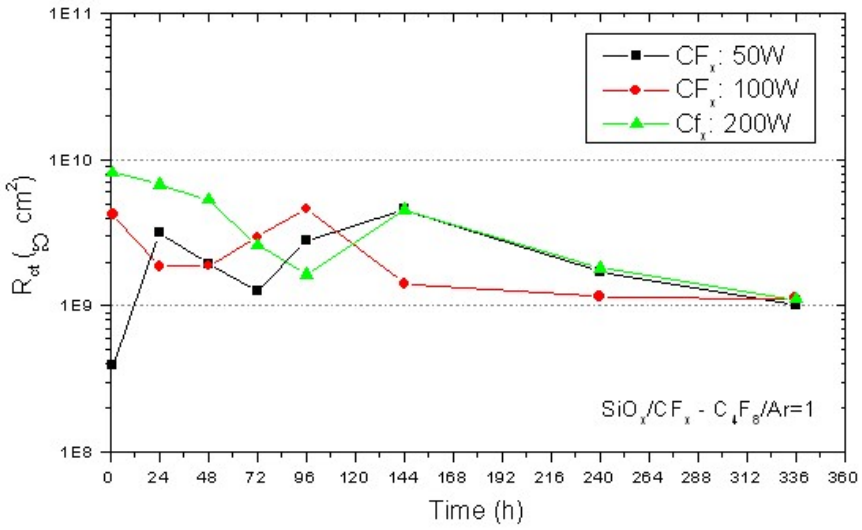

Trend of the R_{ct} values as a function of the immersion time in the NaCl 0.1M solution for SiO_x/CF_x coated steel samples – effect of input power

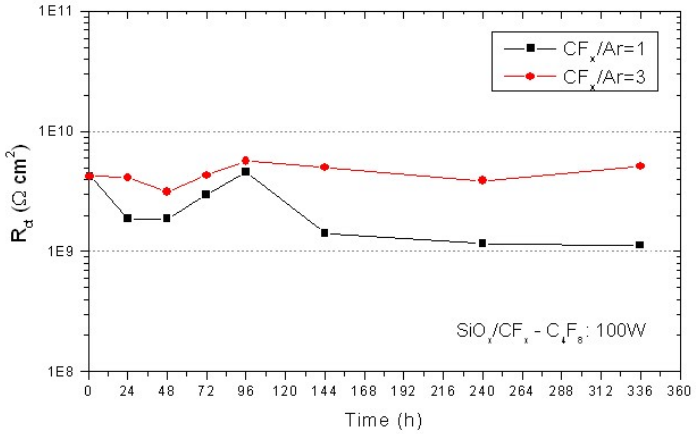

Trend of the R_{ct} values as a function of the immersion time in the NaCl 0.1M solution for SiO_x/CF_x coated steel samples – effect of plasma composition

The morphological analysis of the SiN_xO_y/SiO_x double-layers deposited by UNIBA and characterized from the electrochemical point of view in the sub-task 4.3.2 has been performed by POLITO by means of FESEM microscopy.

Subtask 4.3.3: Characterisation of the coatings in term of wear and corrosion resistance and mechanical properties (**HEF R&D**, **EADS**, **CRF**, **TEFAL**)

Parameters of some of the EADS coatings tested at ICSME are listed in the tables below.

PECVD conditions of EADS coatings

Process	HMDSN	BDMADMS	Oxygen	Nitrogen	Argon	Pressure	Power	T° Sub	Thickness
Nr. 66		1 sccm			30 sccm	0.035 mb	15 W	150 °C	1 µm
Nr. 67		1 sccm	3 sccm		30 sccm	0.035 mb	15 W	150 °C	1 µm
Nr. 68	3 sccm			20 sccm	30 sccm	0.070 mb	45 W	50 °C	1 µm

XPS results

Process	% at.Si	% at.O	% at.C	% at. N	Parameter α' (eV)	
Nr. 66	23.44	14.71	47.87	13.98	***1714.4***	$SiO_{0,63}N_{0,60}C_{2,04}$
Nr. 67	23.85	54.14	16.54	5.43	***1712.1***	$SiO_{2,27}N_{0,23}C_{0,69}$
Nr. 68	26.46	18.57	37.62	17.34	***1714.2***	$SiO_{0,70}N_{0,66}C_{1,42}$

The addition of oxygen to the process strongly increases the oxidic character of the coatings. The figure below represents the Si 2p photoelectron peaks and gives evidences of the presence of Si-O bonds in the EADS-67 sample and Si-N bonds in the EADS-66 and -68 samples. The value of the Auger parameter in the first case is about 1712.1 eV which is characteristic of Si-O bonding and SiO_2-like films. Concerning the samples EADS-66 and -68, the correspondent values are ranging from 1714.2 to 1714.4 eV which is typical of Si-N bonds. It can be assumed that these two coatings are predominantly composed of Si-N bonds embedded into a matrix of carbon atoms. The calculated Auger parameters are in total agreement with the chemical structure defined by means of Si2p photoelectron spectra.

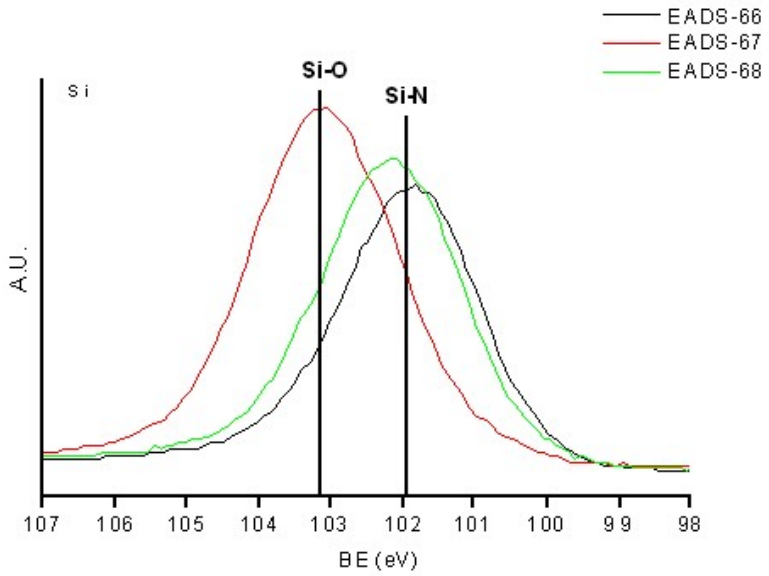

Si 2p photoelectron spectra for the three coatings under study.

The tribological behaviour of the films has been studied at room temperature using a reciprocating pin-on-flat configuration in ambient air (40–50% relative humidity). The evolution of the friction coefficient was recorded using AISI 52100 steel balls 6.00 mm diameter sized for a 1N normal applied load, consistent with maximum Hertzian contact pressure of about 0.7 GPa. The sliding speed was 1 mm/s over a 3.0 mm long wear track. Each sample has been tested twice.

Concerning the friction coefficients, ICMSE observes no significant difference between the samples EADS-66 and -68. The average friction coefficient μ of the coatings is found to be about 0.3. The sample EADS-67 exhibits a friction coefficient of 0.8 which is characteristic of friction coefficients of SiO_2 coatings.

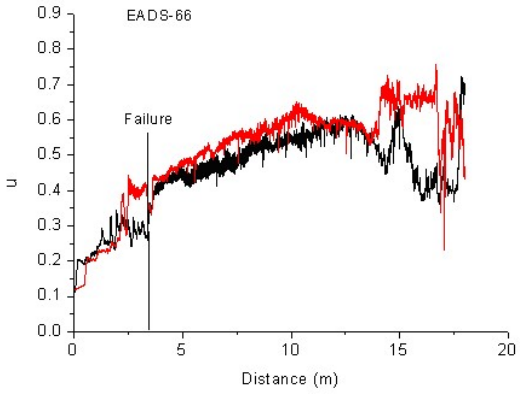

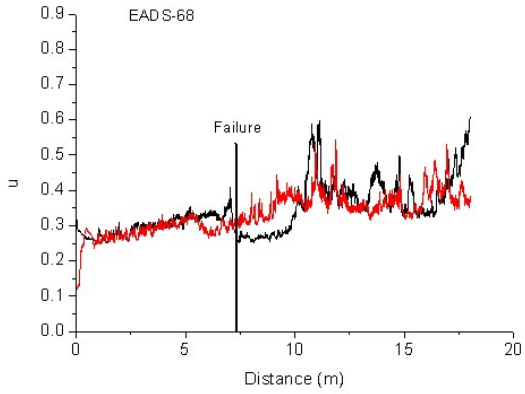

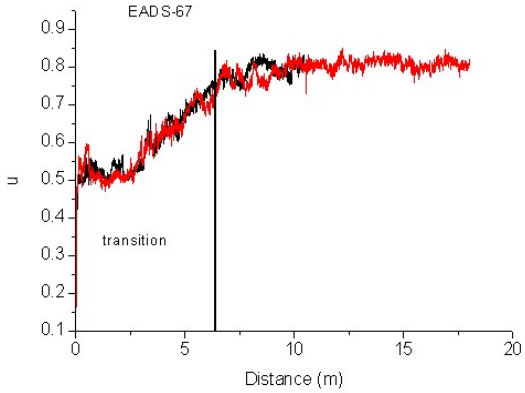

Friction coefficients versus sliding distance for the three samples

The bi-layers investigated by HEF were optimised in term of mechanical properties. The condition of deposition of the 2 layers was found to be important for the mechanical resistance.

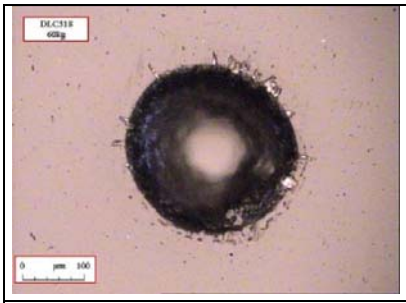	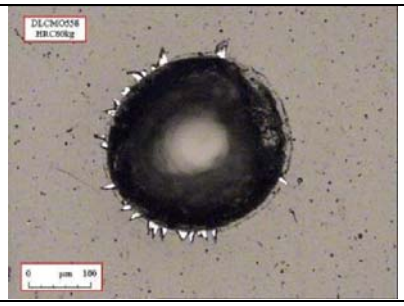	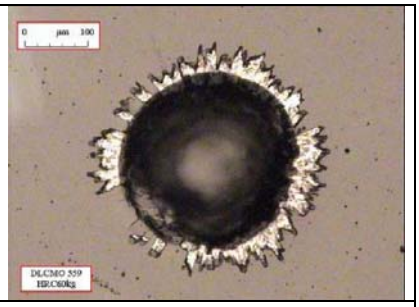
SiCHN(–500V)+DLC (–500V)	**SiCHN(–300V)+DLC(–150V)**	**SiCHN(–150V)+DLC(–150V)**
Pulsed DC PACVD	**Microwave PACVD**	**Microwave PACVD**

The Rockwell adhesion test illustrates the importance of the deposition process and of the deposition conditions on the mechanical behaviour.

Tribological tests

CRF performed tribological tests on different set of disc-samples coated by **HEF** during the project in order to perform the tribological characterisation of the samples and identify the best coating for shim part.
The tests were realised in order to evaluate the friction coefficient and the wear obtained for each coatings developed in the project.
The test was a reciprocating wear test as a ball-on-disc on the OPTIMOL SVR Tribometer.
The two test specimens, ball and disc, which are installed in the test chamber, are pressed on each other.
The top specimen (ball) is oscillated on the bottom specimen at pre-programmed frequency, stroke, load and temperature settings. The specimen contact may either be lubricated or un-lubricated.
The environment in the test chamber (temperature, relative humidity, atmosphere) can also be controlled.

Friction coefficient is automatically calculated as a function of load and recorded throughout the test.
The wear volume and the total friction path are recorded after the test.
In order to simulate the real working conditions of the part (in this case the contact shim/cam in the valve train system of an engine car) the test methodology was developed with the setting of the normal load of the ball against the coated disc, the stroke, the oscillating frequency.
The temperature of the samples was set at 110 °C and the tests were performed in lubricated conditions.

Stroke: 0.5 mm
Frequency: 25 Hz
Load: 20 N (Normal and constant during the test)
Duration of the test: 60 min
Temperature: 110 °C
Test in lubricated condition: Oil SAE 10W – 40

The tested samples presented :
- 2 steel for the shim substrate: 42CrMo4 and 100Cr6
- 3 different coating formulation :
  - SiCH + DLC
  - SiCHN
  - SiCHN + DLC
- different thickness and parameters of the coatings .

The tested samples are reported in the table with the related coating characteristics.

Batch Nr	Shim n.	Substrate	Coating	Total thickness (µm)
A	A11 - A12 - A13 - A14 - A15	42CrMo4	SiCH+DLC	0.3 +1.2
1001	1001 - 1002 - 1003 - 1004 - 1005	100Cr6	SiCH+DLC	1 +1
1006	1006 – 1007 - 1008	100Cr6	SiCHN	1.3
DLC521	30F1 - 30F2 - 30F3	100Cr6	SiCHN +DLC	1.8
DLCMO558	30F4 - 30F5 - 30F6	100Cr6	SiCHN +DLC	2.9
DLCMO559	30F7 - 30F8 - 30F9	100Cr6	SiCHN +DLC	3.6
DLCMO562	30F10 - 30F11	100Cr6	SiCHN +DLC	4.2
DLCMO563	30F13 - 30F14 - 30F15	100Cr6	SiCHN +DLC	4.8
DLCM0628	30F16 - 30F17	100Cr6	SiCHN +DLC	1.1 +0.8
DLCM0633	30F18 - 30F19	100Cr6	SiCH+DLC	1.4 +1.2

In the following graphs is represented the friction coefficient measured during the tests concerning the mentioned samples.

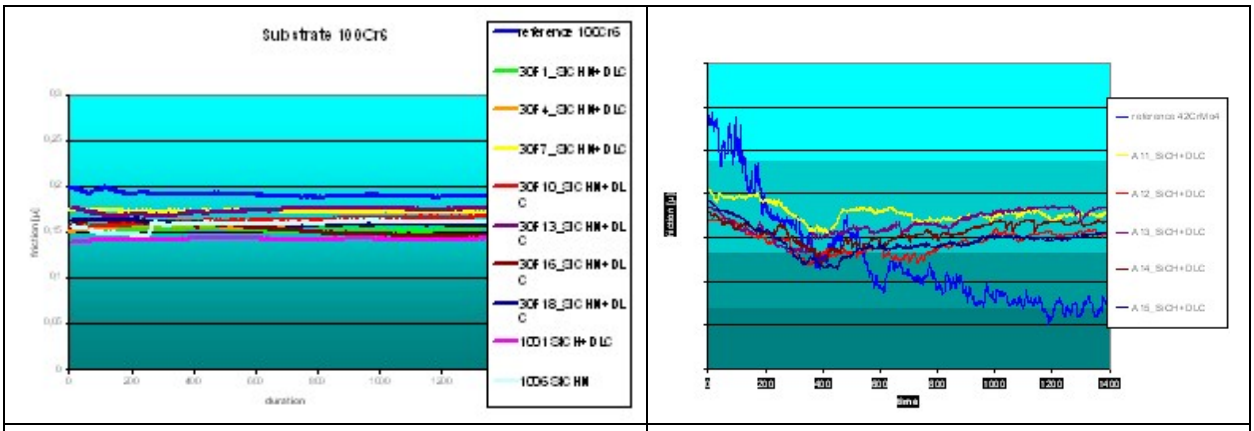

SUBSTRATE 100CR6	SUBSTRATE 42CrMo4

The mean value of the friction coefficient is :

100Cr6 Substrate

Samples	1001	1006	F1	F4	F7	F10	F13	30F16 - 30F17	30F18 - 30F19
Friction coefficient	0.133	0.151	0.154	0.161	0.156	0.167	0.169	0.141	0.152

42CrMo4 Substrate

Samples	A11	A12	A13	A14	A15
Friction coefficient	0.178	0.168	0.179	0.169	0.169

As indicated in the following histogram, where is represented the friction coefficient with the Reference Case (disc in 100Cr6 without coating) , the samples with 100Cr6 substrate and SiCH+DLC coating presented the best tribological behaviour.

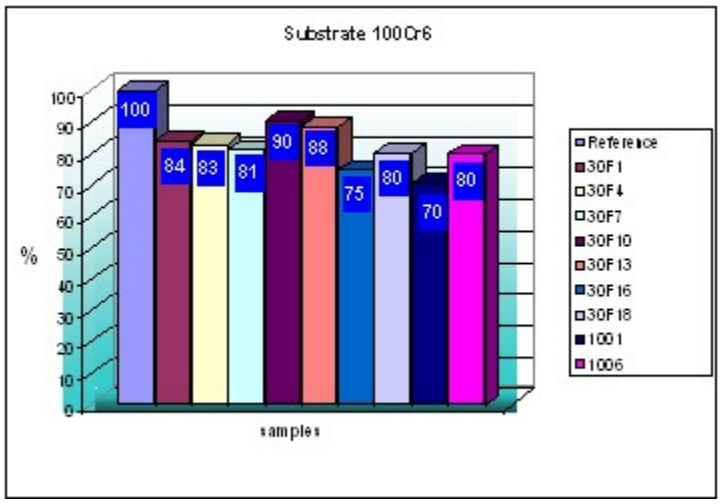

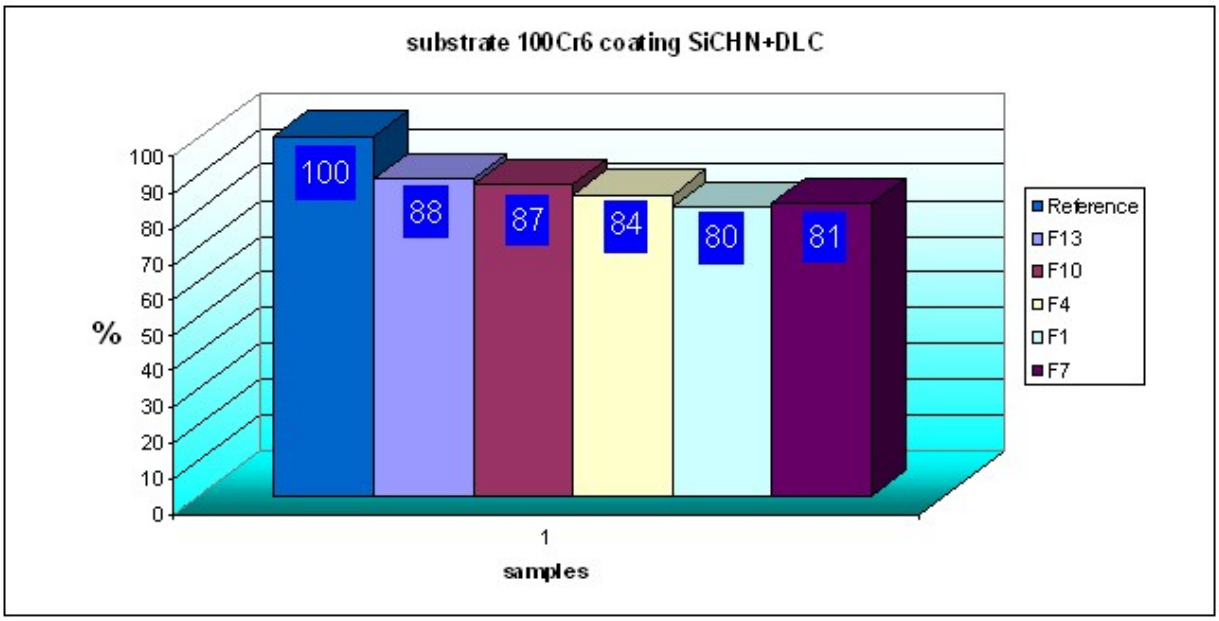

The samples were analysed after the test by scanning electron microscope for a wear evaluation in the contact area.
The samples presented wear (in coated disc and counterpart) with flaking of coating in these configuration:

42CrMo4 substrate and SiCH+DLC coating
100Cr6 substrate with SICHN+DLC coating

The samples with 100Cr6 substrate and SiCH+DLC coating presented the best tribological behaviour (no measurable wear in coated disc and counterpart)

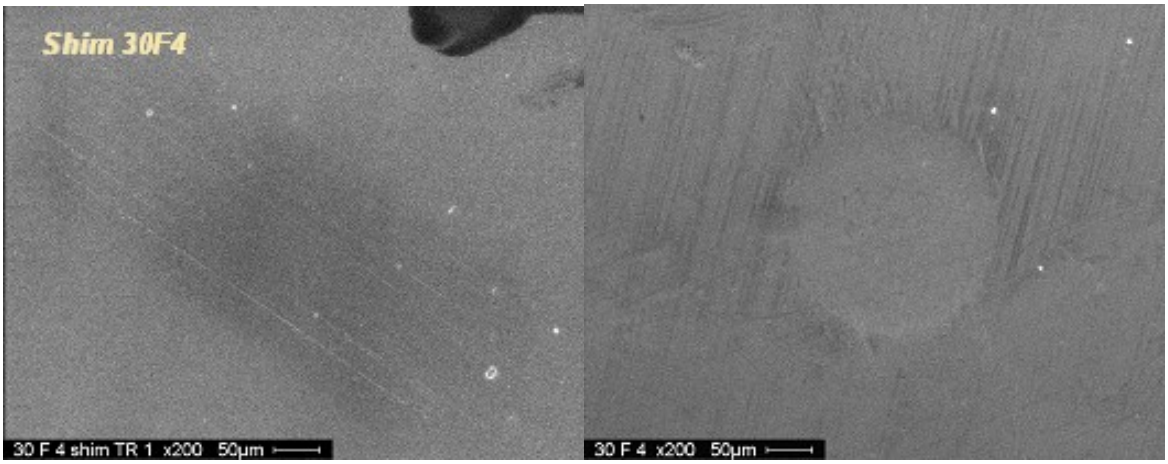
Shim 30F4
30 F 4 shim TR 1 x200 50µm
30 F 4 x200 50µm

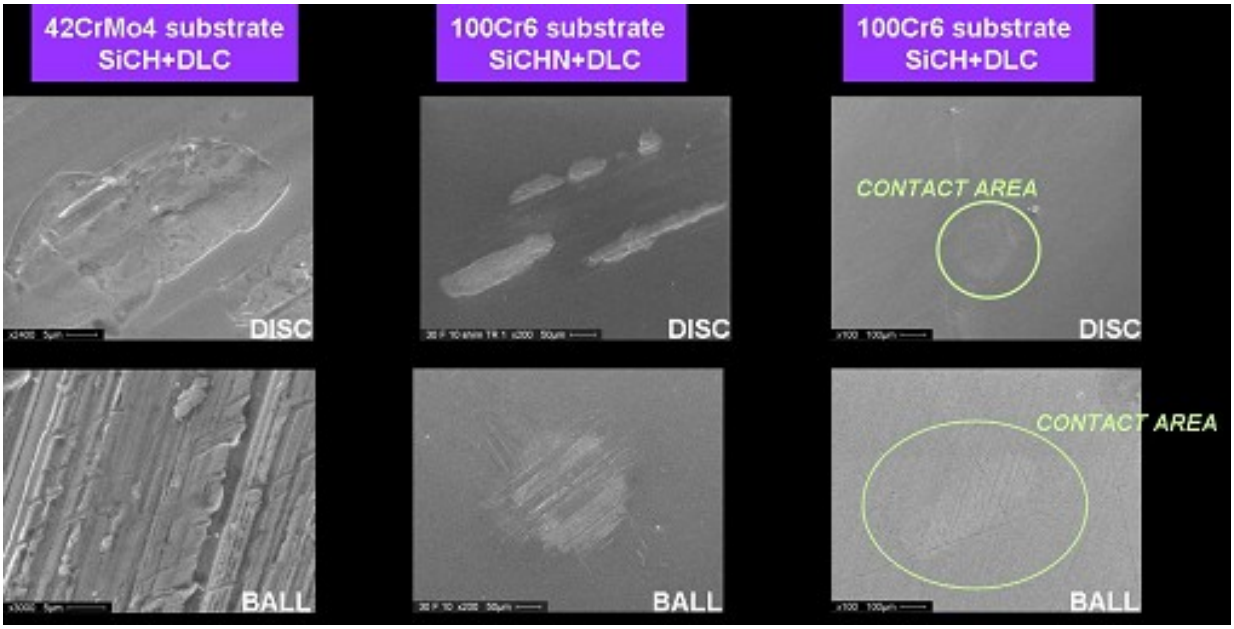
42CrMo4 substrate
SiCH+DLC
100Cr6 substrate
SiCHN+DLC
100Cr6 substrate
SiCH+DLC
CONTACT AREA
DISC
DISC
DISC
CONTACT AREA
BALL
BALL
BALL

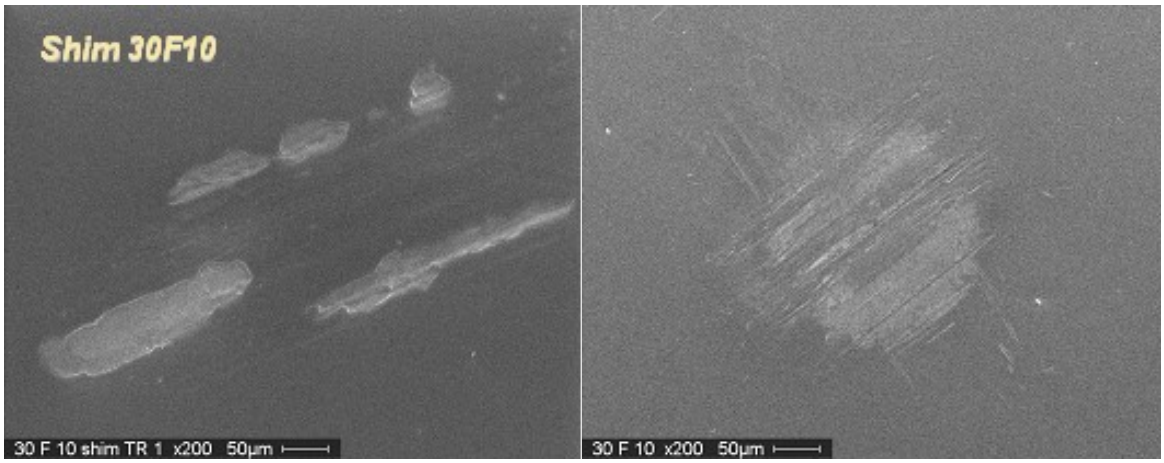
Shim 30F10
30 F 10 shim TR 1 x200 50µm
30 F 10 x200 50µm

100Cr6 SiCH+DLC	Sample N.	1001	1002	1003	1004	1005
	µ	0,133	0,133	0,140	0,143	0,131
100Cr6 SiCHN	Sample N.	1006	1007	1008		
	µ	0,151	0,157	0,150		
100Cr6 SiCHN+DLC	Sample N.	30F1	30F4	30F7	30F10	30F13
	µ	0,154	0,161	0,156	0,167	0,169
42CrMo4 SiCH+DLC	Sample N.	A11	A12	A13	A14	A15
	µ	0,178	0,168	0,179	0,169	0,169

TEFAL has characterised coatings for cookware applications. Requirements are listed below :

Regulations Aspect :

European Regulation Co : Materials in contact with Foodstuffs
n°89/109/CE is replaced by CE n°1935/2004

Specific migration Test :

Applies for polymers or organics
No regulations on metallic substrates

The functional requirements are corrosion resistance, hardness and Easy To Clean (ETC). TEFAL has focussed the research work on this last aspect. The first approach was consisting in contact angle measurement using polar and non polar liquids, assuming that low surface energy could be an indication of ETC.
TEFAL has preformed also an homemade characterisation test to evaluate the coatings provided by UNIBA and HEF R&D. These coatings were based on DLC, fluorinated DLC, SiO_x and SiOC and SiOCNF compounds.
The test consists to burn rice and milk at 210 °C and to try to clean the sample with a white scotch Brite pad. 18 cycles are carried out at a load of 1.5 kg. A detergent is used for this test.

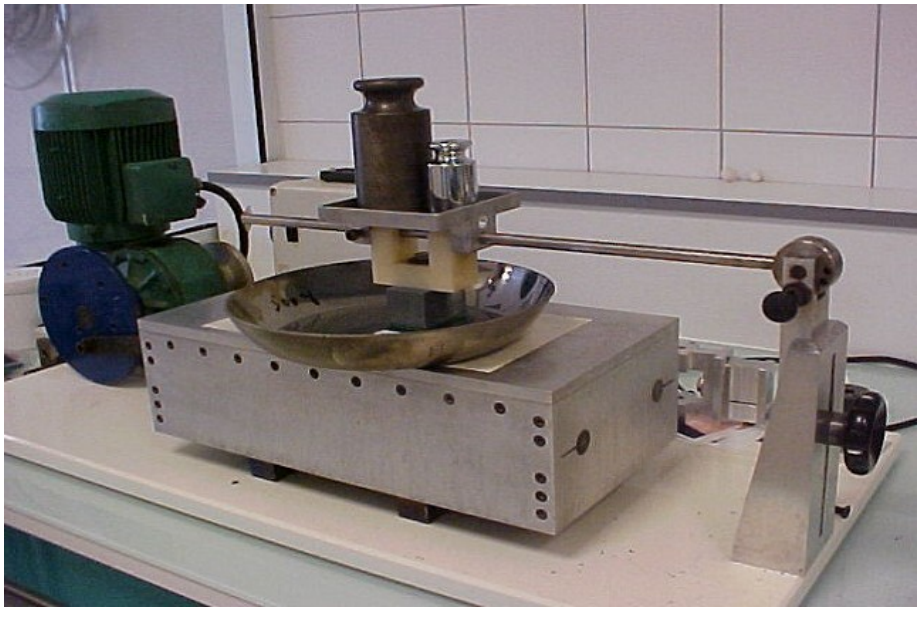

After test, the aspect of samples is characterised and quoted from 0 (bad ETC) to 5 (good ETC).

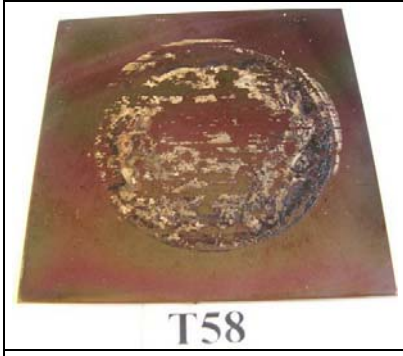	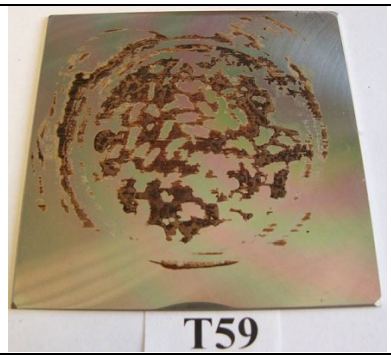	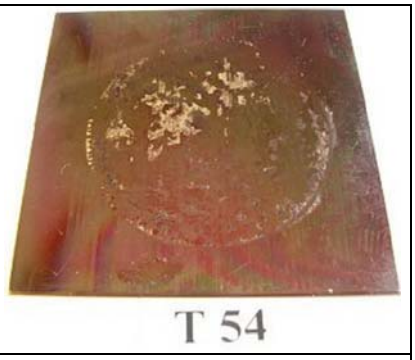
O_2 + BIS	**O_2 + TEOS**	
ETC = 1.5	**ETC = 1.5**	**ETC = 4.5**

The above pictures show some bad behaviour of SiO and SiON based coatings. Using fluorine containing coating has improved in some case the ETC but these coatings are not enough scratch resistant.

Subtask 4.3.4 Optical characterisation of the coatings (**ICMSE**)

The optical characterisation of the transparency properties of the coatings was evaluated at HEF. No coatings were received for UV-VIS measurements at ICMSE during the project.

Subtask 4.3.5 Characterisation of the interface substrate-coating (**UNIBA**, **ICMSE**)

In order to characterise the interface substrate/coating, UNIBA has performed XPS depth profile analysis of the following samples:
- Substrate + plasma coating;
- Substrate + pre-treatment + plasma coating.

Ion sputtering during XPS analysis was carried out by means of 3 keV Ar ion gun.
In the Figure below the atomic percentages profile are reported for a coated aluminum sample with and without O_2 plasma pre-treatment.

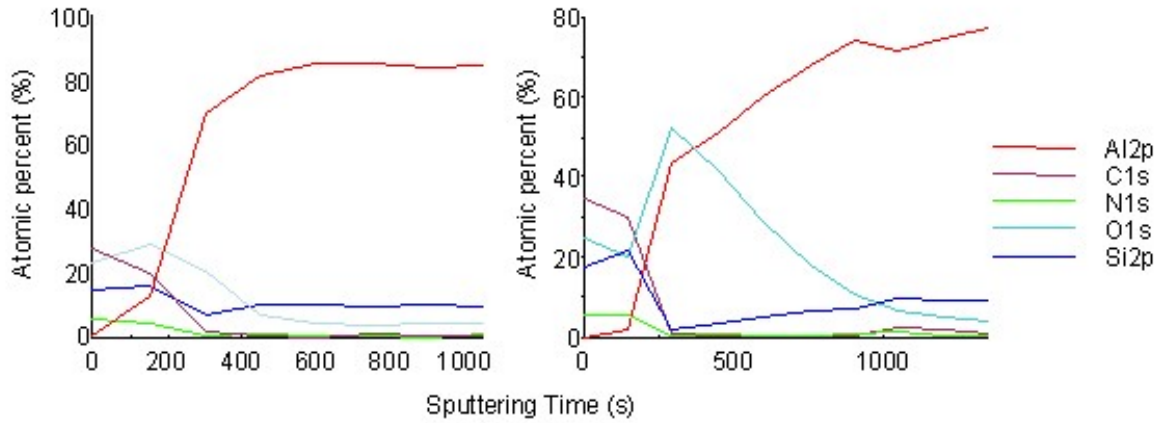

XPS depth profile of SiO_xN_y coated Al substrate without (left) and with (right) plasma pre-treatment

It can be observed that a broadening of the interface results because of an oxidation due to the O_2 plasma pre-treatment, as testified by the oxygen maximum in the profile.. Nitriding of the metal cannot be highlighted. The over oxidation of Al is evident also by the profiling of the Al2P signal reported below: the component at higher BE, relative to AlO_x is more relevant in the oxygen plasma treated sample.

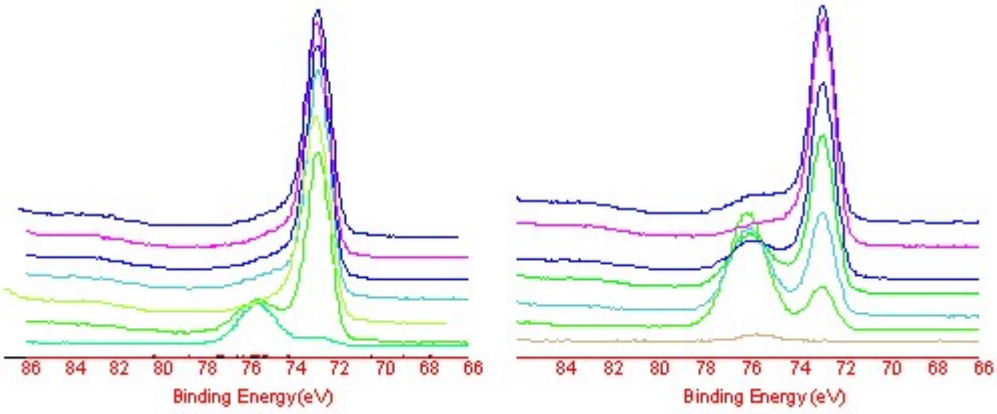

XPS Al2p profile without (left) and with (right) plasma pre-treatment

Similar results have been obtained from the profile obtained onto 42CrMo4, concerning the oxidation of Fe.

It is interesting to notice that when Inox304 is analysed, at the interface there is no modification in the Fe2p depth profile signal but the Cr2p signal presents a major CrO_x content for the O_2 plasma pre-treated sample respect to the untreated one.

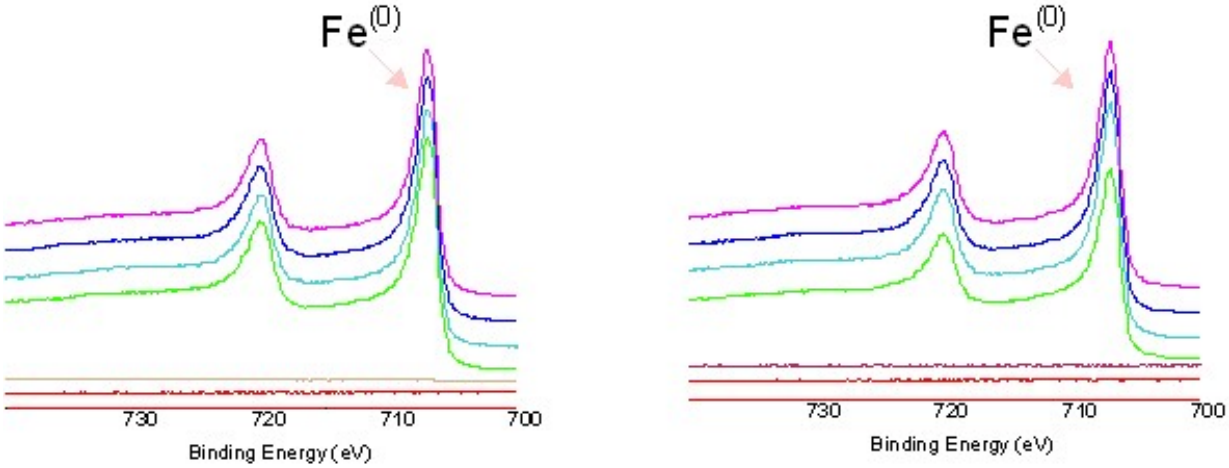

Fe2p signal of Inox304 + SiO_xN_y (left) and Fe2p signal of Inox304 +O_2 pretreatment + SiO_xN_y (right)

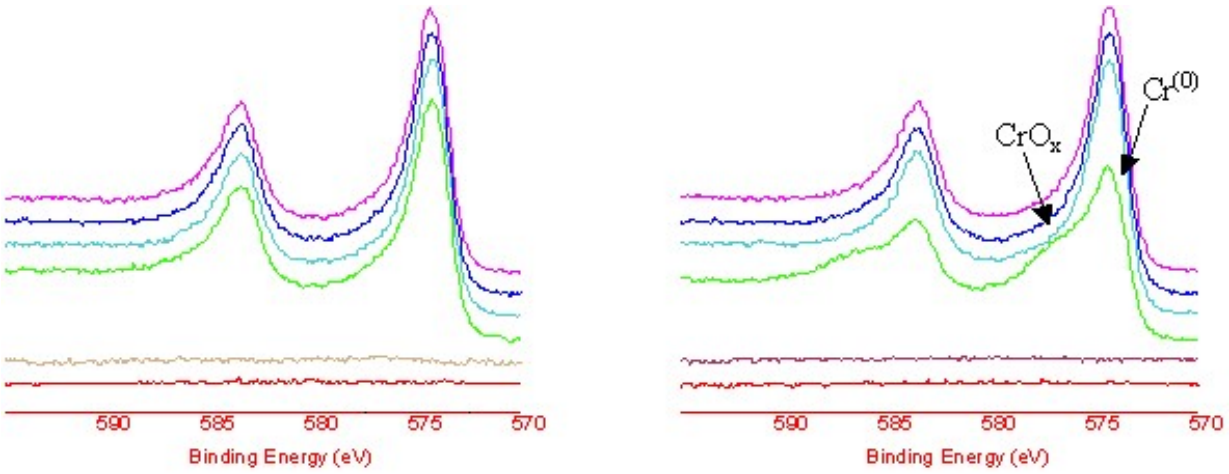

Cr2p signal of Inox304 + SiO_xN_y (left) and Cr2p signal of Inox304 +O_2 pretreatment + SiO_xN_y (right)

1.6.2.3 Task 4.4: Multi-scale approach of the electrochemical behaviour (**INSA**)

INSA was involved in the task 4 to understand the influence of the PACVD Si containing coatings on the corrosion protection of metallic materials. The role of the architecture of stratified coatings was also considered.
The objective was to identify the deposition key-parameters leading to the optimal performance in terms of corrosion protection. To reach such objective, an original 2-step approach was developed, consisting in, first determining the intrinsic electrochemical characteristics of the films and then understanding the electrochemical behaviour of the film once deposited on steel. This approach allows analysing the effects of the galvanic coupling on the degradation of the whole coated part.

Subtask 4.4.1 Coating quality (**INSA**)

Open porosity was estimated by the polarisation curves cross-checking method initiated in the laboratory.

Subtask 4.4.2 Coating chemical inertia (**INSA**)

The chemical inertia was assessed by resonant quartz crystal microbalance.

Subtask 4.4.3 Electrochemical behaviour of coated parts (**INSA**)

The corrosion mechanism was finally explained on the basis of electrochemical impedance spectroscopy. Thanks to a wide interaction between INSA and ICMSE in charge of the structural characterisation, we succeeded in correlating the corrosion behaviour of the films with their chemical nature.
Two series of samples delivered by UNIBA (SiO based coatings) and HEF R&D (SiCH based coatings) partners were characterised. It was established that, in all cases, the intrinsic electrical resistivity of the coating was the key-parameter which controls the protection efficiency.
Analysis of the SiO_x film elaborated by UNIBA revealed an amorphous SiO_2 chemical composition. This film behaves as an insulator, is almost free of open defects, and then protects

the metallic substrate by a barrier layer effect. It was shown that SiO_2 was also efficient to improve the pitting corrosion behaviour of stainless steels.
For the SiCH series, a deep relationship was highlighted between the corrosion rate of the coated parts, and the nitrogen enrichment of the film. Such correlation was explained by semiconductive properties of the coatings. An optimised composition of coating was then proposed.

1.6.2.4 Task 4.5: Understanding phenomena (**INSA**, **ICMSE**)

This task correlates specifically the nature and quality of the coatings, their intrinsic chemical reactivity when immersed in model environment, and their protective effect on the substrate. The multi-scale approach of the electrochemical behaviour of the adhesion layer and their corrosion protection efficiency is fundamental for the understanding of the influence of the structure of the combined, multifunctional coatings on their basic properties. The influence of the architecture (mono or bi-layered structure) on the corrosion protection of steel substrates has therefore been taken into account.
Coatings resistivities deduced from electrical impedance spectra are summarized in next figure:

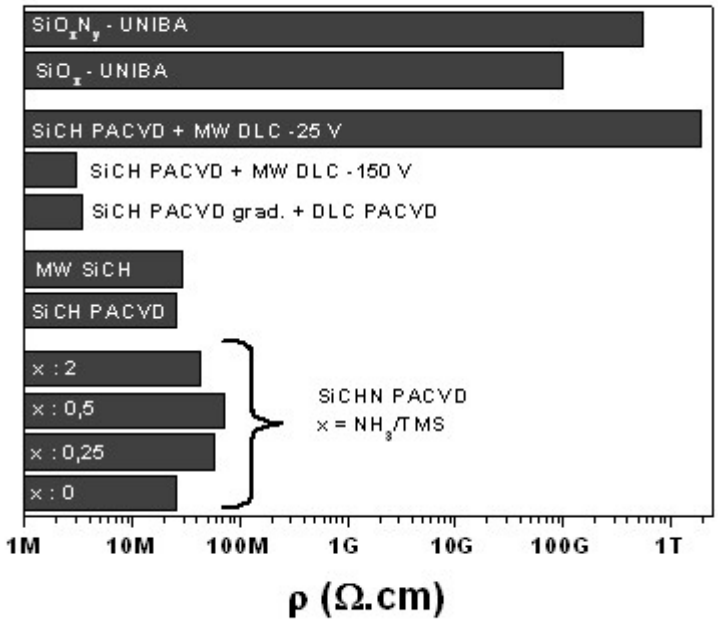

Intrinsic resistivity of various coatings

Charge transport across the layer is directly implicated to the corrosion mechanism. The better corrosion protection is afforded by the higher insulating properties. An insulating behaviour of the coating prevents any galvanic coupling between the coating and its emerged potential defects.

Single coatings

SiO_x: TEM cross-sectional view of SiO_x films prepared by PACVD using TEOS as precursor demonstrated the microstructure of the coating appears very dense and amorphous. No evidences of crystalline features, defects or pores could be seen. The interface between the

substrate and the coating appears very sharp and well defined. By means of XPS and EELS the SiO_2-like character of the coatings was proved (see details on WP1 and WP3). The coating porosity is so low that it can be considered as negligible. Silica-based layers are very promising since they afford excellent corrosion resistance in saline media. The high insulating properties of SiO_x coatings explain their outstanding performance in terms of corrosion protection. No galvanic attack of the substrate can thus occur, and the coating acts as a barrier layer. Moreover, electrochemical measurements, carried out on a laboratory scale, on extended immersion test underline that such high protective efficiency is stable and durable.

SiC_xN_y: It has been demonstrated that the corrosion protective ability of a-SiCN coatings is closely related to their chemical nature, the latter being easily determined by the modified Auger parameter of silicon (α'Si). The corrosion current density and the intrinsic conductivity of the coatings reached the lowest values for an optimum range characterized by N/Si ratios between 0.63 and 0.72. The corresponding α'Si values for the optimum composition are in the range of 1 714.3–1 714.7 eV. Such values correspond to Si–N bonds surrounded by C–C/C–N ''skeletons'' forming a Si–N–C network. This nitrogen incorporation induces an adequate balance between positive and negative free charge carriers leading to high corrosion protectiveness. For even higher N contents, the silicon nitride character of Si-bonds increases, favoring an n-type semi-conductive behaviour which results in a less efficient corrosion resistance. In this study, we have correlated the electrochemical properties with both the chemical and the structural nature of the amorphous SiCN films. Such a procedure can also be applied for other functional characteristics closely dependant on the chemical bonding of the coating.

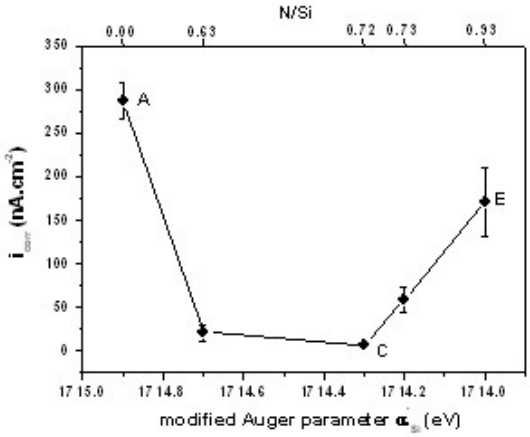

Evolution of the corrosion current density as a function of the chemical characteristics of the different amorphous PACVD SiCN coatings deposited on steel

Multilayer architecture

Whatever the composition, all coatings present a sharp substrate/film interface and are amorphous. The coatings investigated are combination of $SiC_xN_yO_z$ and DLC. It was shown that when z tends to 0 (SiC_xN_y), the corrosion protection effect of the bi-layer system (SiC_xN_y + DLC) was not altered and was slightly increased. When x and y tend to 0 (SiO_z), the DLC top layer shows poor adhesion to SiO_z. When y and z tend to 0 (SiC_x), the corrosion protection of the bi-layer (SiC_x + DLC) is not satisfactory and is less efficient than SiC_x alone. This result is modulated by the nature of DLC top layer.

The porosity of coatings was investigated by electrochemical tests. For all the coatings, the porosity is less than 1 % and can go down to less than 0.0002 %. Except for SiN_yO_z, all the coatings investigated show a high chemical inertia. The evaluation of galvanic coupling of SiO_z on M2 steel has shown that the coatings are really inert. Similar conclusion has been evidenced with SiC_xN_y coatings. In the case of SiC_x coatings, there seems to be a slight coupling with the substrate, however this kind of coating have some effect considering corrosion protection. When adding DLC by classical PACVD on the SiC_x PACVD layer, the slight protection effect by SiCx seems to completely disappear. This behaviour differs much from the mechanism supposed before the project starts, as it was supposed that SiC_x add bad protection effect and addition of DLC could improve the behaviour. When adding soft DLC deposited by the microwave technology to the SiC_x PACVD layer, the corrosion protection is drastically improved.
To conclude, it has been shown that the corrosion protection efficiency and the electrical conductivity were strongly correlated. SiO_2 acting as an insulator and deposited with almost no defects, protects steel by a barrier effect, whereas the corrosion resistance of SiCH and SiCHN layers is influenced by their intrinsic semiconductive properties.

1.6.2.5 Task 4.6: Preparation of materials for validation (**HEF**, **POLITO**)

HEF has deposited coatings on the parts selected by end users and on parts corresponding to a demand identified by HEF. On that last point, HEF has coated steel rods which require both corrosion protection and wear resistance. For this the coating was consisting of a SiCHN sub layer and a DLC top layer. The following pictures shows the first trial for which the polishing carried out according to the method developed in WP1, was not sufficient. Corrosion pits are aligned along the remaining machining grooves. The pits appeared at 72 h while the part was maintained in salt spray test for 167 h.

For the next trial, the polishing was improved. The first corrosion pits appeared after 72h, parts were maintained in salt spray test for 120 h.

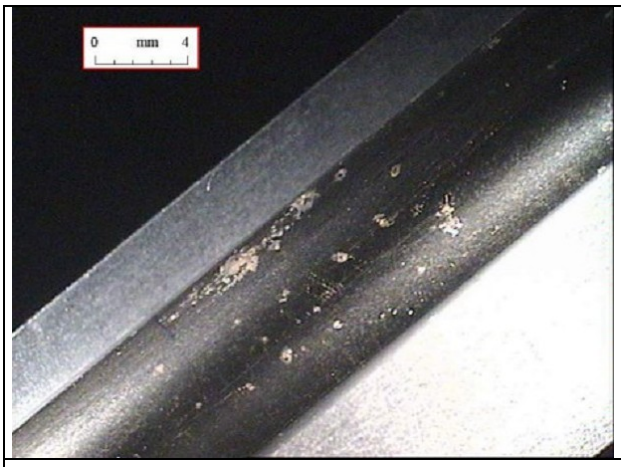	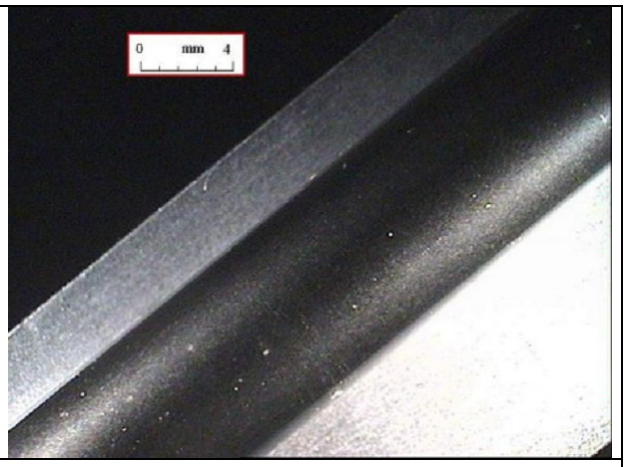
Side oriented toward the axis of the spindle	**Opposite Site**

The corrosion pits are localized on one side of the rod. This side was oriented toward the central axis of the spindle of the rotating substrate holder. On the opposite side, no corrosion pit has formed. Further improvement should be achieved by using 3 rotations substrate holder in order to have an homogeneous coating around the periphery of the rods.

1.6.2.6 Task 4.7: Prediction of the durability of the coated part in service (**INSA**, **POLITO, ICMSE**)

The results of the accelerated corrosion tests (SST according to the ASTM B117 standard method) allow to underline the high protective capability of the MATECO coatings that are able to protect different metallic substrates from galvanic corrosion phenomena. As a matter of fact, galvanic coupling effects are particularly detrimental for any industrial component in working conditions.
The high adaptability of plasma thin films, in particular SiO_x thin films deposited by UNIBA, to the surface roughness and the high electrochemical stability of the films allow to concluded that these coatings can be characterised by good protective properties and can be employed to avoid the detrimental effect due to galvanic coupling on industrial components also near bolt of junctions between different metals.
In order to improve the mechanical/wear properties of the surface, the effect of a DLC top-coat deposited on SiCH based film was tested under tribo-corrosion conditions at INSA. This experiment consists in combining the degradation effects of both the electrochemical corrosion and the wear. From a corrosion point of view, the beneficial effect of the underlayer is confirmed, but only in a temporary manner insofar as the film finally destroys with the test duration. In the case of the duplex SiCH/DLC coated steel, the energy dissipated in the contact is hugely reduced. Moreover, such "self-lubricant" effect is stable with time. After the test, the sample shows no traces of corrosion and the wear track is almost impossible to observe. This layers stratification seems then promising to reduce the degradation of industrial parts in service.

		
Bare steel	**SiCH coated Steel**	**DLC/SiCH coated steel**

1.6.3 WP Assessment and Conclusions

Multifunctionnal coatings have been elaborated and characterised in the WP4. 2 coatings families were defined.
On one side, SiO_x coatings have been found to be very efficient for corrosion protection. This coating can be deposited alone for optical application because of its high optical properties. The main difficulty with this solution concerns the deposition of high thickness to prevent coloration by light interference. This solution was not retained as it is not considered to be economically viable to protect metal coatings on plastic parts which necessitate low deposition rate to keep low the deposition temperature.
SiO_x coatings were also combined with low surface energy top coatings. These top coatings were obtained by addition of fluorine to the coatings. The functional characterisation of these coatings have allowed to evidence that low surface energy is not the only characteristic to consider for Easy To Clean applications. One might also consider micro roughness and chemical inertia which can affect the ETC in the chosen application. The scratch resistance necessary for the ETC application is estimated to be insufficient, the low surface energy coatings are not hard enough.
On the other side, SiCHN coatings were combined with top DLC coatings. The SiCHN base layers demonstrate the possibility to bring corrosion protection. The addition of DLC on SiCHN coatings was possible and showed good adhesion between the 2 layers. SiCHN was chosen instead of SiO_x despite its lower corrosion protection efficiency, because adhesion of DLC on SiO_x was not possible and because SiCHN has higher intrinsic mechanical properties.
Such coatings were deposited on 3 kinds of real parts concerned by mechanical applications and have shown the interest of such solution compared to the state of the art.
The characterisations carried out in this workpackage have allowed to understand the mechanism for corrosion protection of such coatings. It was also shown that the behaviour of the base layer in term of corrosion protection could be affected in some case by the deposition of the top layer. This explains the better behaviour of the combination of SiCHN with DLC compared to classical industrial DLC solutions.

Milestone 4.1 : Establishment of the possibility to obtain the objectives for each multifunctional purpose by coating materials and their combination.
Particularly good results were obtained for the combination of corrosion protection together with friction reduction and wear resistance, including anti fretting. The coatings obtained in this field should be developed and exploited after the end of the project.
The combination of corrosion protection and optical transparency has also been reached but it seems that this solution could be limited for economical reasons as high thickness is required to

prevent interferences of visible light which is not compatible with the required low deposition rate on plastic parts to prevent their degradation by over heating.
For Easy To Clean, low surface energy coatings were obtained but their performance level was not sufficient for the aimed application, especially because this application requires also scratch resistance. One can expect that such coatings could find other applications less sensitive to scratch resistance.

Milestone 4.2 : Defect free coated surface, the coatings should have less than 1% porosity, defined by electrochemical characterisations.
This milestone has been reached by combining the surface preparation method studied in WP1 and the deposition of poorly electrical conductive amorphous coatings developed in WP3 and WP2. The measured porosities were generally comprised between 0.01 and 1% with rather thin coatings, generally less than 3 µm.

1.7 WP 5: Life Cycle Analysis and Socio / Economical / Health Impact (WP Leader: POLITO)

WP Leader POLITO
Participants HEF –CRF – EADS – EPM

1.7.1 Objectives

The objective of this task is to perform an overall analysis of the consequences of the project actions in terms of technical/economical advantages and environmental impact:

- To elaborate an economical study regarding the impact of adopting and implementing proposed technologies;
- To perform a Life Cycle Analysis (LCA) of different coatings developed in order to compare the environmental impact of new coatings in relation to actual ones;
- To define the methods for the recycling of the coating at the end of life;
- To define the economical and environmental impact of such recycling;
- To perform a comparison of results with alternative approaches and discuss their exploitation.

1.7.2 Work performed

1.7.2.1 Task 5.1: Life Cycle Analysis (**HEF, POLITO, EPM, CRF, EADS**) and Task 5.2: Socio / Economical / Health impact (**POLITO**)

Subtask 5.1.1 Removal of the coating by dissolution (**HEF**)

Some trials were made by using solutions including F^- ions. Fluoride solutions are known to make chemical dissolution of silicon containing materials like glass, silica, silicon nitride. The dissolution rate is extremely low on SiCHN coatings. It seems that the increase of carbon content in the coating inhibits the dissolution by fluoride. Some corrosion pits have occurred on the 42CrMo4 substrates where the substrate was not coated. Corrosion inhibitor which protect steel in fluoride solutions should be added. This way is not very promising as it involves hazardous solutions, it produces liquid effluent which have to be neutralized and may interact with the substrate material. In addition, the use of acidic solutions is forbidden on some

materials as it may render them brittle. The work has been focused on the plasma removal (ST 5.1.2) which should be safer for the substrate materials and easier for the handling of small amount of gaseous effluent.

Subtask 5.1.2 Removal of the coating by plasma etching (**HEF, EPM**)

This task is connected to task 2.4 in WP2. The mechanism of coating removal consists in etching the coating by producing chemical reaction with the constituent of the coating. To etch the DLC top layer, an oxygen plasma can be used. The oxygen reacts with the coating and produces volatile species like CO, CO_2, H_2O…. It is necessary to apply a soft ion bombardment to enhance the desorption of the volatile species. For the removal of Si based coatings, the plasma need to be done in a mixture of oxygen and tetrafluoromethane. In the plasma, CF_4 creates some fluorine atoms and some fluorine containing radicals. Fluorine reacts with silicon to form species like SiF_4 which are volatile. The oxygen is used to react with carbon as well from the CF_4 molecule as from the coating. In this case, the soft ion bombardment applied to the coating enhances the desorption hence increases the etching rate.
For coating removal, HEF R&D has built a specific equipment shown in the picture below.

Vacuum equipment for coating removal

This equipment includes a static substrate holder in the bottom of the chamber. The substrate holder is RF biased in order to create the plasma on the parts. The chamber is evacuated by a two stage mechanical pump and allows to operate the plasma between 1 and 10 Pa. Finally, the equipment has three gas lines : Ar, O_2 and CF_4. HEF has used this equipment to determine the removal rate of SiCHN, SiCH and DLC. Process parameters have been optimized to remove the coating without degradation of the surface of the parts. This has been validated on steel and titanium alloys.

Subtask 5.1.3 General study (**POLITO, CRF, EADS**)

One of the main goal of the analysis was to compare different coatings obtained by PA-CVD process, in particular SiO_x and SiCHN/DLC systems, with a Ni/Cr coating obtained by

galvanic process. According to the objectives of the WP, the data collection procedure started sending the questionnaires to the partners involved in the analysis. Specifically, the life cycle data have been supplied by POLITO, UNIBARI and HEF in the case of PA-CVD technology and by an Italian company as far as the galvanic process is concerned. Figure 1 resumes the system boundaries of the considered processes.
Concerning the functional unit definition, it has already been observed that it represented the most important parameter to be set up. At first, the functional unit (FU) was 1 m2 * 1 micron of coated surface: as following described, a different approach will be proposed, using the coating performances to refine the LCA results.

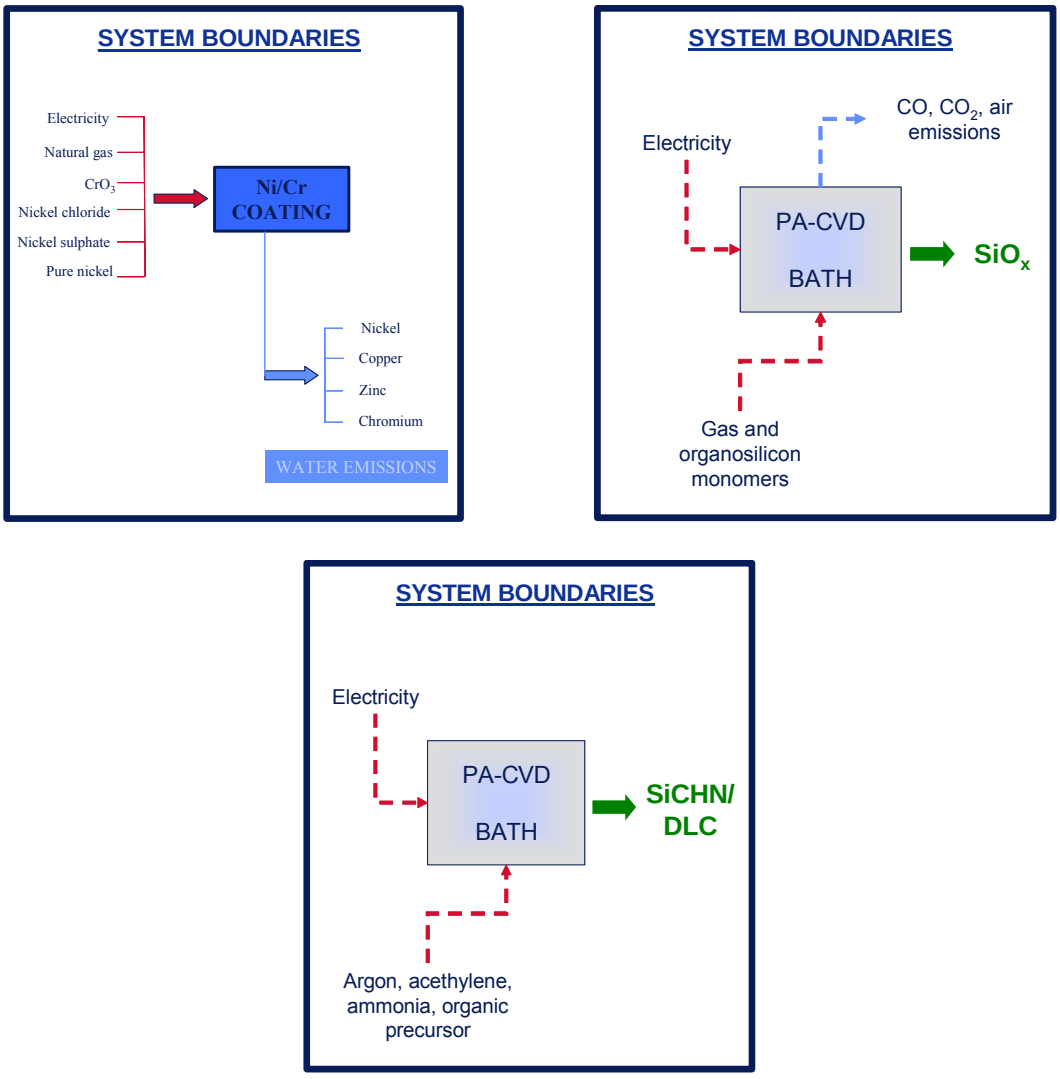

System boundaries of the processes analysed

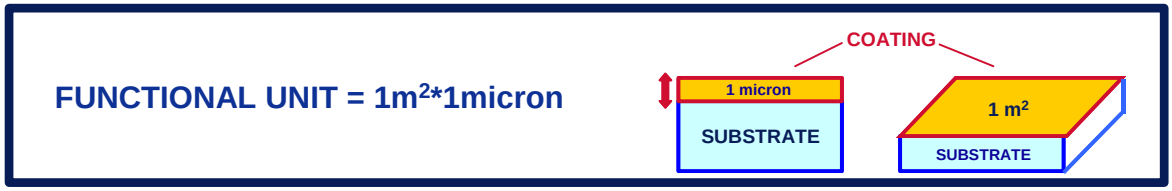

The first approach adopted for the functional unit definition

Following these main lines, Table 1 shows the old results obtained adopting 1 m2 * 1 micron of coated surface as functional unit. The main environmental indicator chosen for the presentation are the GER (*Gross Energy Requirement*), expressed as MJ/FU, and the GWP100 (*Global Warming Potential*), expressed as kg CO_2-eq./FU. It is important to underline that the results have been referred to the Ni/Cr coating (galvanic process = 1).

PROCESS	GALVANIC (Ni/Cr)	PA-CVD (SiO_x)	PA-CVD (SiCHN/DLC)[1]
GER	1	2,3	388
GWP_{100}	1	1,7	62

Old results using 1 m^2 * 1 micron as FU

The study evidenced very high energy consumption and global warming values for PA-CVD processes, especially in the case of SiCHN/DLC coating. The lab-scale conditions and the optimization of the technology were probably the reasons of such performances. Specifically, the figure below shows the old data used for the calculation of HEF coatings.

OLD DATA SUPPLIED BY HEF (SiCHN+DLC)

PROCESS →

STEP	Duration	Energy consumption	Other consumables	Thickness	Area
Pumping	Not available	242 kWh	TMS 173 g NH_3 115 g Ar 497 g		
Heating up to 300°C	Not available				
Keeping temperature at 300°C	Not available				
Plasma etching	Not available				
SiCHN step	Not available			1,2 micron	0,135 m^2
DLC step	Not available	192 kWh	C_2H_2 206 g TMS 232 g NH_3 13 g Ar 497 g	1,5 micron	0,224 m^2
Cooling	Not available				

The old data used for LCA model of SiCHN/DLC coating

As previously said, during the last six months up-to-date data about SiCHN/DLC coating systems have been collected, in order to optimize the life cycle model. In particular, three process setting have been proposed by HEF, as shown in the figure below.

[1] Data referred to a PA-CVD process not optimized: for this reason the results have been called "old".

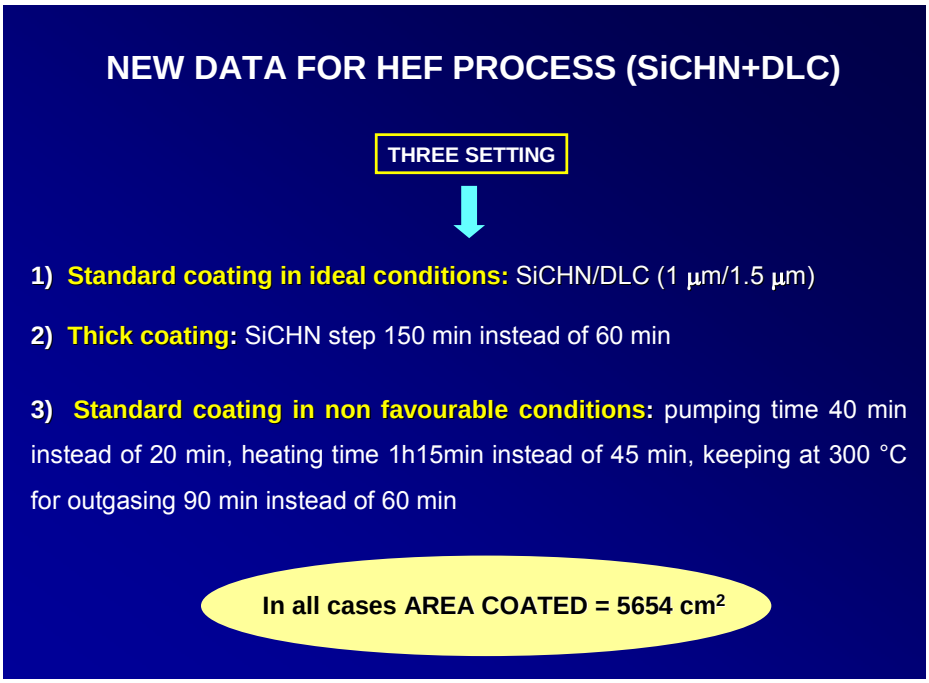

The three setting adopted for LCA model of SiCHN/DLC coating

The optimized data used to rectify the life cycle results are reported in the figure below. It is important to put in evidence that the specific energy consumption strongly decreased, due to the use of a full loaded deposition chamber and to an accurate measurement of electricity utilization.

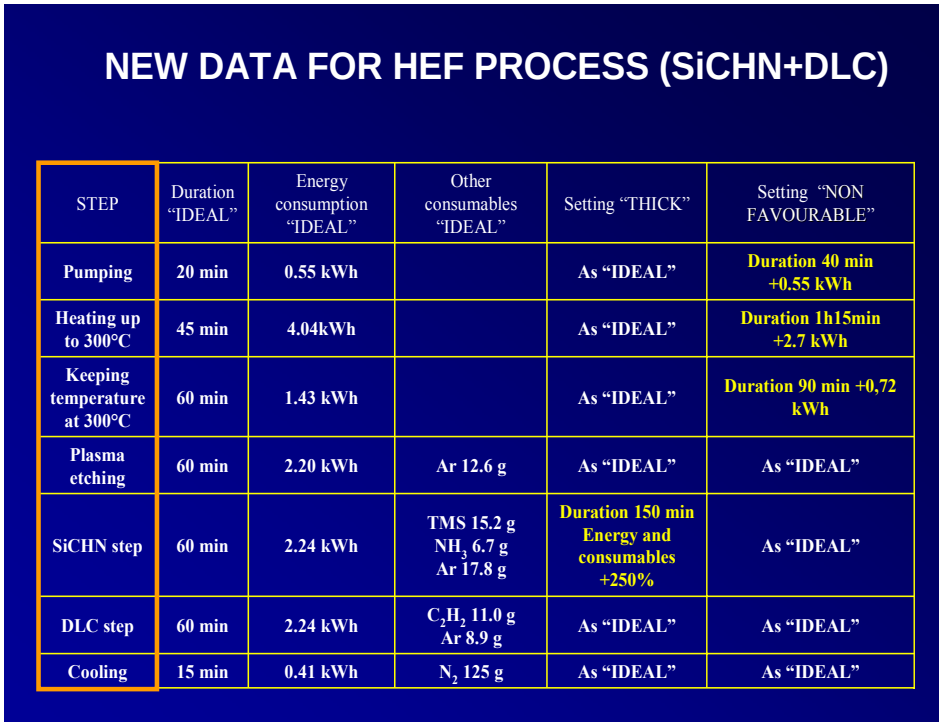

NEW DATA FOR HEF PROCESS (SiCHN+DLC)

STEP	Duration "IDEAL"	Energy consumption "IDEAL"	Other consumables "IDEAL"	Setting "THICK"	Setting "NON FAVOURABLE"
Pumping	20 min	0.55 kWh		As "IDEAL"	Duration 40 min +0.55 kWh
Heating up to 300°C	45 min	4.04kWh		As "IDEAL"	Duration 1h15min +2.7 kWh
Keeping temperature at 300°C	60 min	1.43 kWh		As "IDEAL"	Duration 90 min +0,72 kWh
Plasma etching	60 min	2.20 kWh	Ar 12.6 g	As "IDEAL"	As "IDEAL"
SiCHN step	60 min	2.24 kWh	TMS 15.2 g NH_3 6.7 g Ar 17.8 g	Duration 150 min Energy and consumables +250%	As "IDEAL"
DLC step	60 min	2.24 kWh	C_2H_2 11.0 g Ar 8.9 g	As "IDEAL"	As "IDEAL"
Cooling	15 min	0.41 kWh	N_2 125 g	As "IDEAL"	As "IDEAL"

Optimized data used for LCA model of SiCHN/DLC coating

Starting from this new figures, the LCA model have been revised: the table below shows the optimized results related to 1 m^2 * 1 micron of coated surface as functional unit.

PROCESS	GALVANIC (Ni/Cr)	PA-CVD (SiO_x)	PA-CVD (SiCHN/DLC) "ideal"	PA-CVD (SiCHN/DLC) "thick"	PA-CVD (SiCHN/DLC) "non favourable"
GER	1	2,3	3,7	4,7	4,9
GWP_{100}	1	1,7	0,6	0,8	0,8

Optimized results using 1 m^2 * 1 micron as FU

Concerning the functional unit, it has already been stressed that the results up presented do not take into account the properties of the coatings. For this reason, a different approach was studied in order to introduce salt spray tests to define a correction factor that takes into account the corrosion resistance property of the layer.
In particular, the idea is:

- To refer the results to the galvanic process (Ni/Cr coating = 1) as in the case of previous FU;
- To re-calculate the results using 1 m2 * technical thickness as FU (they are called "GEOMETRIC RESULTS");
- To calculate the "FUNCTIONAL RESULTS" introducing the salt spray tests to define a correction factor (CF).

The correction factor is calculated as follows:

CF = corrosion resistance galvanic process / corrosion resistance considered process

After having calculated the CF, it is possible to obtain the FUNCTIONAL results following the equation:

FUNCTIONAL result = CF * GEOMETRIC result

The figure below compares the functional results of the processes analysed. In the case of PA-CVD process, salt spray tests refer to coatings on 42CrMo4 steel substrate. No data about the corrosion behaviour of "thick" and "non favourable" SiCHN/DLC samples were available: for this reason it has been supposed that the correction factor was the same of the "ideal" samples. The new approach takes also into consideration the Acidification Potential (AP) as LCA indicator.

RESULTS OBTAINED FOLLOWING THE GEOMETRIC AND FUNCTIONAL APPROACH

	GER geometric	GWP_{100} geometric	AP geometric	h_{corr}	Correction Factor	CORRECTED GER	CORRECTED GWP_{100}	CORRECTED AP
Galvanic (1 m² – 16 µm)	1	1	1	350	350/350 = 1	1	1	1
PA-CVD Polito&Uniba (1 m² – 1,5 µm)	0,2	0,2	0,2	168	350/168 = 2,1	0,4	0,4	0,4
PA-CVD HEF OLD (1 m² – 2,7 µm)	65,5	10,4	14	162	350/162 = 2,2	144,1	22,8	30,8
PA-CVD HEF "IDEAL" (1 m² – 2,5 µm)	0,6	0,1	0,1	156	350/156 = 2,2	1,3	0,2	0,2
PA-CVD HEF "THICK" (1 m² – 2,5 µm)	0,7	0,1	0,2	x	350/x if x=156 →	1,5	0,2	0,4
PA-CVD HEF "NON FAVOURABLE" (1 m² – 2,5 µm)	0,8	0,1	0,2	y	350/y if y=156 →	1,8	0,2	0,4

Salt spray test

Coatings deposited onto 42CrMo4

Geometric and functional results for Ni/Cr, SiO_x and SiCHN/DLC coatings

The actual results put in evidence that taking into account only the geometric characteristics of coatings, PA-CVD process requires generally a low quantity of direct process energy with respect to Ni/Cr technology. Also the main environmental indicator values - GWP and AP - are lower than galvanic process. It is expected that considering combined corrosion protection and tribology performances, SiCHN/DLC coating would have largely lower environmental impact than Ni/Cr as wear resistance of DLC (hardness up to 3000 $kg.mm^{-2}$) is much higher than the one of Ni/Cr (hardness up to 1000 $kg.mm^{-2}$) and dry friction against steel of DLC allows coefficient as low as 0.15 while it is around 0.70 for hard chromium plating.

The impact of PA-CVD are mainly due to the high electricity consumption and depend strongly on the process parameters and on the chemical nature of coatings: for these reasons, the country energy mix is a key factor for the environmental performance and the increase of the energy efficiency could be a good way to reduce significantly the burdens of the process.

Introducing the corrosion resistance of coatings as functional parameter, the results change. In particular, due to a correction factor > 1, the impact of SiO_x technology significantly rose, remaining in any case under the Ni/Cr values. As far as SiCHN/DLC process is concerned, it is first possible to see that the energetic and environmental burdens dramatically fell with respect to the old ones (Table 1). Comparing the functional results, the behaviour of GWP and AP indicators is similar to SiO_x process deposition, while in the case of Gross Energy, SiCHN/DLC coatings present the highest values.

The next step would be the LCA study of new different layers deposited by PA-CVD and the definition of a second correction factor in which the corrosion resistance property will be substituted by wear resistance measurement or the combination of both (multifunctional coatings).

Finally, the analysis has been focused on coatings cost evaluation and recycling environmental/economical assessment. In particular, concerning the economical analysis of coatings, it has been decided to evaluate the energetic and the environmental costs of PACVD deposition process. In the case of energy, it has been supposed to carry out the processes in

Italy and in France, starting from an electricity price of 0,1929 €/kWh and 0,1111 €/kWh respectively. In the case of environmental costs, the analysis is based on the prices of CO_2 during the year 2005 (scenario 1 - minimum price 7 €/t, scenario 2 - maximum price 30 €/t).

PARAMETER	COATING	COST
Electricity	SiCHN+DLC "ideal"	**Italy**: 4,5 € **France**: 2,6 €
	SiCHN+DLC "thick"	**Italy**: 5,6 € **France**: 3,2 €
	SiCHN+DLC "non favour."	**Italy**: 5,8 € **France**: 3,4 €
	SiO_x	**Italy**: 1,5 € **France**: 0,9 €

Energetic costs of coatings (data refer to 1 m^2 * technical thickness)

PARAMETER	COATING	COST
CO_2 – Scenario 1 (CO_2 cost = 7 €/t)	SiCHN+DLC "ideal"	**France**: ***0,018 €***
	SiCHN+DLC "thick"	**France**: ***0,023 €***
	SiCHN+DLC "non favour."	**France**: ***0,024 €***
	SiO_x	**Italy**: ***0,030 €***

Environmental costs of coatings (data refer to 1 m^2 * technical thickness). In this case, the energy mix of the country in which coatings are produced has been adopted

PARAMETER	COATING	COST
CO_2 – Scenario 2 (CO_2 cost = 30 €/t)	SiCHN+DLC "ideal"	**France**: ***0,080 €***
	SiCHN+DLC "thick"	**France**: ***0,099 €***
	SiCHN+DLC "non favour."	**France**: ***0,103 €***
	SiO_x	**Italy**: ***0,129 €***

Environmental costs of coatings (data refer to 1 m^2 * technical thickness). In this case, the energy mix of the country in which coatings are produced has been adopted

Concerning recycling, the analysis started from HEF de-coating processes developed in the context of Task 5.1.1 and 5.1.2. In particular, coating removal was tested by using three methodologies:

- A mixture of acids containing fluorine: in this case the DLC overcoat is not attacked, Si containing underlayers are very slowly removed and the steel substrates are corroded;
- Sandblasting: using this technique the surface is destroyed;

- Plasma etching: DLC layer has been removed by RF plasma under O2, while Si underlayer by RF plasma under O2/CF4 mixture. In this case, the results were excellent and parts have not been damaged by the treatment. For this reason, this process has been studied using the LCA approach.

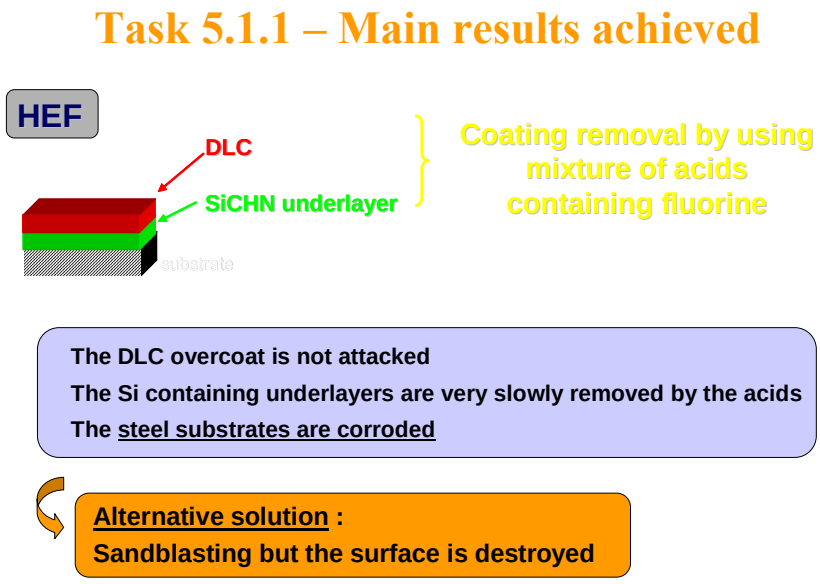

Techniques tested for PACVD coated samples recycling

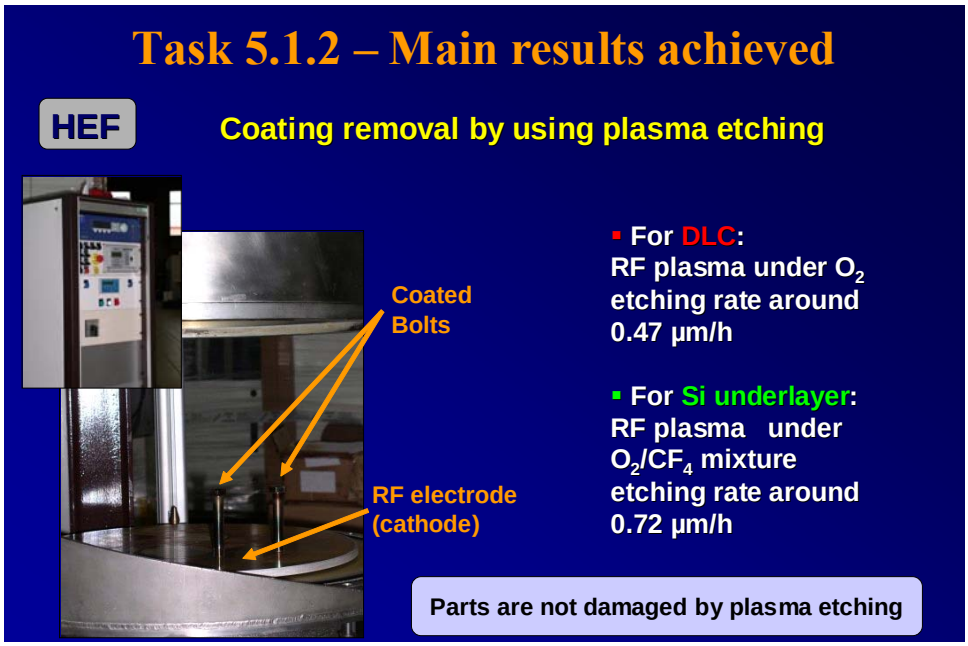

Plasma etching for coated samples recycling

Data have been collected by HEF and the functional unit adopted is 1 m^2 of surface de-coated.

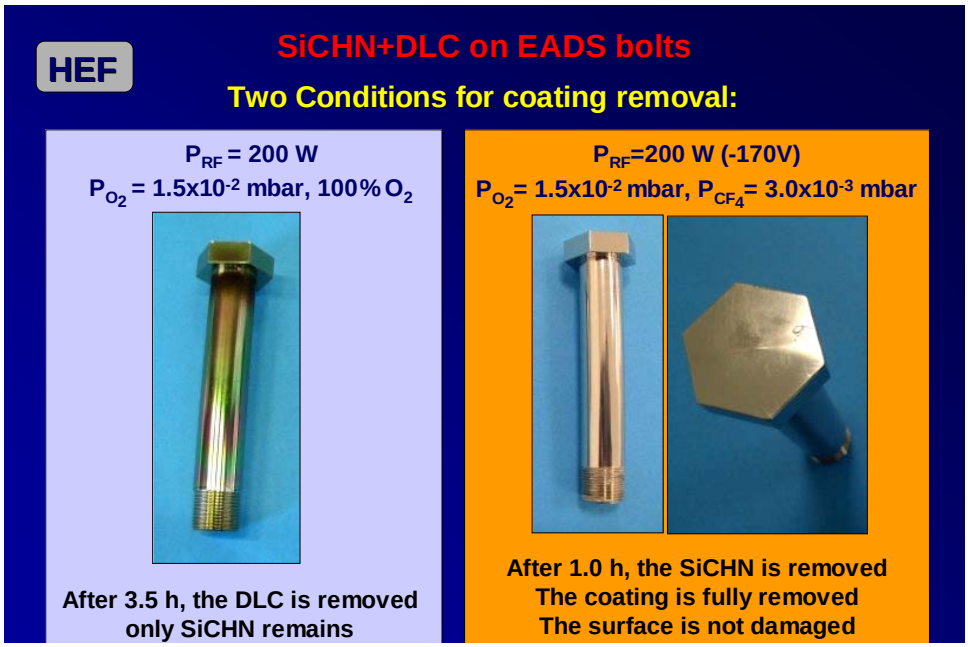

Data used for LCA model of de-coating process

The main environmental indicators chosen for the analysis are the ***GER*** (*Gross Energy Requirement*), expressed as MJ/m^2, and the ***GWP$_{100}$*** (*Global Warming Potential*), expressed as kg CO_2-eq./m^2. It is important to underline that results refer to a de-coating chamber not completely full: for this reason, they could be overestimated.

GER = 896 MJ/m^2 (of de-coated surface)

GWP$_{100}$ = 9,2 kg-CO_2-eq./m^2 (of de-coated surface)

Since the main impacts are linked to electricity use and this parameter is "country depending", the results have been re-calculated using the Italian energy mix, evidencing the effect of electricity production processes.

GWP$_{100}$ = 55,7 kg-CO_2-eq./m^2 (of de-coated surface) – IT Energy Mix

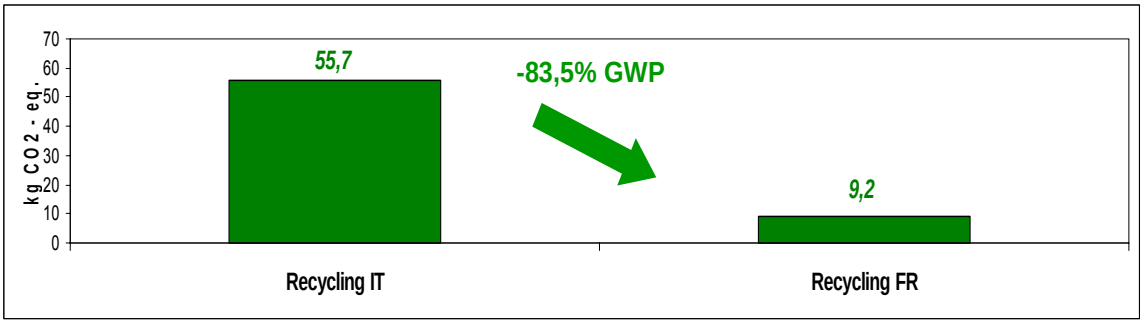

De-coating operations: the effect of the energy mix on the Global Warming

As far as recycling economical analysis, it is possible to follow the same approach adopted for coatings. The results are presented in the Table below.

PARAMETER	COST
GER: 896 MJ/m^2	**Italy**: 15,5 €/m^2 **France**: 8,9 €/m^2
CO_2 – Scenario 1 (CO_2 cost = 7 €/t)	**Italy**: 50,2 kg CO_2/m^2 = ***0,35 €/m^2*** **France**: 8,8 kg CO_2/m^2 = ***0,06 €/m^2***
CO_2 – Scenario 2 (CO_2 cost = 30 €/t)	**Italy**: 50,2 kg CO_2/m^2 = ***1,51 €/m^2*** **France**: 8,8 kg CO_2/m^2 = ***0,26 €/m^2***

Energetic and environmental costs of de-coating operations

1.7.3 WP Assessment and Conclusions

Activities related to WP 5 have started before the theoretical start. It was initially foreseen to start at month 29 which is in the current period covered by the report. More precisely, work related to task 5.1.3 has started early to allow the data collection related to substrates, coatings and processes. These data are used has input in task 5.2 for LCA (Life Cycle Analysis). The refinement of the data collected has allowed to find more accurate results. The work related to coating removal was carried out, using a plasma technology and was based on results issued from the reactor cleaning in WP2.

Milestone 5.1: "Lower environmental impact of the developed coatings"
The LCA was carried out and the coatings were compared to an electrodeposited coating. A series of iteration has been necessary to refine the results. More particularly, it has been necessary to consider industrial batch processes and to consider the coatings performance to evidence the lower environmental impact of the vacuum coatings investigated in the project compared to electrodeposition.

1.8 WP 6: Validation of the coating studied (WP Leader: EADS)

WP Leader **EADS**
Participants **TEFAL – HEF – CRF**

1.8.1 Objectives

The general objectives of this work package comprise the prediction of the durability of the prepared coatings in service and the validation of the results of the new designed materials on functional behaviour.
The work package 6 is divided in coatings combining wear and corrosion resistance (Task 6.1) and coatings on plastic substrate (decorative coating + electromagnetic shielding protection) (Task 6.2).
Work package 6 started at month 19 and lasted until the end of the project (month 36).

1.8.2 Progress towards objectives

1.8.2.1 Task 6.1: Validation for application 1: combining wear and corrosion resistance (**EADS**, **CRF**, **TEFAL**)

Validation for EADS application

The bolts from the EADS application are made of Steel alloy and are prone to fretting corrosion due to vibrations.
To simulate the environment that can result in fretting problems a test rig has been designed and built up at EADS.
The fretting test rig consists of two bolts, connected with a plate and two retainers which are connected to a tensile testing machine. Fretting will occur between the bolts and the bushings which are fitted into the plate. The material of the bolts and the bushings can be selected according to the application.
Forces resulting from a special design of the insert promote vibrations and therefore fretting.

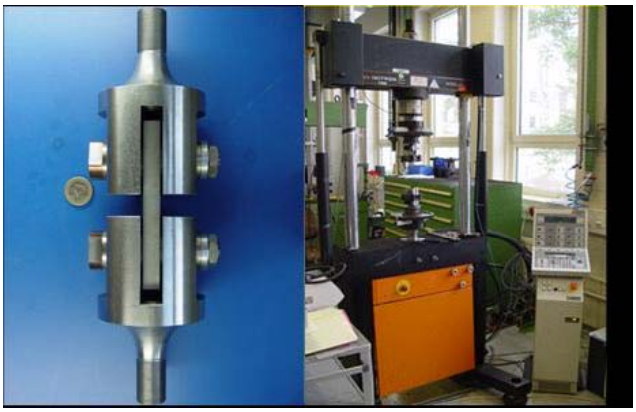

Testing device (left) and tensile testing machine (right)

The test parameters (force, surface pressure, frequency, number of cycles) have been selected according to the EADS application.

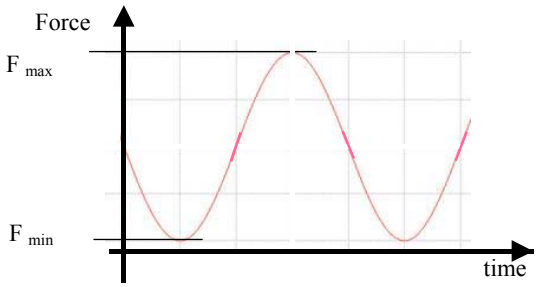

Force progression during one cycle

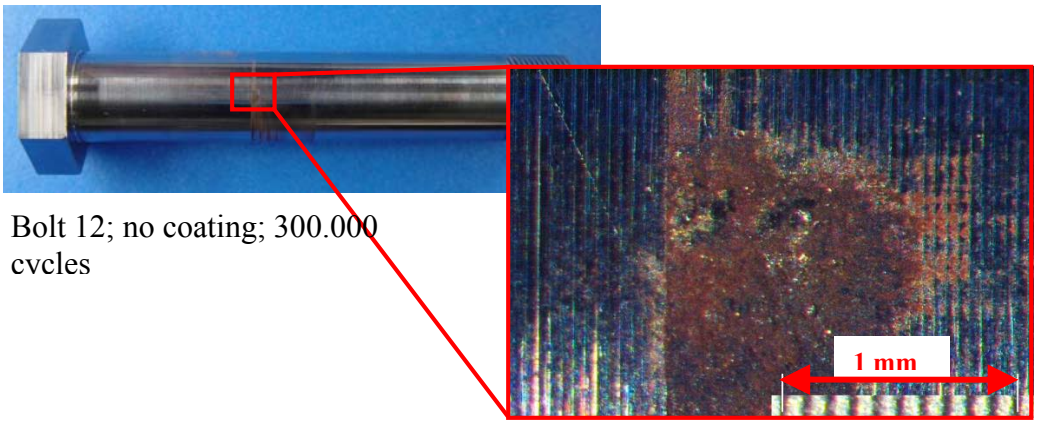

Bolt 12; no coating; 300.000 cycles

Macroscopic damage of bolt after fretting

The picture above shows the typical damage on a steel bolt. This test was performed to demonstrate the capability of the test rig to create fretting damage. The damage occurred after 300.000 cycles without coating or grease.

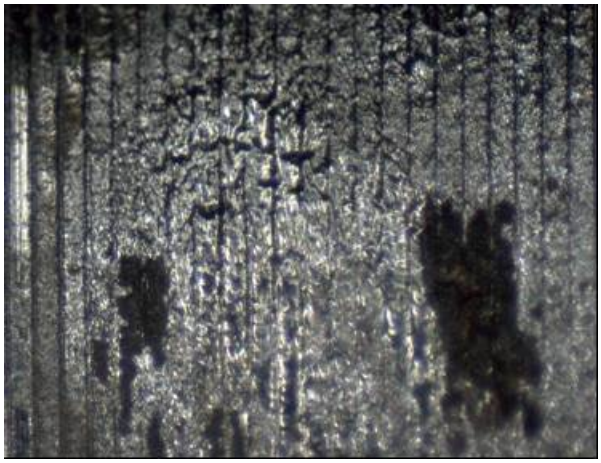

Microscopic damage after cleaning of the fretting area

The figure above shows the microscopic view of the damage after cleaning of the area. Cold welding occurred between bolt and bushing.
The appearance of the fretting area in the SEM is shown in the following images. The area of cold welding is visible.

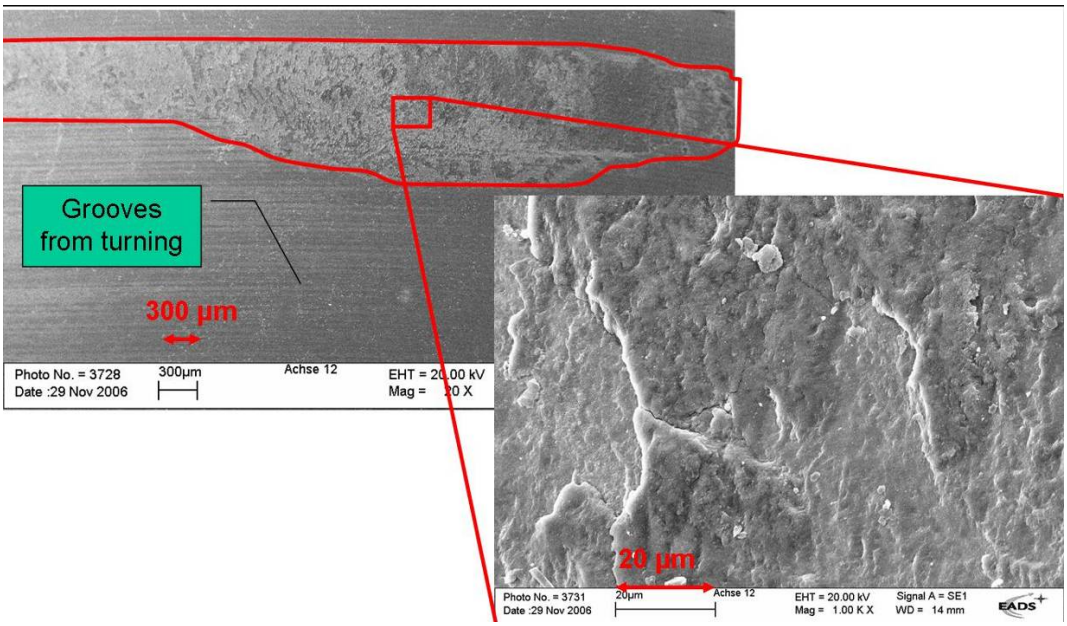

SEM image of fretting area after 1 million cycles

To pass the test a coated bolt has to pass ideally 150.000 cycles in not lubricated condition. After this test the bolt may not show fretting damage.

Test matrix

Based on EADS experience and the results achieved in the MATECO project different promising coatings have been selected for testing.

The coatings of the bolts took place at HEF. All coating structures were based on a multilayer approach with a SiOxNyCz intermediate layer and a DLC like top layer.

Fretting test results

The first test campaign can be divided into two groups: Steel bolts vs Steel bushings and Steel bolts vs Titanium bushings.

If the bolts are uncoated first damages on the surface can be found already after 100.000 cycles fretting test, independently of the bushing material. The use of a special lubricant, supposed to have anti-fretting behaviour, does not significantly improve the test results.

With the MATECO layer on the dummy steel bolt both for the steel and the Titanium bushing even after 2 Mio. cycles only very small markings are visible on the coated bolt.

The following figures show examples of the bad and very good fretting results.

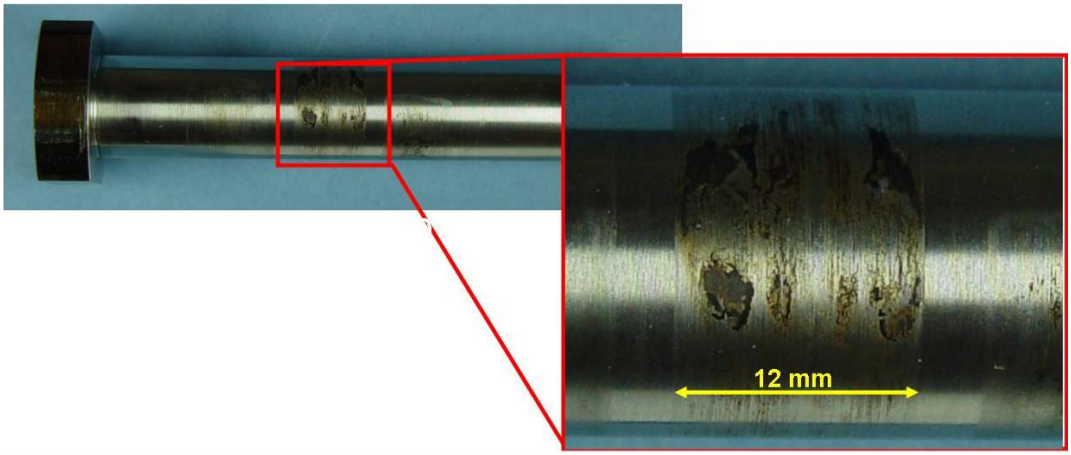

Bolt with special grease against Steel bushing after 1.000.000 cycles

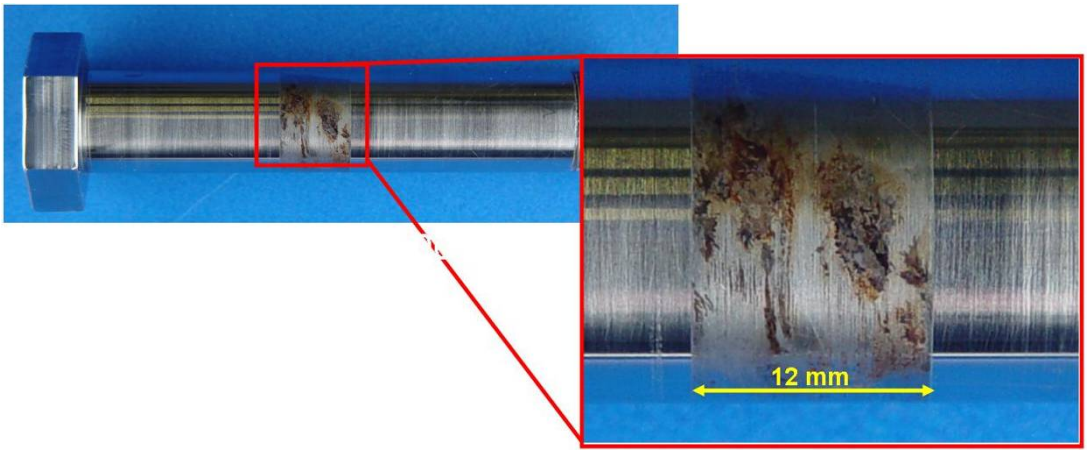

Bolt uncoated vs Titanium bushing after 1.000.000 cycles

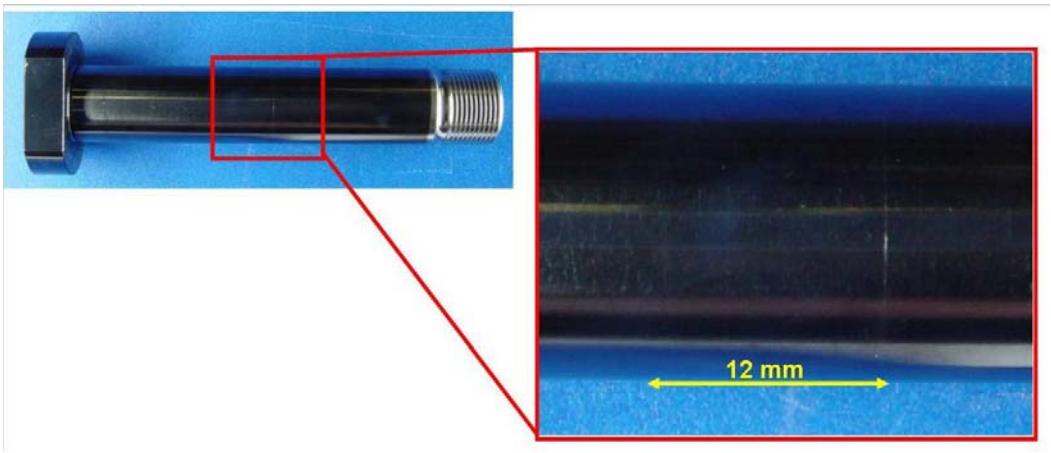

Bolt with MATECO coating against Titanium bushing after 2.000.000 cycles

To exclude a negative effect of the coating process or the multilayer coating on the corrosion properties of the bolts corrosion testing was performed in Neutral Salt Spray Test (EN ISO 7253). After 96 hours no corrosion attack is visible both on the uncoated and on the coated bolt.
Due to the very good results described a second test campaign was started to compare the new coating with state of the art coating systems (besides others thin chromium and nickel).
It was found that the MATECO coating system did show the overall best performance.

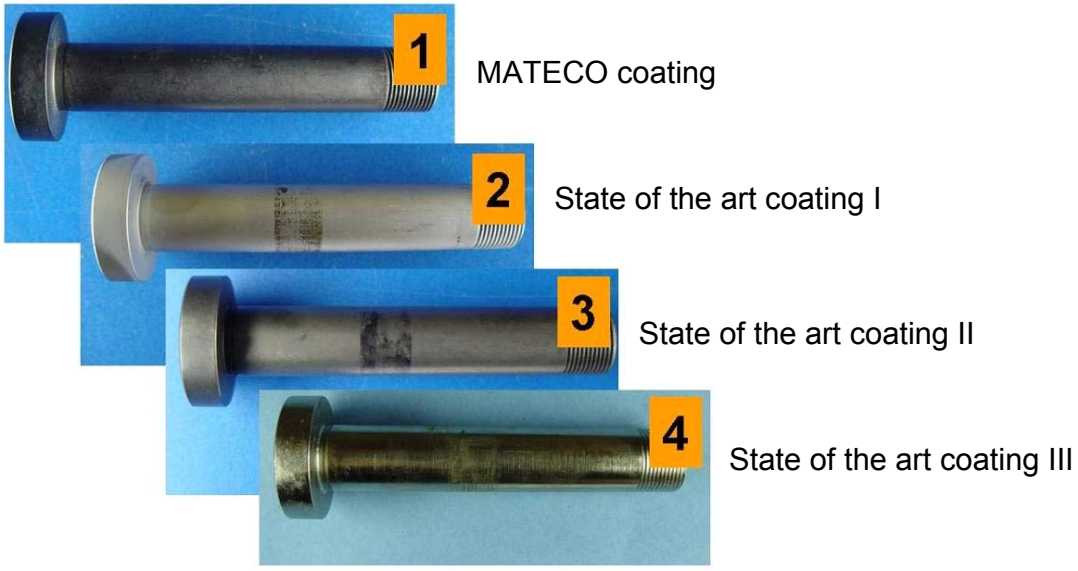

Overview of bolts after 600.000 cycles

Validation for CRF application

General objectives

The general objective of the project is development of an advanced coatings anti-corrosion and able to reduce the friction losses and the part wear.
In the CRF application the coating should substitute a Manganese phosphate surface treatment applied to the shims.

To reach the objective, a Fiat engine has been selected by CRF as representative final demonstrator for the large number of engines produced each year and the long manufacturing life expectancy.

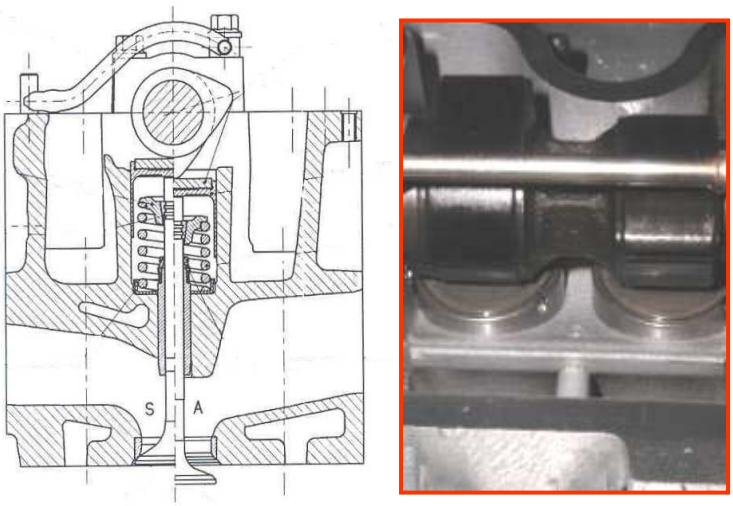

In the project the coupling shim-camshaft is object of interest.

Test methodology

In order to compare the tribological performances of the new shim coatings developed in the project, CRF developed the test methodology and adapted a tribological bench to test a complete valve train system

CRF realised first of all a tribological test on the normal production engine head with shims in alloyed steel and then tested the version with Mateco coated shims.

The tribological test consists in to characterise a standard engine head by measuring torque and component wear in the shim-camshaft system.

A tribological bench test has been adapted to test a complete diesel engine head.

The bench is constituted by an electric motor with a speed range between 0 to 6000 RPM.

The camshaft is joined to the driven shaft by means a mechanical coupling and a torque transducer. A specific lubricating system has been designed in order to adjust oil temperature (from room temperature to 150°C) and oil pressure (15 bar max) according to requirements. A computerised control system is able to control rotation speed, timing cycles, temperature and torque signal acquisition.

According to CRF engine department a representative test cycle has been defined in order to reproduce as much as possible the real working condition of the engine head and standard testing procedures in firing condition.

The testing procedure is constituted by the following steps:
- Metrological control of the part;
- Engine head pre-assembling;
- Engine head assembling;
- Running test with torque monitoring;
- Disassembling;
- Metrological control of the tested parts;
- Running test;
- Disassembling;
- Metrological control of the tested parts;
- Running test;
- Disassembling;
- Metrological control of the tested parts.

The complete test (250h) corresponds to a engine works of 60.000 Km.
Each test is performed with new parts: engine head, camshaft, valves system, tappets, shims, Oil (SAE10W-40).
Each running test is composed by several testing modules, each with the duration of 8h 20'.
At the end of the test running the parts are controlled, measured and weighted in order to evaluate the wear occurred in the shims and camshaft.
CRF tested engine heads with MATECO coated shims and the Reference Case with normal production shims.
The coating developed in MATECO was previously analysed and selected in the Workpackage 4 because of its promising tribological and anti-corrosion behaviour.
The coating selected and applied to MATECO Shims is SICH+DLC on a 100Cr6 substrate.
The first test (Reference Case) concerns the normal production configuration.
In this configuration the shims are in alloyed steel with a manganese phosphate as surface treatment.
The test ran for 250h with the acquisition of torque.

The parts (shims and cams) were measured in order to evaluate the dimensional variation during the test (at time=0, 50h, 100h, 250h).
Then CRF applied the testing procedure to the new engine head with the MATECO coated shims. The test ran for 250h with the acquisition of torque.
The parts (shims and cams) were measured in order to evaluate the dimensional variation during the test (at time=0, 50h, 100h, 250h).
The following results present the comparison between the Normal Production (Head NP), and the head with MATECO coated shims.
The coating developed in MATECO project showed a better behaviour in term of friction torque values than Normal Production configuration at first 200h but increasing friction torque values as test goes on, on the contrary of the NP configuration where the friction torque values decrease as the test is taking place.
Then the wears were valuated in the parts: shims and camshaft.
The camshaft presented wear behaviour of the cams in the coated engine head comparable with the Normal production configuration: the wear was estimated as height difference of the cams.
The shims have been examined by metrological instruments and SEM /EDS analysis at 3 steps of the testing time (50,100,250h).
A visual control and SEM analysis of the shims after the test revealed a delamination of the coating at intermediate steps and a complete removing at the end (250h) in several shims in the MATECO Head.

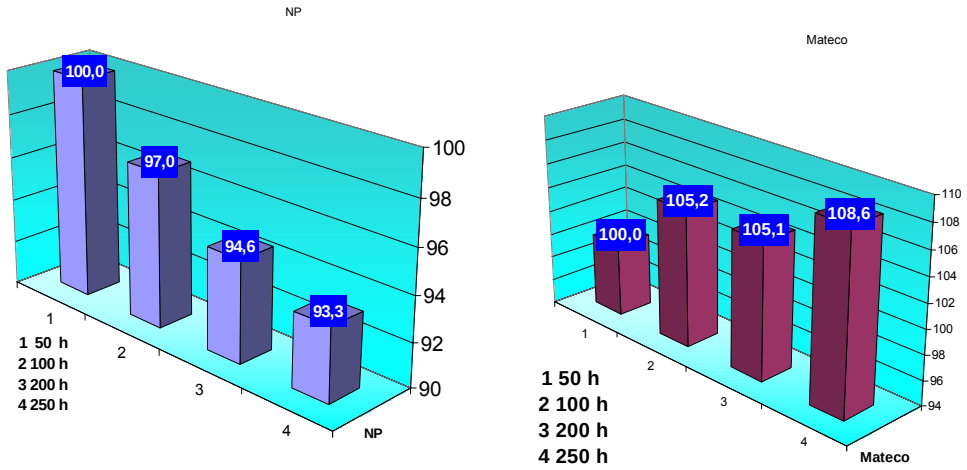

NP Head - MATECO Head : Comparison Friction Torque Related To 50h

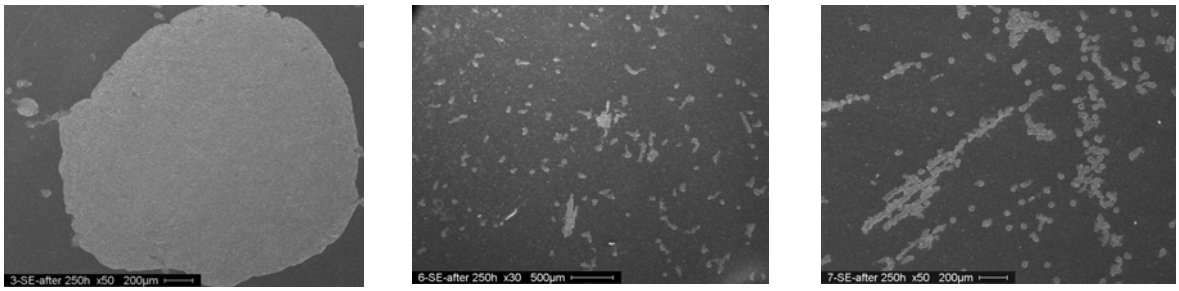

MATECO coated shims nr. 3 – 6 -7 after 250h

The shims with removed coating present a significant variation of profile.

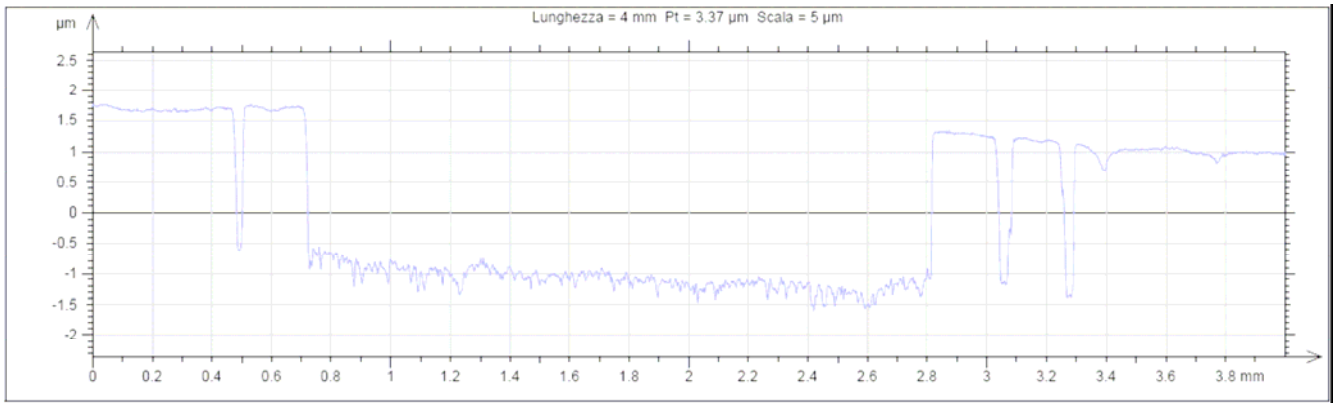

Profile of shim Nr. 3 after the test

Conclusions

As evaluation of the project results, the workpackage 6 foreseen the application of the developed coatings to a demonstrator part in order to assess the behaviour of the material when applied to a real part. So the coating, developed into the MATECO project and indicated as most promising from a tribological point of view in the characterisation phase included in the Workpackage 4, has been applied to the shims of a valve train system of a Fiat engine.

The tests, realised by a tribological bench adapted to test valve train system parts, permitted to evaluate the behaviour of the MATECO coating applied to shims in comparison with the Normal Production ones, in particular taking into consideration the friction torque and the wear/adhesion of the coating.

Concerning to the wear and adhesion of the coating, several coated shims presented delamination of the coating at the intermediate testing steps and a complete take-off at the end of the test.

The friction torque values in the coated shims test were lower than Normal configuration ones in the first 200h, but the values increased during the testing time instead of to decrease as in the Normal configuration : at the end of the test the two cases presented similar values, probably due to the fact that the coating moved out from the MATECO shim.

Validation for TEFAL application

Coatings have been built up on sole plate of iron. The objectives were to try to get both a good sliding property and a hard and corrosion resistance surface.

DLC coatings have been performed by H&F. However, it has been difficult to get homogeneous surfaces due to the size of the iron sole.

Sample n°	Type of coating	Thickness µm	Hardness	Surface Energy		
				Polar	Dispersive	Total
CF 612	Standard F	3,4	2200	5	35	40
CF 613	High F	3,8	330	3	21	24
CF 614	Low F	2,7	1900	3	39	42
CF 701	microwave	4,4	1050	2,5	32,1	34,6

	Angle (water)
	95,5
	86,2
	83,7
	83,8

rather hydrophobic which is not a good result if very good sling properties.

On the picture above, it is shown a DLC coating CFM 701 with fluorine (on the left) and a DLC 612 (on the right) which was inhomogeneous. We could see micro porosity as well which make the surface difficult to clean.

Endurance Test

We load in the iron between 100 and 250 liters of water with different concentration of Ca.
For low concentration of Ca, (hard water) the iron is submitted to thermal shock and we look at the sole resistance.
For high concentration of Ca, we look at the steam going through the holes.

Sliding Test

The smoothness of the sole plate is evaluated by measuring the horizontal force required to pull the iron over the surface of a standard ironing board. The iron is pulled horizontally at a speed of 0,25 m/s. The max force during the movement is measured.
The test is carried out 3 times, the cotton cloth being replaced each time.

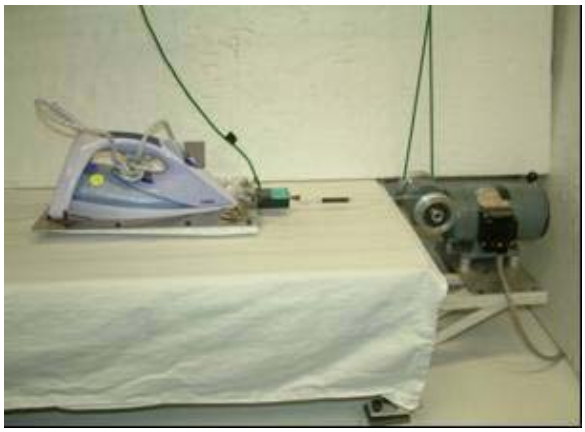

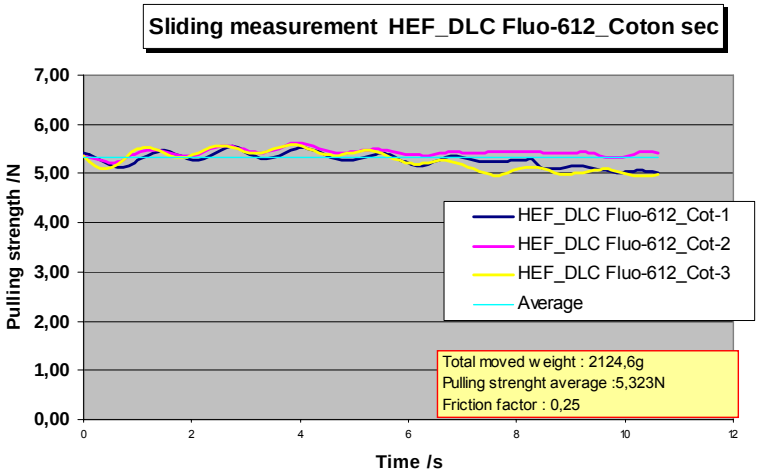

Summary of the results

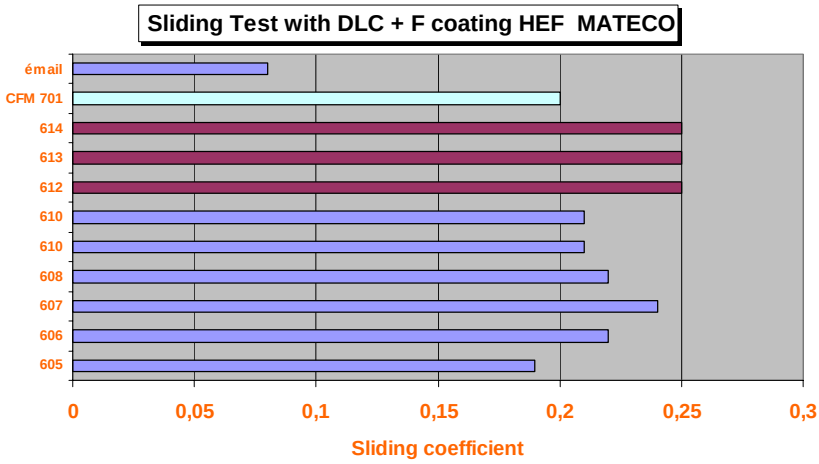

Scratch Test:
Hemispherical WC tip of 1 mm diameter and a force of 20 N with a speed of 35 mm/s. The sole plate is scratched in one direction and the width is measured.

Classes	Width mm
Excellent scratch resistance	X < 0,15
Good scratch resistance	0,15 < X < 0,30
Poor scratch resistance	X >0,3

Results obtained

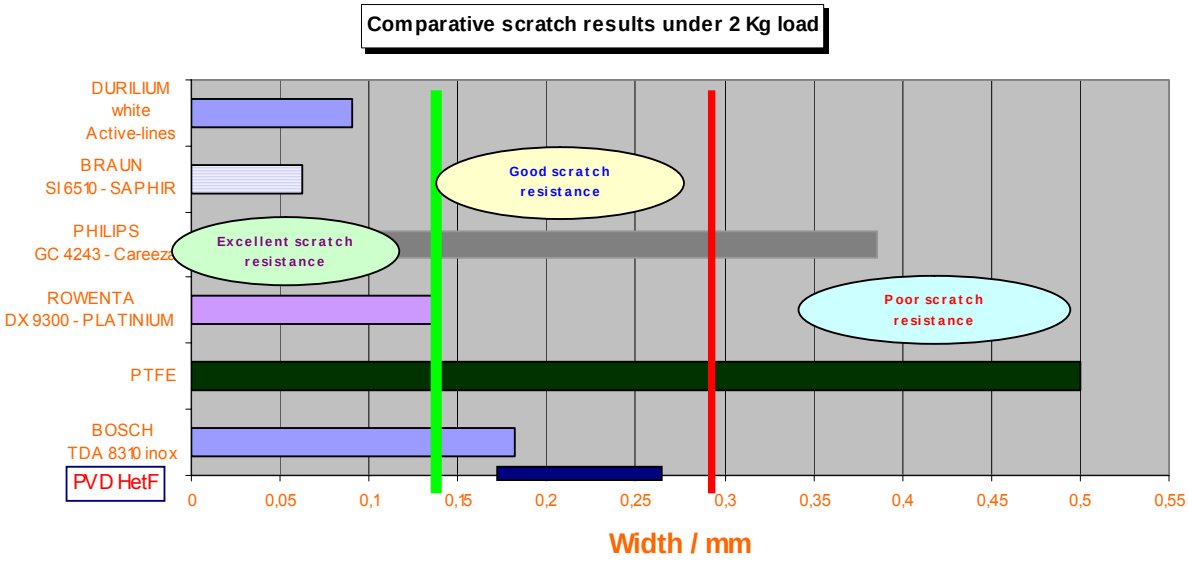

Scratch resistance is good (CFM 701 = 0,26) but this test was done on a first batch of samples and many other coatings should be done in order to assess the performance of DLC coatings.

Conclusion
It has been found with the Wettability measurement (medium angles) that DLC fluorine doped surface has hydrophobic behaviour. (low surface energy) This should help for the cleanliness but is not necessarily good for the sliding behaviour.
Endurance test have just began and are still running
The surface aspect was very poor (color homogeneity, microporosity) due to some machine parameters.
Sliding results are rather good compared with stain less steel but still far from enamels. However, the surface preparation should be discussed as it will have a great impact on the sliding properties.

DLC coatings

E.T.C surfaces for cookware application

New samples have been performed by Uniba for E.T.C surfaces on small samples (50 mm by 50 mm)

High angles have been obtained with CFx adjuvant, however, Easy to Clean test have given bad results probably due to strong links between SiOx species and carbonized foods.

Wettability measurement on new Uniba samples for E.T.C

	Angle Water	**Angle Diodomethane**	**Angle Formamide**	**Energy Dispersive mN/m**	**Energy Pol Acid/basic mN/m**
SiOx 2mm	32,1	47,7	33,5	35,5	12,1
SiOx 1mm +CFx1mm 50 W	103,7	80,3	94,3	17,3	1,4
SiOx 1mm +CFx1mm 100W	113,5	77,1	95,6	19	0,4
SiOx 1mm +CFx1mm 150W	107,8	77,7	95,1	18,7	1,3
SiOx 0,5mm pulsed 25% +SiOxCy Teos 100W SiOx 0,5mm pulsed 25%	42,5	45	28,7	37	14,2

1.8.2.2 Task 6.2: Validation for application 2: on plastic substrate (decorative coating + electromagnetic shielding protection) (**HEF R&D**)

For decorative applications, it was demonstrated that a compromise was difficult to achieve because of antinomic trends : low temperature requires low bias, non compatible with corrosion protection. Transparency requirements could only be achieved with very thin films, which could not provide a reliable corrosion protection. Therefore, it was decided to concentrate on electromagnetic shielding applications, because optical properties were not required.

For electromagnetic shielding applications, the substrate material is polycarbonate with glass fibers reinforcement. The parts are covered with a PVD Ag film. In this case, difficulties previously encountered for Al films are avoided because there is no need of optical properties for the protection of electromagnetic shielding coatings. As a consequence SiCHN films can be tested, which eliminates dissociation problems and limited mass flow previously encountered with HMDSO. Corrosion problems occurring on silver films are related to sulfurizing.

The efficiency of corrosion protection of silver coating is not tested in salt spray chamber like for steel parts, but in sulfurizing atmosphere. Reference test corresponding to customer requirements has a duration of 10min.

Sulphurizing tests are specifically carried out on silver coatings which are used for electromagnetic shielding. Parts are put in a closed container used for dry storage. Drying agents are replaced by a 20mL of sulfurizing solution (ammonium sulphide 0.2%) creating a saturated corrosive atmosphere.

Usual requirement for a good protection is that no tarnishing (presence of brown points) should be observed after 10 minutes in the container.

A silver coated sample and another one with an additional SiCHN top layer were put together in the test chamber. They were observed after 10, 30 and 70 minutes. After 10 and 30 minutes no damage was observed on either part. After 70minutes, the silver coated part exhibits tarnishing at some places, whereas the other one with the SiCHN top film shows no aspect change of the surface.

1.8.3 WP Assessment and Conclusions

The objectives of this work package was the test of the coatings developed in the MATECO project on real parts or at least probes that are close to the real application. The aim was the prediction of the durability of the prepared coatings in service and the validation of the results of the new designed materials on functional behaviour.
For the **EADS** application the MATECO coatings have shown very good results in the fretting test built up during the project. With the best coatings tested even after 2 million cycles no fretting damage can be observed both against steel and titanium bushings.
A substitution of environmental unfriendly coatings like Hard-Chrome or Nickel could be possible with this kind of coatings but further tests are necessary (fatigue, compatibility to service environment).
The coatings deposited by partners contains some species like oxygen and carbon based materials which gives strong connexions with carbonized food and obviously does not fullfill **TEFAL** requirement for “Easy to clean” applications.
DLC based coatings have been tried for few samples for Iron applications, results are promising but it would need much more trials and more conditions in order to find the best compromise.
The sliding properties were rather good but many other tests should be done to pursue this investigation.
CRF evaluated the developed coatings taking into consideration corrosion resistance and tribological behaviour. The coatings developed in the project presented in CRF application an efficient corrosion protection, but the tribological properties were not completely satisfactory.
In fact the tested coating applied to shim components in the engine valve train system, presented a delamination and a complete removing after the test in the contact area.
The promising results related to the friction torque in the coupling shim-camshaft for the MATECO coating, in comparison with the actual treatment, push on to proceed with further investigation and development in the coating deposition to reach the necessary adhesion.
For HEF, it has appeared that despite the excellent corrosion protection efficiency of SiOx coatings and their high optical transparency, the deposition of such coatings for decorative application on plastic parts is not economically viable. The deposition of SiCHN coatings for the protection of silver coatings has given good results. The coatings are coloured but this is not a problem for the protection of electromagnetic shielding silver coatings. The coatings on gas spring rods carried out in WP4 have shown a real breakthrough compared to the state of the art related to corrosion protection by vacuum deposited coatings. The progress achieved is reinforced by the fact that tribology properties brought by DLC allow to increase further the interest of such PACVD coatings compared to classical corrosion protective coatings.

Section 2 – Dissemination and Use

2.1 Exploitable knowledge and its use

Result no	Description of knowledge	WP	Contact partner	Documentation available (deliverables and others)	Other partners involved	Status*	Key code*
R 1.1	Development and modelling of new materials	1 & 3	ICMSE UNIBA			IP /NSY/ C	SEC/ WAIT/ PAT/ PUB
R 2.1	Vapour deposition process	2	HEF EPM	D2.2 Reactor Design		IP	WAIT
R 4.1	Coatings properties	4	HEF	No		IP	PAT
R 5.1	Validation	5	EADS POLITO			NSY	
R 6.1	Sample preparation	5	Tefal			IP	WAIT

**Status: IP = In Progress, NSY = Not Started Yet, C = Completed, N.A. = Non applicable. Key code: SEC = Secrecy approach foreseen, WAIT = Secrecy needed while waiting for completing, PAT = Patenting (or other protecting measures) foreseen, PUB = Dissemination of results foreseen*

2.2 Publications

These are the articles that the consortium has planned to publish within the next months.

POLITO

Study of the corrosion protective properties of PECVD SiOx and SiNx thin films
E. Angelini, S. Grassini, F. Rosalbino, F. Fracassi, R. d'Agostino, S. Laera, F. Palumbo
Proceedings of the European Corrosion Congress, **EUROCORR 2005**, that will be held in Lisbon on September 2005

Low-pressure plasma treatments for corrosion protection of metals
E. Angelini, S. Grassini, A. Palma, F. Rosalbino, F. Fracassi, F. Palumbo, S. Laera, R. d'Agostino
Proceedings of the Italian **Corrosion Congress,** which will be held in Ancona on July 2005

Comparison between eco-profiles of innovative PA-CVD and traditional galvanic coatings"
B. DeBenedetti, S. Grassini, L. Maffia
Accepted for the publication in the Proceedings of the ICMAT 2005 that will be held in Singapore.

INSA

Role of new PACVD silica based coatings on the corrosion protection of steel substrates

Enhancement of surface characteristics of passivable materials without losing their corrosion self-protective properties

2.3 Cooperation with other projects / programmes

Corresponding partner	Project concerned	Programme concerned	Purpose of meeting/discussion	Date of meeting / cooperation
HEF	HARDECOAT	FP6 - NMP	Seminar with similar STREP project	10/01/2006

It is planned to perform cooperation with the HARDECOAT Project consortium. Indeed, it is planned to perform a common meeting between both project's coordinators in order to exchange some non-confidential results obtained within each project.